The solid state interaction of palladium with SiC

Jeaneth Thokozile Kabini

Submitted in partial fulfilment of the requirements for a degree of

MAGISTER SCIENTIAE

in the Faculty of Natural and Agriculture Sciences at the University of Pretoria

Supervisor: Prof. C.C. Theron

December 2012

DECLARATION

I, Jeaneth Thokozile Kabini declare that the dissertation, which I hereby submit for the degree of MSc in Physics at the University of Pretoria is my own work and has not been submitted by me for a degree at this or any other tertiary institution.

Signature: .....

Date: .....

ACKNOWLEDGEMENT

- First and foremost I would like to thank God my heavenly Father and creator for always being my provider. In Him I live, I move and I have my being.
- I would also like to thank my flexible supervisor Prof. CC Theron for his guidance and encouragement through out this study. Thank you Prof. for walking baby steps with me into becoming a researcher.
- A special thank you to the former head of department of physics Prof. JB Malherbe for his comments, thoughts and support and for affording me an opportunity to travel and present my research in progress at an international conference.
- I would like to sincerely thank the entire physics department at the University of Pretoria for doing such excellent research and for taking graduate students from different backgrounds and turning them into scientist that will benefit our beautiful country in the years to come.
- To my friends and fellow students whom I have learned and struggled with: Mxolisi Mukhawana, Joseph Kuhudzai, Thulani Hlatshwayo and Zenande McOtshana, thank you guys for being my surrogate family in Pretoria. A special thank you to Eric Njoroge, for reading through my work and for his fruitful suggestions. May your journey be rich and interesting as mine.
- I would definitely like to express my extreme gratitude to my lovely family for their continual love and support. My mother Molly Tshilidzi Mudau, my sister's Emsion, Hlengiwe and Sindiswa and of course my brother Zeblon. To my aunt Rose Kabini, thank you for your tireless love and support.
- A special thank you to the South African Nuclear Energy Corporation (NECSA) for the financial assistance provided through out this study.
- I dedicate this work to my late father Mjoinelwa Kleinbooi Kabini, thank you dad for always believing in me and for the gift of education!
  'Ulale ngoqolo Hlalithwa elimnyama namadodana'.

Abstract

The solid-state interaction of palladium (Pd) with single crystal silicon carbide (6H-SiC) before and after annealing has been investigated using Rutherford backscattering spectrometry (RBS) in conjunction with RUMP simulation package, time-of-flight elastic recoil detector analysis (ToF-ERDA), glancing incident X-ray diffraction (GIXRD) and scanning electron microscopy (SEM).

A thin layer of Pd (500$\mathring{A}$) was deposited onto a clean 6H-SiC substrate at room temperature. The prepared diffusion couples were then annealed in vacuum at different annealing temperatures for a maximum period of 1 h. The annealing temperature ranged from 200^0C to 800^0C. The composition of the as-deposited and the annealed samples was measured by using a He^+ beam with an energy of 1.6 MeV. The ToF-ERDA measurements were performed on the as-deposited sample by using a high energy copper beam (about 30 MeV) for elemental depth distribution. The GIXRD measurements performed on the samples were able to identify the phases that form before and after annealing. The SEM micrograph obtained during this study gave some insight on the surface morphology of the samples before and after annealing.

Our results obtained during this study showed that Pd reacts with SiC after annealing at 400^0C resulting in the formation of metal-rich silicides and some unreacted Pd. Annealing at higher temperatures (500^0C and 600^0C) produced metal-rich silicides, which continued to grow until all the Pd has been consumed. Annealing at even higher temperatures (700^0C and 800^0C), the metal-rich silicides disappear and the silicon rich silicides start appearing. These appear by simply consuming the metal-rich silicides, resulting in the formation of two or more phases. The behaviour of the interaction between Pd with 6H-SiC is different than the Pd-Si system. The reaction temperature of the Pd/SiC are much more higher than those of the Pd/Si system. That is, Pd reacts with Si at temperatures as low as 250^0C, while it starts to react with SiC at an annealing temperature of 400^0C. In addition to this silicides such as Pd_9Si_2, Pd_4Si form at the initial reaction temperature followed by the formation of the Pd_2Si phase at the temperatures above 600^0C for the Pd/SiC system. Meanwhile in the Pd/Si system the Pd_2Si phase remains stable even after annealing at 800^0C. No carbon compounds were observed in the temperature range used in this study and the formation of silicides were found to be accompanied by the formation of free carbon which remained immobile in the system.

Contents

List of Figures

List of Tables

Chapter 1

Introduction

1.1 Introduction

Solid-state science comprises of a wide field of fundamental knowledge from mineralogy to quantum physics and from designing of high temperature materials to the development of telescopes and other electronic devices used in everyday life. Materials are important because anything that is used is made of some form of material. Over the past years material science has evolved enormously and its relationship to technology is self-evident.

Joining of metals or alloys to ceramic or semi-conductor materials is important for a variety of applications. Silicon carbide (SiC) is one of the materials with a large interest due to its unique properties such as corrosion resistance, high strength and high modulus (Park *et al.,* 1999). It can also be joined with metals or alloys for various applications. In many of these applications interfacial reactions between SiC and metals / alloys is of vital importance and can influence the functionality and the performance of the material. Thus the study of the growth and morphological development of the reaction zone together with the chemical reactions taking place between the metal and SiC has to be understood, and it is in this field that this thesis will make a contribution.

The interaction of metals with SiC under different conditions is important for the functionality of a device application. Hexagonal SiC (6H-SiC) can be used in a variety of device applications, due to its useful properties for photonic applications at short-wavelength, high frequency and high temperatures. To create such devices, SiC must be joined with different metals and this may result in the quality of the SiC being compromised. The main culprit for the deterioration of the device functionality can be from the intermixing and reaction at the metal-SiC interfaces found in these devices. During the reaction process, the performance of the SiC is controlled to a large extent by the stability of the interface at different temperatures.

For this study palladium (Pd) was chosen as a metal of interest. Its chemical interaction with SiC has been of great interest to researchers because of their applications as ohmic or Schottky contacts in electronic devices. In this devices the interface reaction between the SiC and Pd may lead to structural instability and thus deteriorating the mechanical properties of SiC. Another application for Pd with SiC is in coated fuel particles used in the high temperature gas-cooled nuclear reactors such as the South African Pebble Bed Modular Reactor (PBMR). These fuel particles generally consists of fissile phase kernel centered in the pebble. The kernel is coated with carbon (Pyrolytic Carbon) and SiC layers which act as a containment for fission products that form during fuel burnup (van der Berg *et al.*, 2009). Some of the fission products formed in the kernel, very often migrate to the coating layers and interact with the coating layers. Pd is one of the fission products which has been found accumulating in the inner SiC layers. Pd has also been reported to attack the SiC layers resulting in the corrosion of SiC (Minato *et al.,* 1994). This corrosion of SiC layer by Pd has raised some concerns about the integrity of SiC as an effective barrier for fission products.

1.2 Properties of SiC

SiC is a robust material with a wide-range of unique properties. It has a high breakdown electric field strength, excellent thermal conductivity and thermal stability which makes it ideal for operations in high temperature and high frequency environment. In addition to the above-mentioned properties SiC is a chemical inert which allows it to resist most chemical attacks. It is also a hard material due to the high bond strength resulting from the short bond between the Si and C (Zolnai, 2005).

In any of the SiC structures, the SiC tetrahedral are joined to each other at their corners, i.e. two neighboring tetrahedral share a corner atom. Figure 1.1 shows the carbon atom at the center of the tetrahedron surrounded by four silicon atoms tetrahedrally. The *c*-axis coincides with one of the Si-C bonds, the triangular base of the tetrahedron opposite to this bond is normal to the *c*-axis and defines a *c*-plane (Pirouz and Yang, 1992).

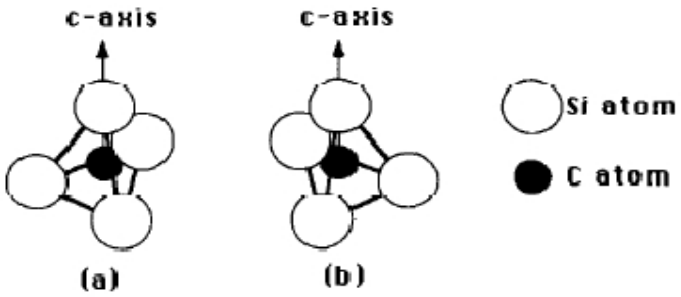

Figure 1.1: (a) SiC tetrahedron with the c-axis coinciding with the vertical Si-C bond , (b) the twinned variant of the SiC tetrahedron (Pirouz and Yang, 1992).

SiC consists of a number of different polytypes. The polytypes depend highly on the varied stacking order of Si and C closed packed atomic planes. There are more than 200 polytypes currently known resulting from the wide variety of preferred stacking sequence (Snead et al., 2007). The difference between these polytypes lie in the way in which Si-C close packed planes are stacked. These large number of possible combinations of this stacking sequence, results in SiC exhibiting a phenomenon known as polytypism. Polytypism, a one-dimensional polymorphism is a phenomena of stacking different crystal structure with the same chemical composition. Polytypism occurs in some close-packed structures and the change in crystal structure is given along the *c*-axis. Figure 1.2 shows the closed-packed structure system.

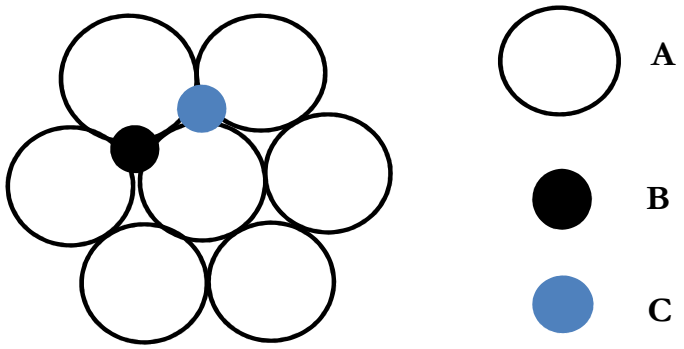

Figure 1.2: Closed-packed structure system.

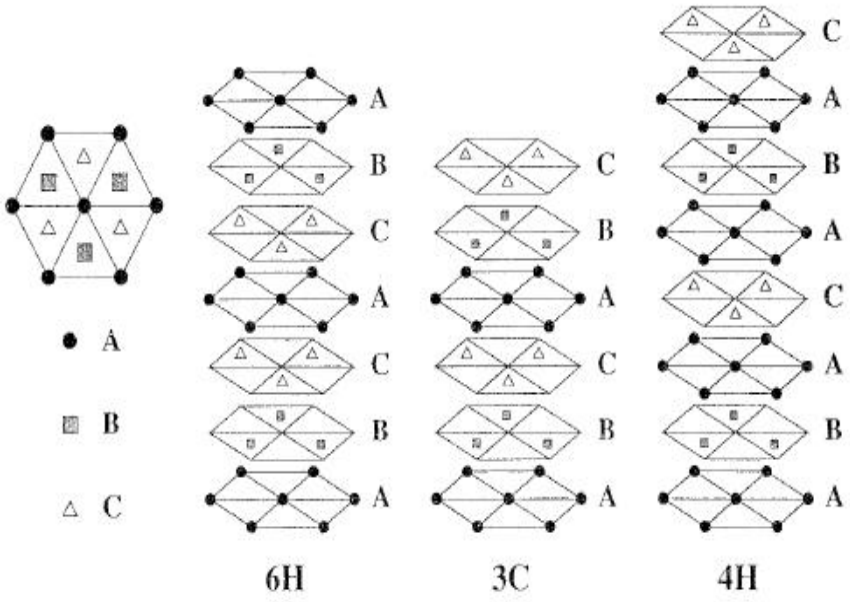

Figure 1.3: Bi-layer arrangements of 3C, 6H and 4H-SiC polytype, (Syväjärvi, 1999)

.

Each layer of atoms along the *c*-axis in a close-packed structure can occupy three different positions A, B, C with the Si-C pair considered as one unit. Thus the letters A, B, C represent a double layer of Si and C atoms. From this, different polytypes can be constructed by stacking the A, B or C atoms in different ways. If the first double layer is positioned in the plane A, the following plane can either be positioned at B or C. After the stacking sequence of the polytype is formed, the crystal with the given polytype is constructed by repetition of the polytype stacking sequence.

The resulting crystal structures of SiC are cubic (C), hexagonal(H) and rhombohedral(R). These polytypes can be described by using the Ramsdell notation (Sōmiya *et al.*, 1991). The stacking sequence of the 3C-SiC, 4H-SiC and 6H-SiC polytypes are shown in figure 1.3. This notation system indicates the number of layers in the unit cell and the letter represents the structure of the crystal. The only polytype that exhibits the cubic symmetry is the 3C polytype also known as β-SiC. The other non-cubic polytypes are all classified as α-SiC.

1.3 Properties of Palladium

Pd has an FCC crystal structure and a high melting point of 1554.9^0C which makes Pd ideal to be used in high elevated temperature environments. It is also known as a refractory and catalytic material. When Pd is in contact with SiC it is known to form compounds with Si known as silicides. These silicides can come in a number of different forms with a formula of Pd_xSi or Pd_xSi_y, where $x = 1, 2, 3$ and $y = 1, 2, 3$ etc. The most known silicides to form are PdSi (orthorhombic), Pd_2Si (hexagonal and rhombohedral) and Pd_3Si (orthorhombic).

1.4 Literature Overview of Pd/SiC interaction.

Extensive studies have been carried out on the metal-SiC interactions. In a paper by Bhanumurthy and Schid-Fetzer, (2001), the interface reaction between SiC with metals such as Cr, Zr, Ni and Pd where investigated in the temperature range of 700-1300^0C by employing bulk diffusion couples. For the interaction of Pd with SiC, the samples were prepared by making a "sandwich" type bulk diffusion couple consisting of a 6H-SiC, Pd, Hot Isostatic Pressing (HIP) (6H-SiC/Pd/HIP-SiC). The reaction products were identified by using SEM / energy dispersive x-ray analysis (SEM/EDX) and electron probe microanalysis (EPMA).

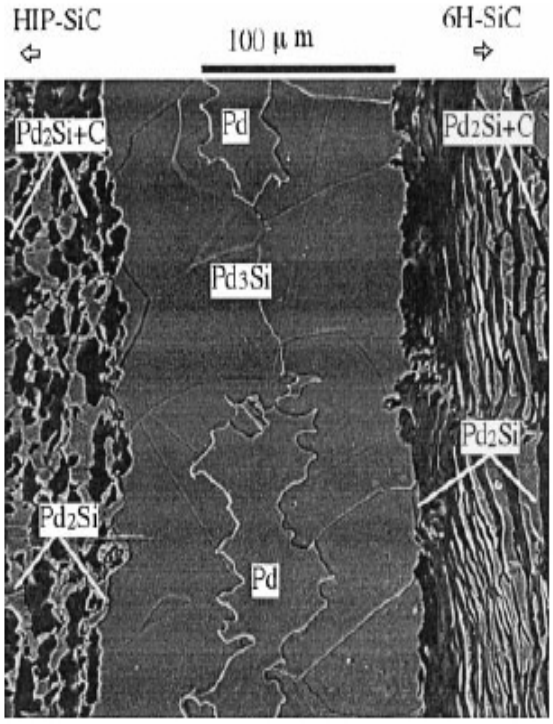

Figure 1.4: A secondary electron image of the 6H-SiC/Pd/HIP-SiC diffusion couple annealed at 750^0C (Bhanumurthy and Schid-Fetzer, (2001)).

Pd foils of approximately 250μm were cut to the size of the single crystals of 6H-SiC, HIP-SiC and were loaded into a diffusion bonding furnace with a pressure of 4-8 MPa in argon atmosphere for annealing. The prepared diffusion couples were annealed in the temperature range of 700^0C-1300^0C up to 200 hours (h). After annealing the samples were embedded in a resin, cross-sectioned and polished to 1μm diamond finish. The microstructure of the reaction zone was carried out by optical microscopy and SEM. The composition profiles were obtained by using EPMA.

The results showed that after annealing at 750^0C for 85 h Pd had reacted and a variety of phases in the reaction zone were formed and are shown in figure 1.4. The interface reaction between the 6H-SiC/Pd/HIP-SiC showed a development of the periodic structure consisting of Pd_2Si and graphite. The formation of the Pd_2Si phase close to the Pd_3Si without the graphite and the formation of the Pd_2Si with the graphite (Pd_2Si + C) in the dark band close to SiC was observed. The reaction layers (periodic layered structures) were observed to be generally sharp for the couple made from the monocrystalline SiC (6H-SiC/Pd) compared to the polycrystalline SiC (Pd/HIP-SiC). The formation of these periodic bands are found to depend on a number of certain properties. That is, to form a periodic structure metal must be the most dominant diffusing species and the carbon atoms must be practically immobile. Since the carbon atoms do not form compounds with Pd, silicides such as Pd_2Si, Pd_3Si and Pd_2Si + C resulted.

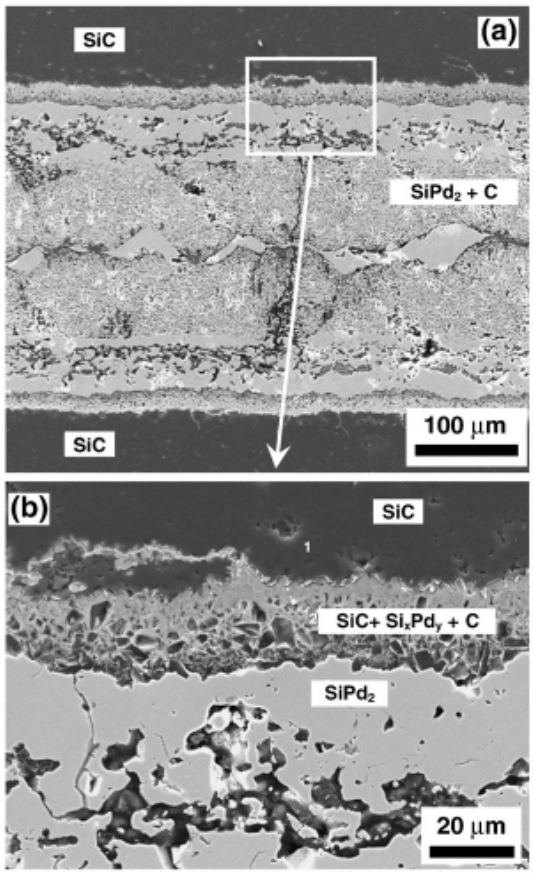

Figure 1.5: Pd-SiC interface annealed at 1000^0C for 10 h (Demkowicz *et al.*, 2008).

Demkowicz *et al.*, (2008), studied the high temperature interfacial reaction of SiC with Pd and rhodium at temperatures of up to 1600^0C by employing bulk diffusion couples. The intermetallic phases at the ceramic-metal interface were observed using SEM, EPMA and transmission electron microscopy (TEM). The diffusion couples were prepared by placing a metal foil with a thickness of approximately 0.25mm between two polished ceramic disks or between a polished ceramic disk and graphite spacing. The prepared diffusion couples were placed in a tube furnace and a small normal force was applied to promote good contact between the surfaces. The samples were then annealed at 800^0C for 10 h, 1000^0C for 10 h and 1000^0 for 50 h as well as 1200^0C for 10 h. After annealing the samples were cross-sectioned and polished to 1μm finish. The metal-ceramic interface were then analyzed using SEM, EPMA and TEM.

Figure 1.5 shows the SiC-Pd diffusion couple annealed at 1000^0C for 10 h. Microprobe composition data showed that Pd_2Si and Pd_2Si+C regions formed in the reaction zone. The region adjacent to the SiC (b) appears to be a mixture of incompletely reacted SiC grains, carbon and Si_xPd_y intermetallics. The Pd/Si ratio in this region was found to be approximately 1.7. No formation of periodic layered structures was observed in this study.

Roy *et al.*, (2002), performed studies on the Pd/β-SiC interface using secondary ion mass spectrometry (SIMS) and Rutherford backscattering spectrometry (RBS). This was done to investigate a reaction or interdiffusion at the Pd/β-SiC interface upon prolonged

annealing at different temperature in air. Epitaxially grown β-SiC film (on Si substrate) were first degreased before any Pd film deposition. Pd film was deposited on each substrate simultaneously by thermal evapouration. A thickness of Pd film of 0,18μm was deposited. The samples were then annealed in a resistive heated furnace at different temperature with a ramp rate of 30^0C/min. Both the as-deposited and annealed samples were then studied by SIMS and RBS to determine the compound composition as a function of depth.

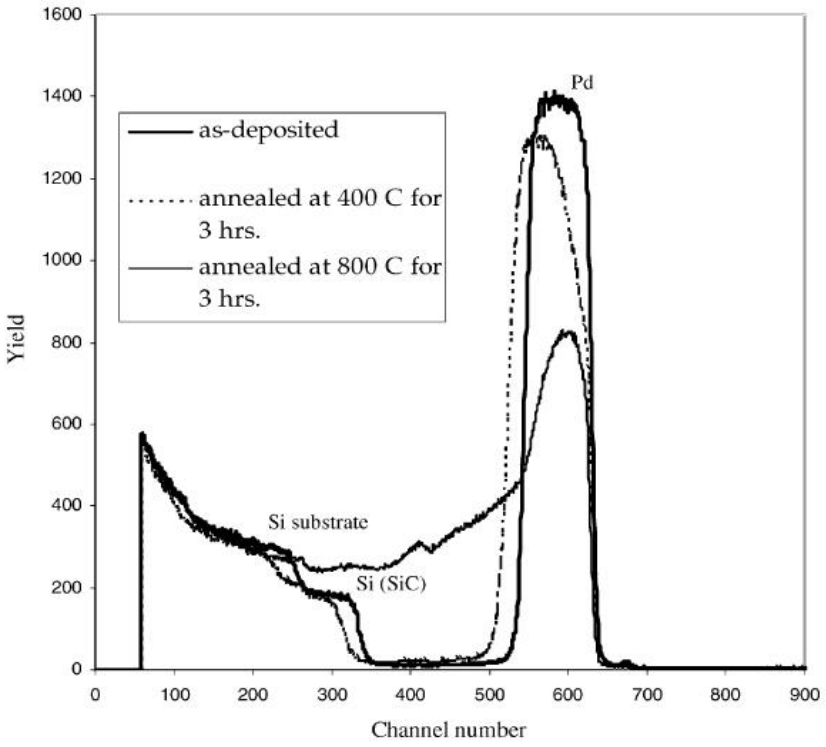

Figure 1.6: RBS spectra of Pd/β-SiC interface before and after annealing at 400^0C and 800^0C (Roy *et al.*, (2002)).

Figure 1.6 shows the backscattering spectra of the as-deposited and thermally annealed Pd/β-SiC interface. The Pd/β-SiC were annealed at temperature of 400^0C for 3 h and 800^0C also for 3 h. The sharp edge of the Pd signal for the as-deposited sample indicated a pure Pd top layer. The spectrum annealed at 400^0C in air for 3 h, showed a rounded leading edge of the Pd peak. This indicated less number of Pd atoms per unit energy loss in the top layer which was attributed to the interaction of SiC with Pd. Inside the Pd layer, the Pd:Si atomic ratio was found to be close to 3:1 indicating the formation of Pd_3Si with a thickness of 150nm.

The spectrum for the sample annealed at 800^0C was found to be different from that of the as-deposited as well as the 400^0C annealed samples. The interdiffusion of Pd and Si and a very high content of Si was observed throughout the sample. The out-diffused Si from the substrate was smeared through out the Pd matrix with a graded atomic concentration of about 68% on the top surface to about 55% in the interior. Phase determination could not be performed from RBS at this temperature due to the influence of Si atoms from the substrate.

Pia *et al.*,(1984), investigated the reaction of Pd and Ni with SiC (unspecified polytype) during thermal annealing by using X-ray diffraction (Read camera) and RBS. In preparing the sample, the SiC substrates were first degreased and loaded into an e-beam evapourator. Pd was evapourated onto the SiC with a thickness of about 0.1μm. The samples were then annealed in vacuum over a temperature range of 400^{0}C to 900^{0}C at 100^{0}C intervals maintained at 30 minutes at each temperature. The samples were then investigated by X-ray diffraction for phase identification and by RBS for compound composition and depth profiling.

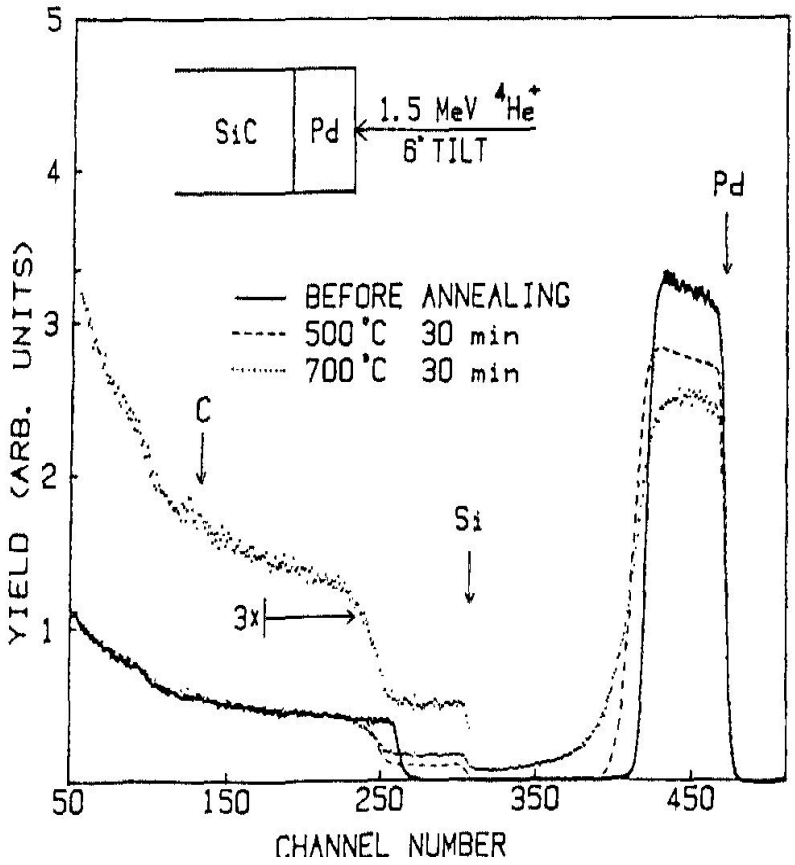

Figure 1.7: Backscattering spectra of Pd/SiC before and after annealing at 500^{0}C and 700^{0}C (Pia *et al.*,(1984)).

Thermally annealed Pd on SiC showed no detectable reaction after annealing at 400^{0}C. Figure 1.7 shows the backscattering spectra of Pd/SiC samples before and after annealing at 500^{0}C and 700^{0}C. The spectra show that the Pd has completely reacted with SiC after annealing at 500^{0}C. The atomic ratio of Pd:Si in the reaction product at this temperature was found to be 2.9. The sharp rear edge of Pd signal observed in the backscattering spectra indicates that the silicide-SiC interface is relatively uniform after annealing up to 600^{0}C. At 700^{0}C Pd begins to diffuse into SiC. The atomic ratio of Pd:Si in the reaction product after annealing at 700^{0}C was found to be 2.2. Due to the low sensitivity of the backscattering technique the amount of carbon dissolved into the Pd silicide could not be determined.

X-ray diffraction results indicated the formation of metal-rich silicides Pd_3Si formed first after annealing at 500^0C. This was followed by the formation of Pd_3Si and Pd_2Si after annealing at 700^0C. The Pd_2Si silicide was observed after annealing at 800^0C and 900^0C.

Veuillen *et al.,* (1999), investigated the reaction of the Pd thin-films on a clean and Si-rich 6H-SiC surface by using low-energy electron diffraction (LEED), photoelectron spectroscopy (UPS and XPS), atomic force microscopy (AFM) and glancing-incidence X-ray diffraction (GIXRD). The samples were prepared by evapourating a thin-film of Pd ($20\mathring{A}$) on the substrate maintained at room temperature and annealed at a temperature range of 600^0C to 800^0C. The reaction of the thick film was investigated by depositing an additional $100\mathring{A}$ of Pd at room temperature and annealed in the same temperature range. Veuillen *et al.*, (1999), found that Pd reacts with SiC at room temperature forming Pd_2Si at the interface. The $20\mathring{A}$ layer produced Pd_2Si islands covering the SiC surface after annealing at 600^0C. Carbon did not react with the Pd. For the $120\mathring{A}$ thin Pd layer, annealed at 800^0C the surface became very rough and was found to consist of high micrometer sized islands of the Pd_2Si surrounded by amorphous carbon.

1.5 Scope of investigation

Chemical reactions occurring in and between two substances, in this case between the metal Pd and the semi-conductor 6H-SiC may result in the formation of other substance(s). When the two reactants are brought together a reaction will occur until such a time that a stable state is reached, this of course will depend strongly on the kinetics involved. When this state is reached and depending on the number of components involved in the chemical reaction a single phase, two phase or many phases may develop.

Literature for ultra thin-film diffusion couples (nm scale) has shown that Pd reacts with SiC at room temperature to form a phase Pd_2Si (Veuillen *et al.,* 1999). These phase occur as islands covering the SiC surface. The work done on bulk diffusion couples (μm) has shown that Pd reacts with SiC (β-SiC) to form silicides at temperatures as low as 400^0C (Roy *et al.,* 2002). The formation of metal-rich silicides are found to form first at low temperatures followed by the formation of Si-rich silicides at high temperatures. This is also followed by the formation of a uniform phase Pd_2Si after annealing at 800^0C and 900^0C (Pai *et al.*, 1985). Literature has shown that during a chemical interaction between Pd and 6H-SiC in bulk diffusion couples, the reaction zone will consist of repeating patterns of reaction products and graphitazation resulting from the carbon atoms dissociating from the Si in the SiC compound. These repeating patterns of reaction products are the so-called periodic layered structures (Park *et al.*, 1999). These periodic structures may be the final / complete results of the solid-sate reaction process.

Therefore, in our work, we investigate the metallurgical interaction of Pd with 6H-SiC at low and elevated temperature for thin-film diffusion couples. We also aim to investigate the temperature at which Pd starts to react react with SiC and form silicides for thin-film samples and identify the phases that form after annealing at low temperatures of 200^0C up to high temperatures of 800^0C. This study also aims to investigate the reaction morphology of Pd/SiC together with the phase formation sequence of Pd/6H-SiC.

1.6 Outline of the dissertation

In this work several techniques were used in investigating the reaction morphology between Pd and 6H-SiC. These included the RBS technique which was used to determine the layer-by layer composition together with RUMP simulation software package. Time of flight - elastic recoil detector analysis (ERDA) to determine the elemental distribution, GIXRD for phase identification and SEM for surface analysis. Thus this thesis is organized as follows: **Chapter 1** gives an introduction to the metal-SiC interaction, the overview of the scope of investigation and discusses previous work done on metal-SiC interfaces. **Chapter 2** gives the theory of silicide formation and also highlights on the reaction morphologies found in ternary systems. **Chapter 3** presents the experimental techniques, methods and procedures followed in preparing the samples and obtaining the results. In **Chapter 4**, the results obtained are presented and disscused. The conclusion or the summary of this work together with the reccomendations for future studies are given in **Chapter 5**.

Reference

Bhanumurthy K., Schmid-Fetzer R., 2001, Compos. Part A-Appl. Sci. **32**, 569.

Demkowicz P., Wright K., Gan J. , Petti D., 2008, Solid State Ionics **179**, 2313.

Minato K., Ogawa T. , Fukuda K., Shimizu M., Tayama Y. ,Takahashi I., 1994, J. Nucl. Mater. **208**, 266.

Pai C.S., Hanson C.M. and Lau S.S, 1985, J. Appl. Phys. **57**, 618.

Park J.S., Landry K. and Perepezko J.H., 1999, Mat. Sci. Eng. A 253, 279.

Pirouz P. and Yang J.W., 1993, Ultramicroscopy **51**, 189.

Roy S., Basua S., Jacoba C., Tyagi A.K., 2002, Appl. Surf. Sci. **202**, 73.

Sōmiya S., Inomata Y., 1991, Silicon carbide ceramics: Fundamental and solid reaction, Elsevier science publishers, LTD, p.4.

Snead L., Nozawa T., Katoh Y., Byun T., Thak-Sang B., Kondo S. and Petti D., 2007, J. Nucl. Mater. **371**, 329.

Syväjärvi M., 1999, PhD thesis, High growth rate epitaxy of SiC: growth processes and structural quality, Linköping University.

van der Berg N.G., Malherbe J.B., Botha A.J., Friedland E. and Jesser W.A, 2009, Surf. Interface. Anal. **42**, 1156.

Veuillen, J.Y., Nguyen Tan, T.A., Tsiaoussis, I., Frangis, N., Brunel, M. and Gunnella, R., 1999, Diam. Relat. Mater., **8**, 352.

Zolnai Z., 2005, "Irradiation-induced Crystal Defects in Silicon Carbide", PhD Thesis, BUTE-DAP, Department of Atomic Physics, pg.4.

Chapter 2

The theory of Silicide formation

This chapter covers the fundamental principles needed in the formation of silicides for both binary systems and ternary systems. It is not within the scope of this thesis to describe the complete processes involved (kinetics) in the formation of the phases.

2.1 Introduction

The formation of phases in both bulk and thin-film systems has been of academic interest over the past years. Thin-film systems received attention in the sixties when Lepselter and Andrews introduced the metal silicides as contacts on silicon integrated circuits (Ottaviani, 1984). This introduction of metal silicides as contacts then triggered a large interest in the study of properties of thin-film silicides. The electrical and metallurgical properties were the two main aspects considered.

In order to understand the interfacial chemistry of the reaction zone, it is important for one to know the thermodynamics and kinetics of the system under considerations. By knowing the kinetics one can determine how much of a phase can be formed and on the other hand, by knowing the thermodynamics one can determine which phases are stable at certain conditions In principle, a complete set of both thermodynamic and kinetic data should allow the prediction of the compositional and morphological evolution of the reaction zone. However, in practice, attempting to make predictions on phase formation does not prove to be an easy task even in simple binary systems.

The difference between bulk and thin-film materials, apart from the scale, is the annealing time and temperature needed for phase formation to occur. One can generalize that for thin-film systems the time needed is short and the temperature is low for obtaining a desired amount of the reaction product, whereas in bulk systems longer annealing times and high temperatures are needed. The other difference is that in time, sequential phase formation is expected in the thin-film systems and simultaneous phase formation sequence is expected in bulk systems.

Over the years kinetic models have been developed (d'Heurle and Gas, 1993 and Dybkov, 1992) in an attempt to explain the sequential phase formation in thin-film system. Several studies have also been performed in order to predict the first phase that forms in various thin-film systems after annealing (Walser and Bené, 1976., Bené, 1982., Ronay, 1983., Pretorius, 1993.). A number of the proposed models for phase formation have been based on direct predictions from the phase diagrams. Although phase diagrams make it possible to determine which compound may form during the reaction in a system, one should note that phase diagrams are usually equilibrium diagrams while thin-film interactions and the sequence of phases formed reflect kinetics behavior. Therefore phase diagrams alone cannot be used in predicting the first phase formation.

2.2 Thermodynamics

2.2.1 Mass Action law

In general, a chemical reaction is written as

$$\Sigma_i \nu_i R_i = \Sigma_j \nu_i P_j \tag{2.1}$$

where ν_i and ν_j denote the stoichiometric coefficiency and R_i and P_j are the reactant species and product species respectively (Kubaschewski and Alock, 1979). When the system is at equilibrium there is a fixed relation between the activities of the components, this relation is called the mass action law, and is given by

$$K_p = \frac{P_j^{\nu_j}}{R_i^{\nu_i}} \tag{2.2}$$

where K_p is called the equilibrium constant. The equilibrium constant K_p is of great interest to scientist and it cannot be determined directly by measuring the concentration components at some selected temperature, but it can be obtained by using thermochemical calculations.

2.2.2 Phase diagrams

Phase diagrams are the pictorial representation of the domains of stability of various classes of structures (one phase, two phase, three phase, etc), that may exist in the system (Laurila and Molarius, 2003). They are most commonly represented in the temperature-pressure-composition space. They may be constructed from the knowledge of Gibb's energy curves as a function of variables but till present they are easily accessible by experimentation. A number of phases formed during the chemical reactions may be present in an equilibrium system of the phase diagrams and a number of phases that may be present in a system equilibrium is not arbitrary. If F is defined as the degrees of freedom that may be varied independently without altering the number of phases present then we have that:

$$F + P = C + 2 \tag{2.3}$$

where

- P is the number of phases
- C is the number of components present
- 2 stands for the variable temperature and pressure

Equation 2.3 is known as the phase rule. Since the equilibria in complex systems depends on many different variables, phase diagrams tend to be very complicated. In this study only the systems where the pressure variable can be neglected are considered.

To represent the phase diagrams on paper, two variables have to be chosen with the other variable remaining constant. To represent the phase equilibria in ternary systems at constant pressure, a three-dimensional construction is required. In many practices carried out for ternary systems the temperature is kept constant. Therefore the most quantitative ternary phase diagrams are presented as isothermal cross-section at certain temperatures. The compositions in the ternary systems are plotted using an equilateral triangle sometimes referred to as the Gibbs triangle. In this thesis, two types of phase diagrams will be appearing (a) the binary composition against temperature diagram and (b) Isothermal cross-section of a ternary composition against temperature diagram. For both of these diagrams the pressures of the systems are kept constant.

2.3 Solid-State diffusion

In solid-state studies no reaction can occur without diffusion. In this section diffusion phenomena occurring in solid-state is described. No attempt is made to give a complete overview on the diffusion of solid state, only the theory which is relevant in the formation of silicides is described. An important tool in studying diffusion phenomena is the so called diffusion couple, which consists of two starting material brought into contact with each other and are annealed for an appropriate time over a chosen temperature.

An ideal crystalline solid consists on an undistorted lattice equilibrium position where all the positions are occupied by the proper atoms. For diffusion to occur in such crystals a large amount of energy would be required to break the bonds between the lattice atoms, making it possible for atoms to jump and exchange positions. However, perfect crystals do not exist, the perfect infinite array of lattice points is always affected by the distortion called defects. These defects are important in a sense that the chemistry of solids cannot be understood without the knowledge of the nature and properties of these defects.

Defects in solids are classified into four categories :

1. Point defects : Vacancies, Interstitial and Impurities
2. Line defects : Dislocation
3. Surface defects : Grain boundaries and Interfaces
4. Macroscopic defects : Pores, cracks, etc

The presence of these defects and structures, such as vacancies and interstitials and other defects such as dislocations and grain boundaries enhances the mobility of atoms. Each of these categories has its own effects on the physical and chemical properties of the crystals. In this study we will only consider the effects of diffusion.

2.3.1 Mechanism of Diffusion

Solid-state diffusion in solids is different from that of diffusion of gases and fluids due to the structural constraints imposed by the solid. Diffusion in solids involves the movement of atoms or ions under the influence of some driving force. The driving force could be thermal, chemical, mechanical or electrical. Diffusion of atoms through a solid can occur in several ways; via the atomic lattice, this is the so-called volume or bulk diffusion or via the surface or grain boundaries, this is known as the short-circuit diffusion.

The volume or bulk diffusion occurs in a perfect single crystals at high temperatures and the short-circuit diffusion is found to be mostly dominant at low temperatures and occurs in polycrystalline materials. In this study volume diffusion is considered and a number of diffusion mechanism can be derived and these mechanisms play an important role in the atomic movements in metals. In semiconductor, there are two major mechanism of diffusion; vacancy mechanism and interstitial mechanism and these are considered in the next section (Shewmon, 1989).

2.3.2 Vacancy Mechanism

In vacancy mechanism the atoms move by exchanging places with the neighboring vacancy. That is, unoccupied vacancies in a crystal lattice provide a favorable route for atomic diffusion where atoms from the adjacent sites can jump into the nearby vacancies. The movement of these atoms to the vacancies in a solid is caused by the random thermal motion. Every now and then an atom will acquire enough vibration energy to jump to the neighboring vacant space.

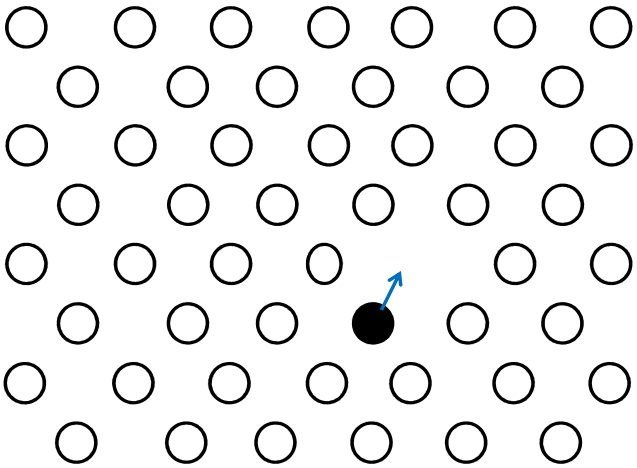

Figure 2.1: Vacancy diffusion mechanism in solid-state.

2.3.3 Interstitial Mechanism

Atoms diffusing interstitially can move through the crystal by jumping directly into the neighbouring interstitial sites without displacing any of the lattice atoms. These diffusing atoms are usually smaller than the lattice atoms making it easy for them to move from one interstitial site to the next. This mechanism is dominant for small impurities such as H, He and Li. The interstitial mechanism is commonly referred to as the direct interstitial mechanism. Another form of the interstitial mechanism is the interstitialcy mechanism where self interstitials push one of their neighbours into an interstitial position and occupy the lattice site previously occupied by the atom it has displaced.

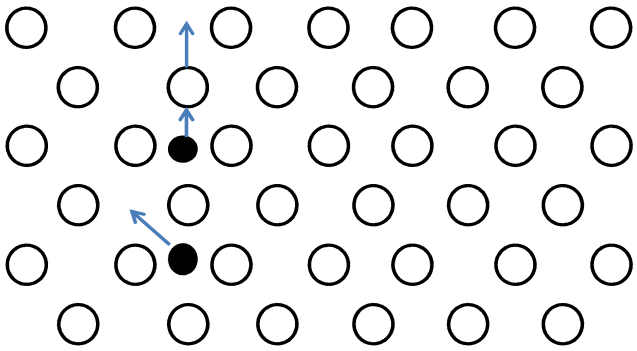

Figure 2.2: Interstitial diffusion mechanism in solid-state.

2.4 The laws of diffusion

General

The mention of the diffusion automatically brings to mind Fick's laws of diffusion. One-dimensional diffusion in a diffusion couple can be described by Fick's first law of diffusion (Crank, 1975) as:

$$J = -D\frac{dC}{dx} \tag{2.4}$$

where

- J is the flux of the diffusing component
- C is the concentration of the component
- D is a diffusion coefficient and
- dC/dx is the concentration gradient

The flux is proportional to the negative of the concentration gradient, the negative implying that the flow of matter is from high to low concentration. The diffusion coefficient is highly dependent on temperature and it is also a function of the diffusing species as well as the material through which it diffuses.

2.4.1 Diffusion in binary systems

When two metarials are brought into contact at elevated temperatures interdiffusion takes place and intermetallic compounds begin to grow. The thickness of the compounds formed in the diffusion couple can be directly related to the interdiffusion coefficient in the compounds. If these coefficients are known the composition and the layer thickness of the diffusion zone can, in principle, be calculated (Jan et al., 1993).

Diffusion in binary systems is considered a result of concentration gradient, or in terms of Fick's law (for one-dimension case)

$$\tilde{J}_i = -\tilde{D}_i\frac{\partial C}{\partial x} \tag{2.5}$$

In this case the diffusion coefficient is called the interdiffusion and it measures the mobility of both elements in a binary system. The corresponding flux is called the interdiffusion flux.

A combination of Fick's first law and the law of conservation of matter yields Fick's second law given by:

$$\frac{\partial C}{\partial t} = \frac{\partial}{\partial x}(\tilde{D}\frac{C}{\partial x}) \tag{2.6}$$

Where $C(t)$ is the concentration of the species of interest as a function of time. The advantage of this equation lies in the fact that if the concentration is known at some earlier time $t = 0$, then the concentration at a later time can be calculated provided that the interdiffusion coefficient $\tilde{D}$ is known.

To calculate the interdiffusion coefficient, equation 2.6 was initially solved by Boltzmann in 1894 and derived by Matano in 1933 (Devendra, 2005). However, this model is only valid in the situation where the total volume remains constant. If the volume changes, a modified second

law of Ficks has to be used (van loo, 1971). The interdiffusion coefficient determined by the Boltzmann-Matano analysis is given by equation 2.7. This interdiffusion coefficient is determined as a function of composition on the concentration profiles of diffusion couples.

$$\tilde{D}(C') = -\frac{1}{2t}\left(\frac{\partial x}{\partial C}\right)C' \int_0^{C'} x dC_i \tag{2.7}$$

The Boltzmann-Matano method does not involve a concentration gradient, therefore it is not applicable to diffusion couples containing phases with narrow, unknown region of homogeneity. To solve this problem Wagner introduced an integrated diffusion couple D_{int} which is a material constant, by integrating $\tilde{D}$, thereby loosing the concentration gradient (Rijnders, 1996).

$$\begin{aligned} D^i_{int} &= (x^+ - x^i)\frac{x^+ - x^i}{x^+ - x^-}\frac{(\triangle x^i)^2}{2t} + \\ &\frac{\triangle x^i}{2t}\cdot\left[\frac{(x^+ - x^i)\sum_{\nu=2}^{\nu=i-1}\frac{V^i_m}{V^\nu_m}(x^i - x^-)\triangle x^\nu + (x^i - x^-)\sum_{\nu=i+1}^{\nu=n-1}\frac{V^i_m}{V^\nu_m}(x^i - x^\nu)\triangle x^\nu}{x^+ - x^-}\right] \end{aligned} \tag{2.8}$$

Since the Dint is a material constant its value does not depend on the starting material in the diffusion couple. If all the Dint of a system are known the concentration profile can be calculated for each annealing time and couple type. Equation 2.8 has been used for determining the interdiffusion coefficient for the Ni-Si system (G$\ddot{u}$lpen, 1995).

2.4.2 Diffusion in ternary systems

In a binary system, the chemical potential of each component increases continuously with its concentration. However, in ternary systems a component can diffuse also along the chemical potential of other components (Wakelkamp, 1991). Therefore for multicomponent diffusion Ficks law has to be extended. In a volume-fixed frame, the extended form of Fick's law for a single phase ternary system is given by (Osinski, 1983)

$$\tilde{J}_1 = -\tilde{D}^{(3)}_{11}\frac{\partial C_1}{\partial x} - \tilde{D}^{(3)}_{12}\frac{\partial C_2}{\partial x} \tag{2.9}$$

$$\tilde{J}_2 = -\tilde{D}^{(3)}_{21}\frac{\partial C_1}{\partial x} - \tilde{D}^{(3)}_{22}\frac{\partial C_2}{\partial x} \tag{2.10}$$

where component (3) is chosen as the dependent one. To describe the diffusion process in ternary systems four interdiffusion coefficients are needed for each phase. Therefore the interdiffusion coefficients $\tilde{D}^{(3)}_{11}$ and $\tilde{D}^{(3)}_{22}$ represent the influence of the concentration gradients of components 1 and 2 on the interdiffusion fluxes of components 1 and 2 respectively. The other two cross interdiffusion coefficients $\tilde{D}^{(3)}_{12}$ and $\tilde{D}^{(3)}_{21}$ also represent the influence of the concentration gradients of components 1 and 2 on the interdiffusion fluxes of components 2 and 1 respectively.

Thus Fick's second law for a single phase ternary systems can be written as:

$$\frac{\partial C_1}{\partial t} = \frac{\partial}{\partial}\tilde{D}^{(3)}_{11}\frac{\partial C_1}{\partial x} + \frac{\partial}{\partial x}\tilde{D}^{(3)}_{12}\frac{\partial C_2}{\partial x} \tag{2.11}$$

$$\frac{\partial C_2}{\partial t} = \frac{\partial}{\partial}\tilde{D}^{(3)}_{21}\frac{\partial C_1}{\partial x} + \frac{\partial}{\partial x}\tilde{D}^{(3)}_{22}\frac{\partial C_2}{\partial x} \tag{2.12}$$

To determine the interdiffusion coefficient as a function of concentration from Fick's second law, the Boltzmann-Matano analysis is also applied. The Boltzmann-Matano solution for equation 2.11 and 2.12 becomes (Osinki, 1983)

$$\left|\tilde{D}^3_{i1}\frac{\partial C_1}{\partial x}+\tilde{D}^3_{i2}\frac{\partial C_2}{\partial x}\right|_{C'_i}=\frac{1}{2t}\int_{C_i}^{C'_i} xd(C_i), i=1,2 \tag{2.13}$$

2.5 Kinetics Consideration

For a system consisting of two materials namely A and B, A being a metal and B being Si. When the metal material A is deposited onto a substrate B such as Si, these materials will be separated by an A/B interface which is not thermodynamically stable, however upon heating this interface tends to become more stable and the elements A and B tend to have minimum activity (Gas and d'Heurle, 1993). To understand the evolution of this interface, the phase diagrams are mostly used.

The thin-film solid state reactions are vastly different from those of bulk reactions due to their sequential appearance of phases, the absence of certain stable phases and the rapid kinetics of formation. The metal-Si diffusion couple will lead upon annealing to successive formation of different silicides starting with the metal rich silicide to Si rich silicides (Poate *et al.*, 1978). The kinetics of silicide growth are classified into three categories namely, diffusion-controlled, nucleation controlled and reaction-rate controlled kinetics.

2.5.1 Diffusion-controlled kinetics

In binary systems, a large number of metals are found to react with Si at a temperature below that of 500^0C to form silicides that can grow according to the diffusion-controlled kinetics. An example of such silicides are Ni_2Si, NiSi, Ru_2Si_3, Pd_2Si, CoSi, MnSi and Pt_2Si (d'Heurle and Gas, 1986). Table 2.1 shows the silicides whose formation is diffusion-controlled and the temperatures which they appear. The sequence of the phase formation of these silicides does not necessarily follow the sequence found in the binary phase diagrams. In analyzing the kinetics of these kind of phases, a case where only one phase is formed is considered. To establish or determine if the solid-state reaction is diffusion-controlled, the squares of the thickness of the thickness of the reacting layers obtained form the Rutherford backscattering spectrometry spectra (which provides information about the composition of the reacted layer and its thickness) is plotted against time for different temperatures. When this is done a series of straight line is obtained. These straight lines are the characteristics of diffusion-controlled kinetics and their convergence near zero implies parabolic growth rate (see figure 2.3).

The slopes of these straight lines provides a quantity called diffusivity which is a function of diffusion coefficient. The relationship between the diffusion coefficient and the temperature is given by the Arrhenius equation

$$D=D_0 exp(\frac{-Q}{RT}) \tag{2.14}$$

where

- D is the diffusivity
- D_0 is the pre-exponential factor
- Q is the activation energy

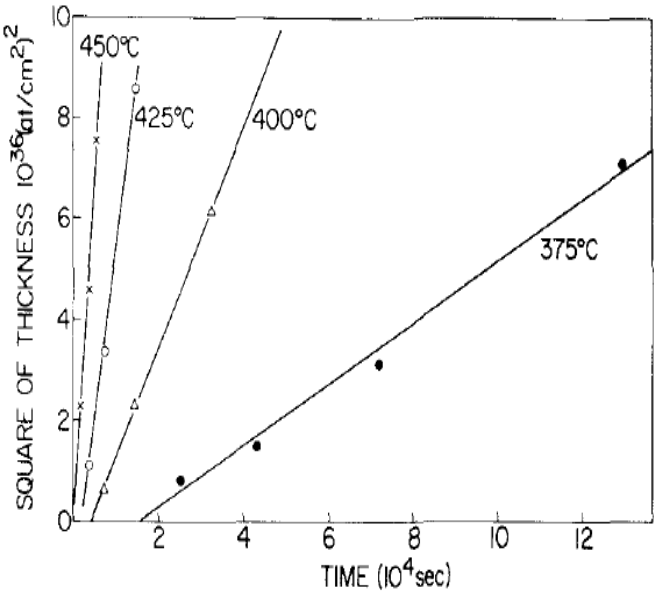

Figure 2.3: The square of the thickness of the growing layers plotted as a function of time (d'Heurle and Gas, 1986).

The quantity of diffusivity can be displayed on the Arrhenius plots, where the natural logarithm of the diffusion coefficient is often plotted against the temperature reciprocal and the slope of this curve gives an activation energy of diffusion as shown in figure 2.4. Where the slope of the curve is the activation energy Q and the y-intercept is the pre-exponential factor D_0.

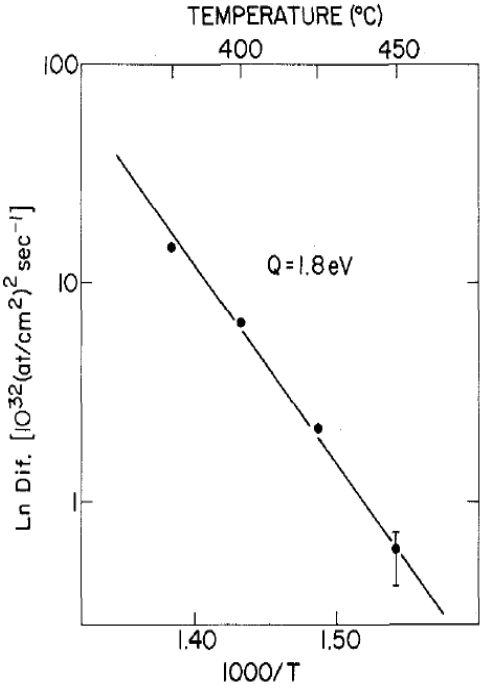

Figure 2.4: Arrhenius plot of the slopes with activation energy (d'Heurle and Gas, 1986).

The activation energy obtained from the graph, is not the activation energy of the diffusion, but contains the sum of the quantity of activation energy for diffusion Q_{diff}, the temperature exponent for the variation of concentration gradient Q_{sol} and the activation energy for heat adsorption Q_{ads} which has an opposite sign to all the others and must be added for the grain boundary diffusion . Thus the sum of the activation energy can be written as $Q_{diff} + Q_{sol} + Q_{ads}$ (d'Heurle and Gas, 1986).

Table 2.1: Silicides whose formation is diffusion-controlled and the temperature at which they appear (Gas and d'Heurle, 1993).

					Co_2Si-350	Ni_2Si-200	Cu_3Si-150
			MnSi-425	FeSi-450	CoSi-350	NiSi-275	
$TiSi_2$-425	VSi_2-600	$CrSi_2$-520			$CoSi_2$-400	$NiSi_2$-380	
Zr_5Si_4-670						Pd_2Si-175	
					RhSi-350		
	$NbSi_2$-645	$MoSi_2$		Ru_2Si_3-350			
HfSi-525		WSi_2-800		Os_2Si_3-450	IrSi-400	PtSi-300	

2.5.2 Nucleation-controlled Kinetics

Nucleation occurs as a result of a competition between the gain in Gibb's free energy $\triangle G$ of the newly formed interface and the increase in the surface energy $\triangle\sigma$ resulting from the extra interface formed. Several silicides are known to occur via the nucleation controlled reactions such as $Mn_{11}Si_{19}$, PdSi, $HfSi_2$, Rh_4Si_5 and Rh_3Si_4. These silicides tend to form at very high temperatures.

The process of nucleation is associated with an increase in free energy which is compensated by an equivalent or greater decrease due to the formation of the new phase (d'Heurle and Gas, 1993). Therefore only the reaction characterized by the small gain in free energy can be nucleation-controlled.

Table 2.2: Silicides whose formation is nucleation-controlled and the temperature at which they appear (Gas and d'Heurle, 1993).

ScSi-900	$TiSi_2$-900	$Mn_{11}Si_{19}$-55	$FeSi_2$-55	$CoSi_2$-500	$NiSi_2$-800
				Rh_4Si_5-825	PdSi-735
	$ZrSi_2$-625			Rh_3Si_4-925	
	$HfSi_2$-685		$OsSi_2$-740	$IrSi_3$-940	

Table 2.2 above gives the type of silicides whose formation is nucleation controlled and the temperature at which these silicides are appear. Silicides from the rare-earth metals appear to be widely dominated by the nucleation phenomena.

The difference between the nucleation-controlled and the diffusion-controlled kinetics is very small and this difference is influenced by a small change in the formation process. That is, changing from a crystalline to amorphous Si and the associated increase in free energy of the reaction is sufficient enough to change from a nucleation-controlled reaction to a diffusion controlled reaction (d'Heurle and Gas, 1993). For example, the formation of the $NiSi_2$ silicide is the diffusion-controlled controlled reaction when

$$NiSi + \text{a-Si} \longrightarrow NiSi_2$$

and it becomes nucleation controlled when

$$NiSi + c\text{-}Si \longrightarrow NiSi_2$$

2.5.3 Reaction-controlled Kinetics

Some silicides are reported to form linearly with time, these silicides are known to be reaction-controlled. An example of such silicides are $TiSi_2$, VSi_2, $CrSi_2$ and $NbSi_2$ and the thickness of the growing layer in these silicides is observed to increases linearly with time (Theron,1997). The observation of the linear growth indicates that the rate at which the reaction takes place is constant, that is, the kinetics of reaction itself controls the growth of silicides. Also in this case the activation energy of growth for the reaction controlled kinetics is higher than the diffusion-controlled kinetic. The activation energy of the reaction controlled kinetics is determined in a similar manner as the diffusion-controlled reaction, except that the relationship between the thickness and time is linear (Theron, 1997).

Some silicides have been reported to be either linear with time or parabolic (d'Heurle and Gas, 1993). A good example of such growth is the $TiSi_2$, where the thick layers of the $TiSi_2$ can grow without any diffusion problem, since most of the limiting step from the beginning of growth is diffusion. In other cases the growth of $TiSi_2$ can be nucleation-controlled. The scheme for the formation of the $TiSi_2$ is as follows: diffusion controlled growth for the first phase and at high temperature by nucleation controlled growth for the second phase. This will eventually result in a complex kinetic behavior, where the individual characterization of each phase will be hard to extract. Thus in cases like these where the formation of the silicide is either linear or parabolic will strongly depend on experimental parameters such as the quality of the metal-Si interference, crystallinity of the Si substrate, purity and reactivity of the metal film, temperature that may influence both efficiency of the diffusion barrier and nucleation difficulties.

2.6 Phase Formation in binary systems

2.6.1 Metal-Si

In binary systems the metal-Si reaction on the thin-film may to some extend differ from those on bulk reactions in sequential apparence of phases, absence of other phases and very rapid kinematics of formation. The characteristics of the formation of silicides in the thin-films is analysed by taking into account the kinetics of solid-state reaction and the role of the experimental conditions encountered in the metal-Si thin-film reaction such as low temperature, high density of interfaces (Gas and d'Heurle, 1993).

2.6.2 Single phase growth

The growth of a phase A_xB_y by reacting material A and B requires three stages (1) creating of an additional interface (2) diffusion of A and/or B through the A_xB_y and (3) chemical reaction between A and B at the interface A/A_xB_y and A_xB_y/B leading to the formation of an intermediate compound. When the reaction starts the thickness of A_xB_y phase is very small and either of the elements A and/or B are available at the interface for the formation of the phase. Thus the only limitation for the growth of A_xB_y is the capacity of the interface to form a new phase (Gas and d'Heurle, 1993).

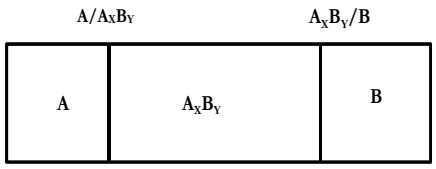

Figure 2.5: Schematic representation of the growth of the phase A_xB_y by solid-state reaction between A and B.

The growth of the A_xB_y is no longer controlled by the interfacial reaction when its thickness increases and the path that A or B atom has to cross becomes lesser and lesser. When this happens the thickness of the A_xB_y becomes a parabolic growth. This is the so-called 'linear-parabolic growth'.

2.6.3 Simultaneous growth of phases

When two or more phase grow simultaneously the kinetics of growth of each phase will depend not only on the charectaristics of that phase but on the charectaristics of all the phases present in the A/B diffusion couple. In the system with two phases forming at the same time, say (A_2B and AB) only the movement of atom A is considered. The growth of A_2B will take by the following reaction, at the interface of A_2B/AB.

$$A + AB \longrightarrow A_2B$$

The growth of AB occurs at both the A_2B/AB and AB/B interface with the reaction of

$$A_2B \longrightarrow AB + A$$

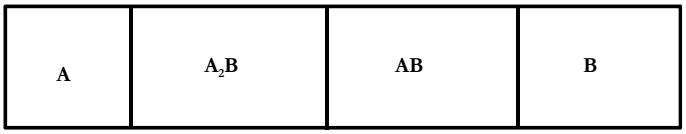

Figure 2.6: Schematic representation of the growth of phases A_2B and AB by solid-state reaction between A and B.

2.6.4 Pd-Si and Pd-C system

In order to obtain a correct ternary phase diagram it is important to start with a good set of data for the binary system. For the Pd-Si-C system only the Pd-Si and the Si-C and Pd-C are considered.

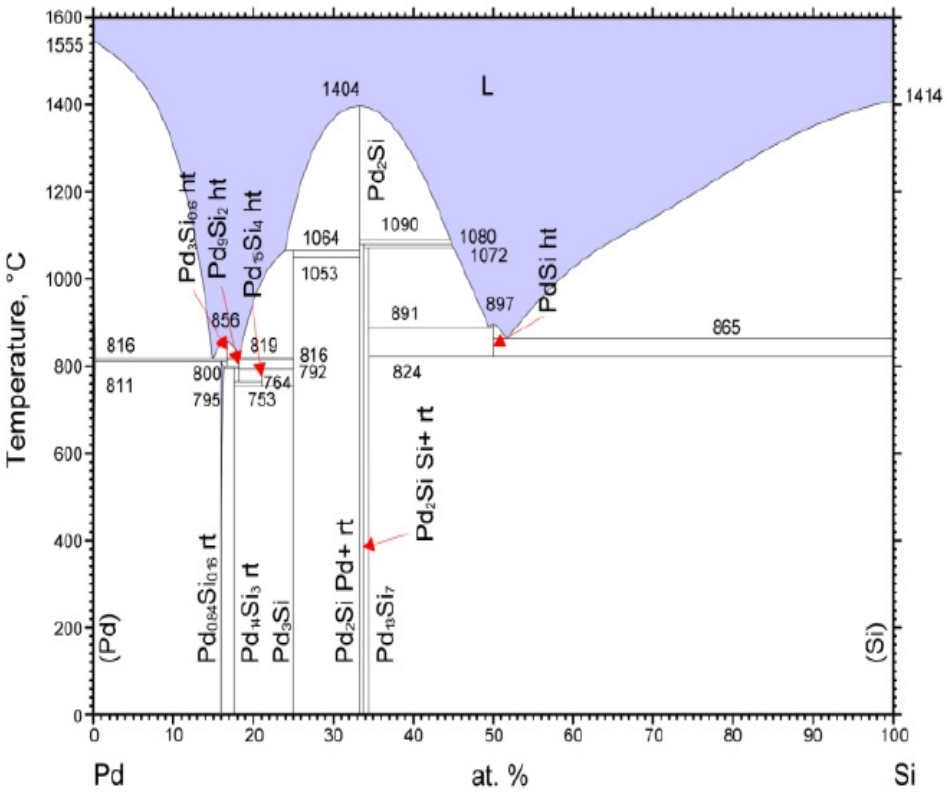

Figure 2.7: Schematic presentation of the Pd-Si phase diagram (Du *et al.*, 2006).

Figure 2.7 shows a calculated Pd-Si phase diagram (Du *et al.*, 2006). In a metal-Si system many compounds exist and in most cases more than one phase is observed. The general behavior is that compounds grow consecutively or sequentially and not simultaneously. Generally, the appearance of a new phase in phase diagrams is accompanied by the reduction of a metal layer or the disappearance of the previous compound (Ottaviani, 1984). In a binary system is found that the near noble metals first form metal-rich silicides and more Si-rich silicides grow before equilibrium is reached. The phase diagram in figure 2.7 shows the existence of several compounds such as Pd_9Si_2, Pd_3Si, Pd_2Si and PdSi. In the phase diagram, the Pd_9Si_2 phase is appearing at the temperature of 800^0C and it decomposes at low temperatures. The Pd_3Si phase is appearing at both low and high temperatures while the PdSi phase is found to be appearing at even higher temperatures but only exists for a short-range of temperatures of 888^0C-908^0C.

Figure 2.8 shows the calculated Pd-C phase diagram (Du *et al.*, 2006). The solubility of carbon in Pd is reported to be vanishingly small. Carbon is found to have a solubility of 0.02% by weight at 1700^oC in Pd (Selman *et al.*, 1970).

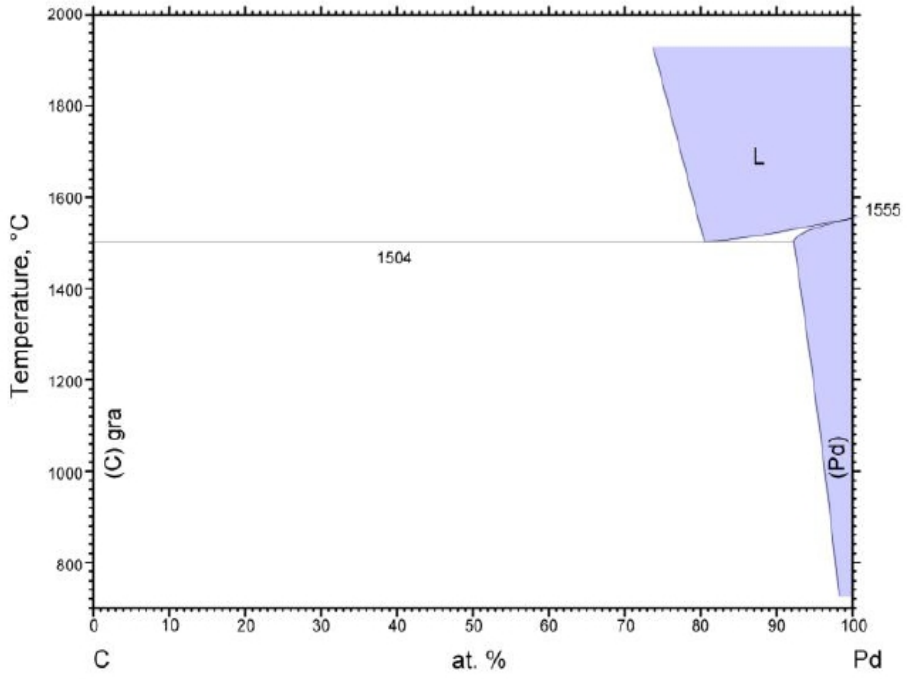

Figure 2.8: Schematic presentation of the Pd-C phase diagram (Du *et al.*, 2006).

2.7 Phase formation in ternary systems

2.7.1 Metal-SiC

The behaviour of the interaction of metal with SiC has been studied in detail by Park *et. al.*, (1999). The reaction product sequence and the interface morphology in metal-SiC reactions was found to mainly depends on the contact material. The metal-SiC reaction modes have been separated into types: type (I) and type (II). Type (I) consists of a system where there is no compound formation in the metal-carbon binary system and a three-phase region (SiC-silicide-C) exists in the isothermal phase diagram. Type (II) consists of a system where atleast one compound exists in the metal-carbon binary system and the existing ternary phases are in equilibrium with the silicide and a carbide. Figure 2.9 shows two schematic representation of a ternary diagrams of the SiC-X(I) and SiC-X(II) system with the diffusion pathway. The X(I) indicates the element in the type (I) reaction system and X(II) indicates the element in the type (II) reaction system.

For the SiC/X(I) interface reaction, the reaction mode includes interdiffusion reaction producing a silicide and a free carbon as shown below

$$\mathrm{Me} + \mathrm{SiC} \longrightarrow \mathrm{Silicide} + \mathrm{C}$$

where Me stands for metal. The formation of silicides in this case is associated with producing a free carbon so that there is mass balance. The diffusion pathway of the type(I) reaction mode is indicated by solid arrows as shown in figure 2.9(a). In the SiC/X(II) interface reaction there is formation of carbides and silicides as reaction products as shown below. The reaction pathway in these reaction type is shown by the solid arrow in figure 2.9(b),

$$\mathrm{Me} + \mathrm{SiC} \longrightarrow \mathrm{Silicides} + \mathrm{Carbides} + \mathrm{Me}_x\mathrm{Si}_y\mathrm{C}_z$$

where Me stands for metal. The ternary diagrams in figure 2.9 shows that the properties of the contact material affects the final diffusion pathway and morphology. Figure 2.10 shows the sequence of phases formed with respect to the contact material.

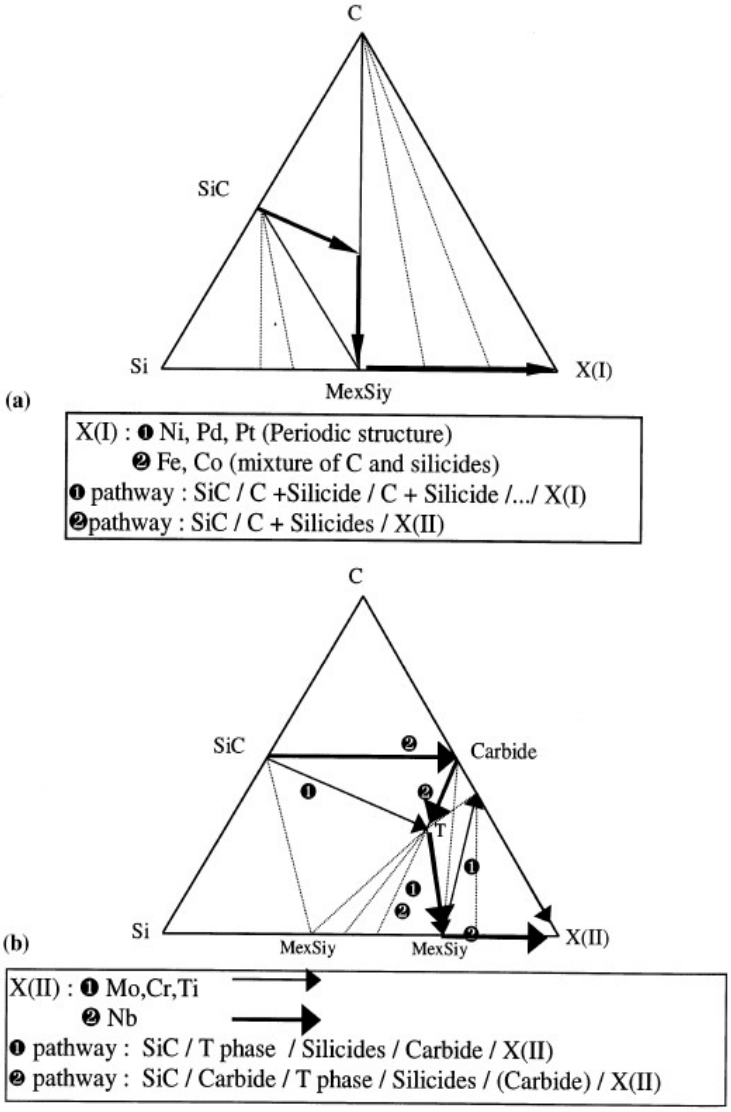

Figure 2.9: Schematic presentation of the ternary phase diagram and the reaction pathway of X(I)/SiC and X(II)/SiC (Park *et al.*,1999).

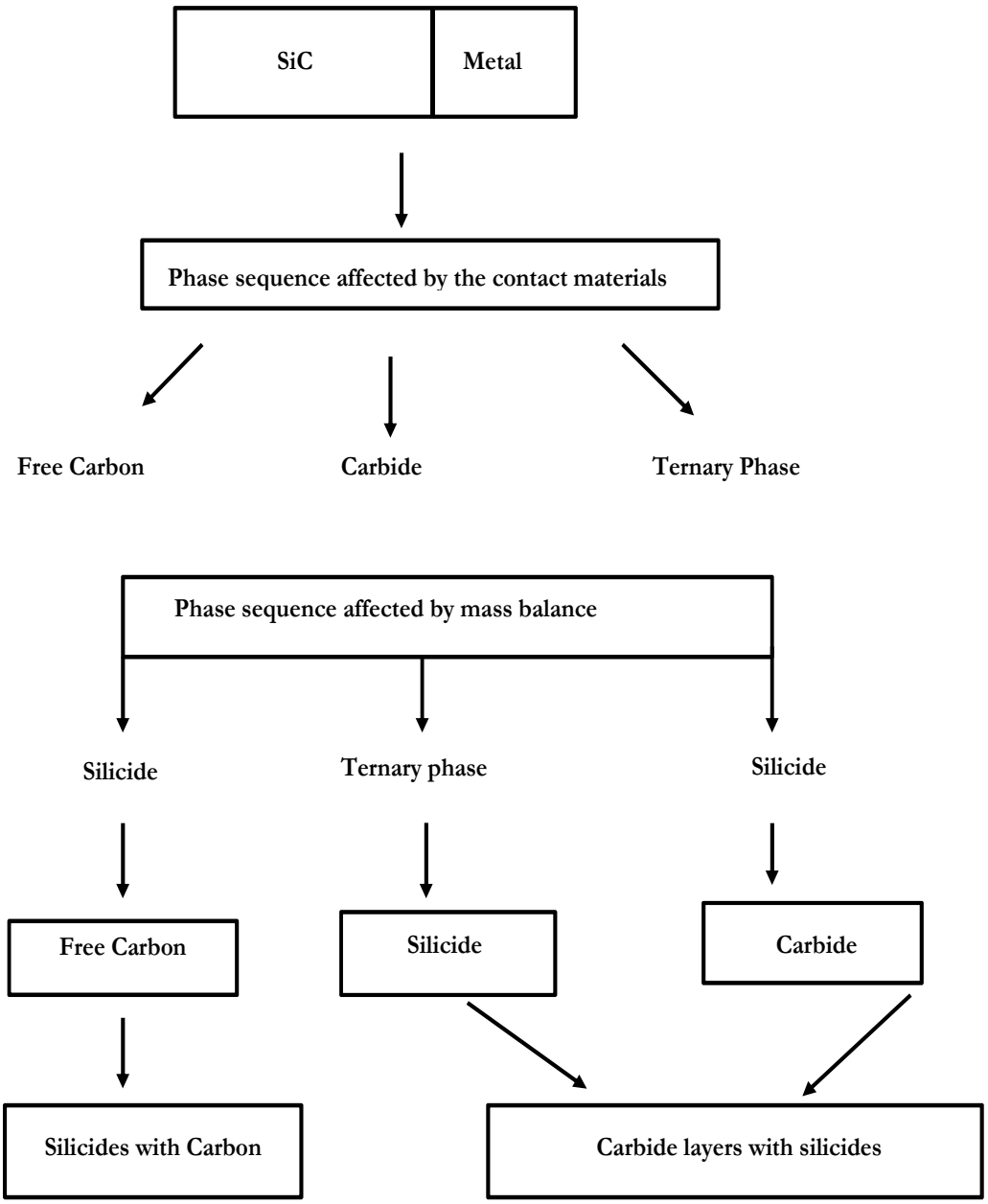

Figure 2.10: A schematic representation showing the sequence of products with respect to the contact material taken from Park *et. al*, (1999).

2.7.2 Concept of diffusion path

It follows from the phase rule that, if two phases are in equilibrium with each other there is no degree of freedom left for the concentration to adapt itself. In the case of the ternary systems it follows from the phase rule that there exists one more degree of freedom. That is, if there are now two phases in equilibrium, there is a one more degree of freedom left for the concentration to adapt freely. This means that in a ternary system two phases can co-exist in equilibrium over a range of composition. This means again that if there is only one reaction product, we obviously have one phase or a single phase reaction zone. If there are more reaction products we can then have multi-phase diffusion or a two phase reaction zone.

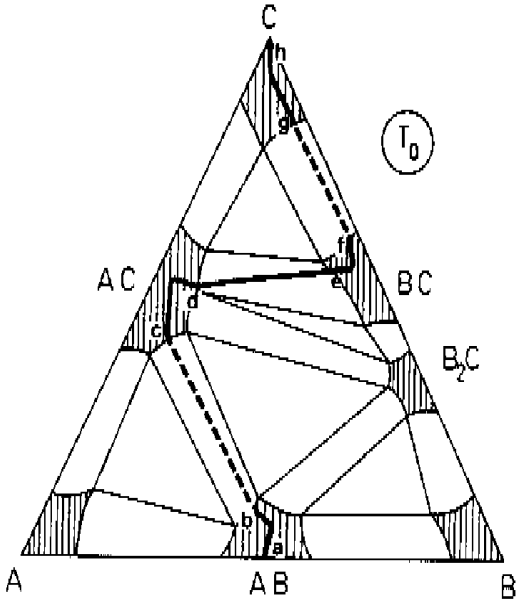

Figure 2.11: An isothermal ternary system A-B-C with a plotted diffusion path of the diffusion couple in figure 2.12 (Osinski, 1983).

Considering a hypothetical A-B-C isothermal section of a ternary phase diagram at a certain temperature T_0 shown in figure 2.11. Two phases AC and BC have developed and are separated by a non-planar (wavy) interface and the phases are in local equilibrium with each other. The concentration profile in this system is measured parallel to the diffusion direction and the concentration is measured on a line perpendicular with the diffusion direction as shown in the corresponding diffusion couple in figure 2.12. The measured concentration are then plotted with dotted lines on the ternary phase diagram as shown in figure 2.11. The plotted points are the so-called diffusion path. Therefore the diffusion path shows a plot of a ternary phase diagram presenting the average composition along the diffusion couple.

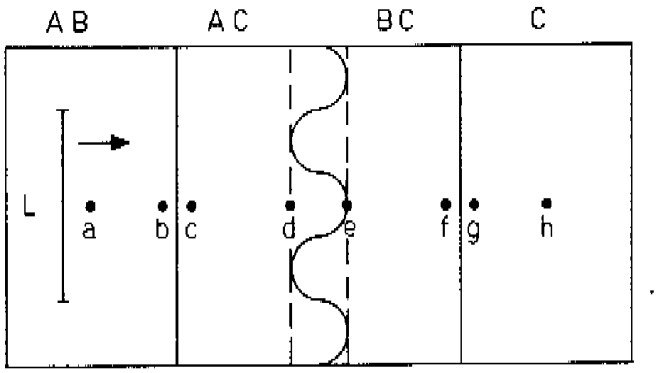

Figure 2.12: Layer sequence in the hypothetical ternary diffusion couple A-B-C (Osinski, 1983).

2.7.3 Reaction layer morphologies

The diffusion path explained in the previous section represents the specific arrangement of phases in a diffusion couple under conditions where each phase is in equilibrium with its neighbouring phase. If A in figure 2.11 is in contact with B, the intermediate phase AB will form in the following sequence A—AB—B. For this interaction, this is the only diffusion path that can take place. Now if A is in contact with BC, there are more than one possibility of diffusion paths. The most likely diffusion paths will be BC—AC—AB—A and BC—AB—AC—A. If the component C is immobile, as it has been found in most ternary systems (Bhanumurthy and Schmid-Fetzer, 2001), the conditions which favour the formation of layered structures and aggregate structures are presented below.

Chang and Kao (1994), studied the application of the thermodynamic conditions in the Si-Me-C system governing the formation of structural composites via solid-state displacement reaction. Their study explained that, for a layered arrangement of BC—AC—AB—A shown in figure 2.13, where A diffuses through the layer AB and AC to react with BC at the BC/AC interface to form AC. The reaction at this interface is given by

$$A + BC \longrightarrow AC + B$$

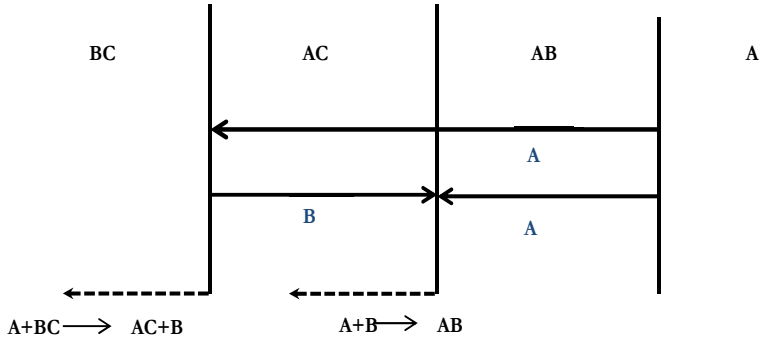

Figure 2.13: Ternary BC/A diffusion couple. Take from Chang and Kao, (1994).

The growth front of the layer AC was found to be towards left, since A reacts with BC to form AC. The element B formed in this reaction then diffuses through AC to react with A, which diffuses through AB to form AB at the AC/AB interface according to the following reaction:

$$A + B \longrightarrow AB$$

The growth front of the layer AB was also found to be towards the left since it grows at the AC/AB interface.

This study also found that for the interface BC/AC, where the rate-limiting step for the reaction at this interface is the rate at which A atoms reach the interface. As shown in figure 2.14. A diffuses to point 2 faster than point 1, therefore the growth front at point 2 grows faster than at point 1. This results in the planar interface between BC and AC being stable. Also if A arrives at point 4 much sooner than at point 5 the AC/AB interface will be stabilized. Since both the interfaces are stabilized a layered structure will be developed.

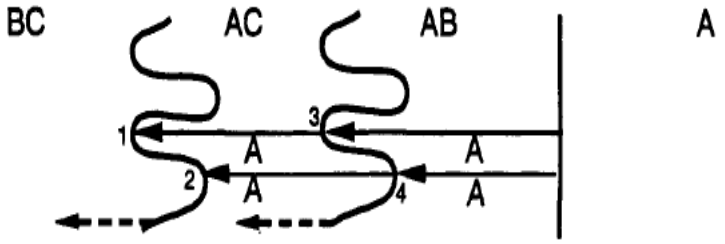

Figure 2.14: Interfacial stability of BC/AC and AC/AB in the ternary diffusion couple. Take from Chang and Kao, (1994).

If the diffusion of B through AC is now slower than than that of A through AB, B becomes the rate-limiting step through AC. Figure 2.15 shows that B reaches point 7 sooner than point 8, therefore the interface at point 7 will grow faster than at point 8 creating the instability at the AC/AB interface resulting in the formation of an aggregate structure.

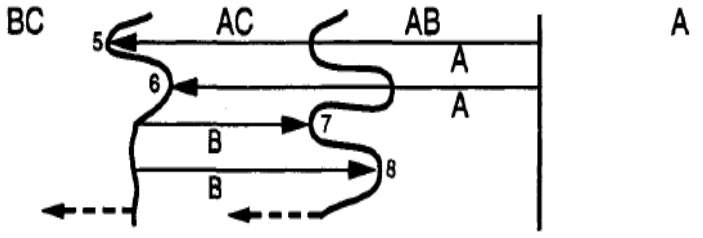

Figure 2.15: Interfacial stability of BC/AC and AC/AB in the ternary diffusion couple. Taken from Chang and Kao, (1994).

There are three common elementary morphologies that take place in ternary diffusion couples: layered structures as shown in figure 2.14, aggregate structures as shown in figure 2.15 and periodic

layered structures which is characterized by regular repetition of bands of precipitates of the reaction products. The periodic layer reaction morphology is considered in the following section. Figure 2.16 to 2.18 shows a schematic overview of elementary morphologies in ternary solid state diffusion couple (Rijnders, 1966).

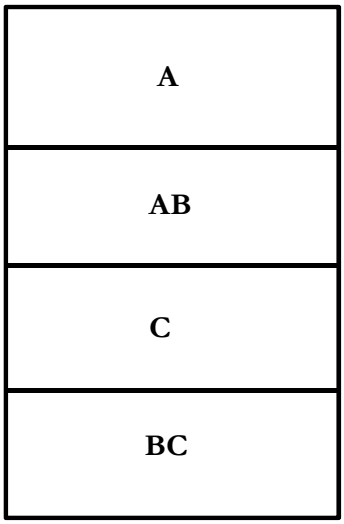

Figure 2.16: Reaction layer morphology in ternary solid-state diffusion couple forming simple layered structures.

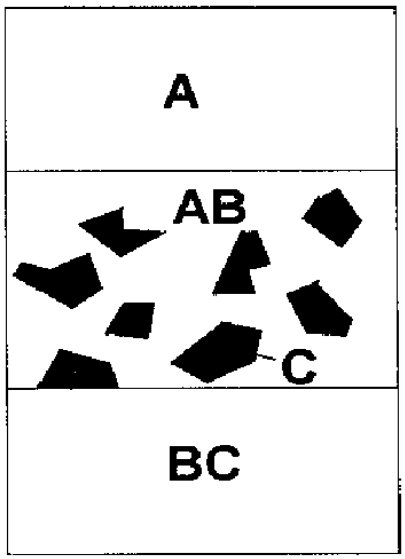

Figure 2.17: Reaction layer morphology in ternary solid-state diffusion couple forming aggregate structures. Taken from Rijnders, (1991).

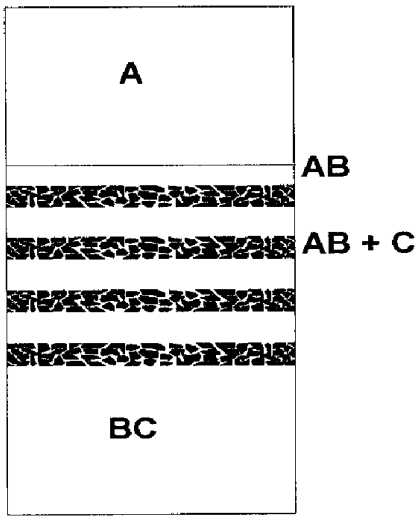

Figure 2.18: Reaction layer morphology in ternary solid-state diffusion couple forming periodic layered structures. Taken from Rijnders, (1991).

2.8 Solid-state reaction of SiC with non-carbide forming metals.

In a binary diffusion couple the phase sequence is completely determined by thermodynamics after long annealing time and the concentration profile is a reflection of the phase diagram. In these couples only single phase regions can exists because of the phase rule. However for metal-SiC systems the situation is different because they contain more than two components, therefore it follows that two-phase regions are possible. In a ternary couple many possible concentration profiles can occur and therefore prediction of the phase sequence is very difficult or even impossible. For the proper prediction one needs the values of all the ternary diffusion coefficient in the different phases together with the exact phase relations.

Metals which do not form carbides (Fe, Pt, Co, Ni and Pd) react with SiC to form silicides and leave carbon (immobile) as a side product. This will result in a multiphase reaction layer containing layers of silicides mixed with the immobile carbon. The morphology of the reaction layer varies from isolated precipitates of carbon to distinct periodic structure. The periodic layered structures observed in diffusion couples are much more similar to the Liesegang bands (Kao and Chang, 1993). However, the Liesegang phenomena has not been observed in the solid-solid system and only two components are involved in the formation of the formation of the Liesegang bands while three components precipitate in the reaction for the formation of the periodic layered structures.

2.8.1 Pt-Si-C

In the study of the reaction of Pt a non-carbide forming metal with SiC, where Pt is non-carbide forming metal van Loo and Kodenstov, (1998) reported the interaction between SiC and Pt over a temperature range of $973 - 1023$K.

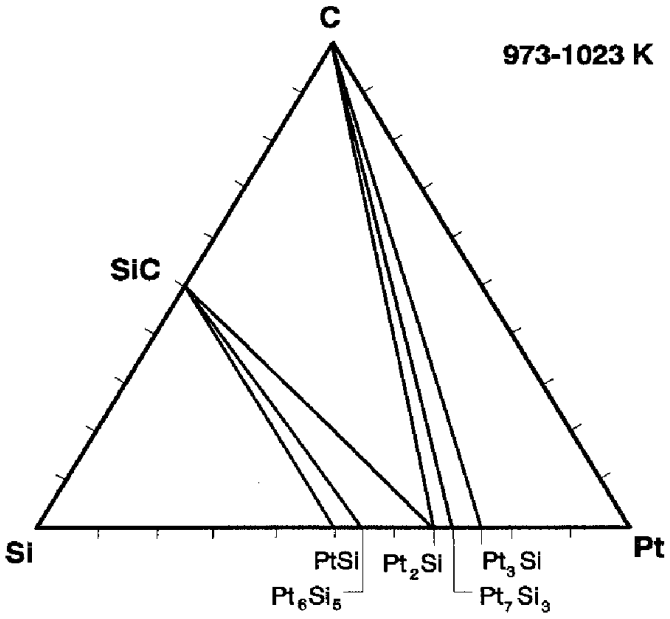

Figure 2.19: Isothermal Pt-Si-C phase diagram, (van Loo and Kodenstov, 1998).

It is possible to predict the phase sequence in the reaction zone using just the isotherm of the Pt-Si-C phase diagram shown in figure 2.19. In this study van Loo and Kodenstov, (1998), explained that "the thermodynamic activity of the carbon is one and in the SiC it is lower than one. Therefore it is impossible for the carbon formed by the interfacial reaction to diffuse through the reaction zone towards a graphite phase at the metal side, because it would then have to diffuse against the gradient of its chemical potential". This then results in the carbon being immobile in the system.

Figure 2.20 shows the reaction zone of the Pt/HIP-SiC interface annealed at 1023K for 36 h. The resulting products were found to be Pt_2Si, Pt_3Si and Pt_7Si_3 with carbon. The formation of the periodic layered bands are clearly visible in the reaction zone morphology. These included the bands of carbon embedded in the Pt_7Si_3 phase. A two-phase carbon-containing zone (Pt_2Si + C) is also observed next to the SiC. A Pt_3Si phase which does not contain any carbon is also observed.

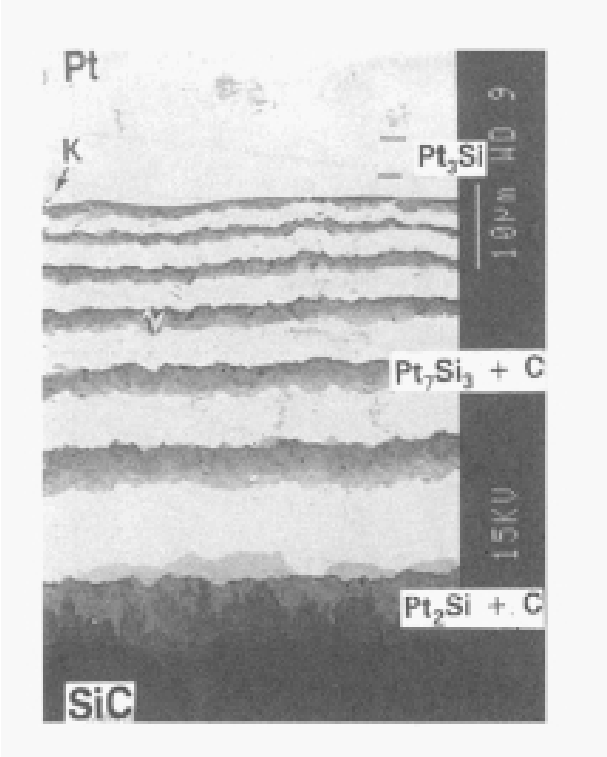

Figure 2.20: Morphology of the reaction zone in the Pt/HIPSiC diffusion couple (van Loo and Kodenstov, 1998).

2.8.2 Ni-Si-C system

Figure 2.21 shows the backscattering secondary electron (BSE) image of an Ni/SiC reaction couple annealed at 900^0C for 40h. Ni is a non-carbide metal, therefore only binary phases between Ni and Si are expected to form and the carbon remains immobile in the system. The reaction products are observed in both sides of the initial interface. The Ni diffuses into the SiC and the SiC decomposes to react with Ni to form silicides and free carbon. The Ni_2Si phase with graphite is found to form close to the SiC followed by the formation of the Ni_5Si_2 with graphite which is close to the Ni_3Si layer. The observed product sequence is Ni / Ni_3Si / Ni_5Si_2 + C / Ni_2Si + C / SiC.

Bhanumurthy and Schmid-Fetzer, (2001) also studied the Ni/SiC diffusion couple after annealing at a temperature of 900^0C for 24 h and based on their investigations the diffusion paths were plotted for 6H-SiC/Ni isothermal sections of NiSiC at 850^0C as shown in figure 2.22.

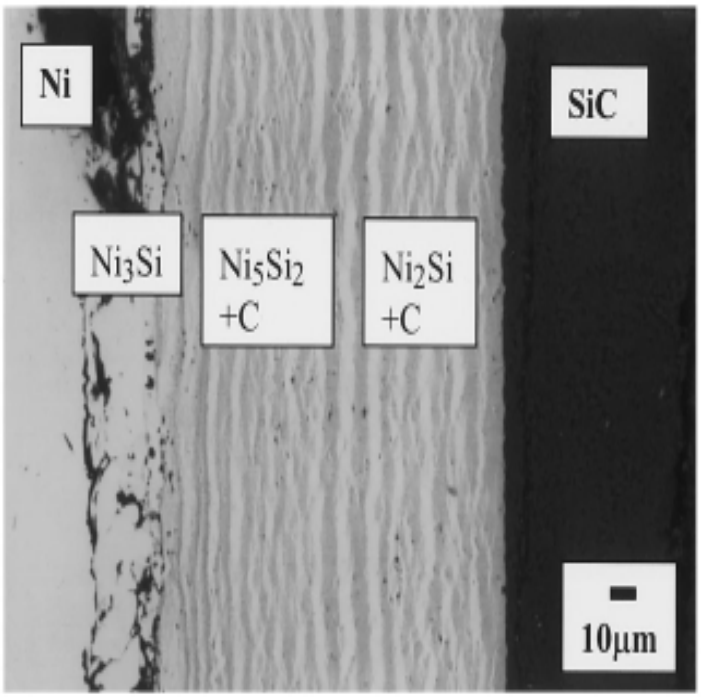

Figure 2.21: BSE image of the Ni/SiC diffusion couple annealed at 900^0C for 40 hours (Park et al., 1999).

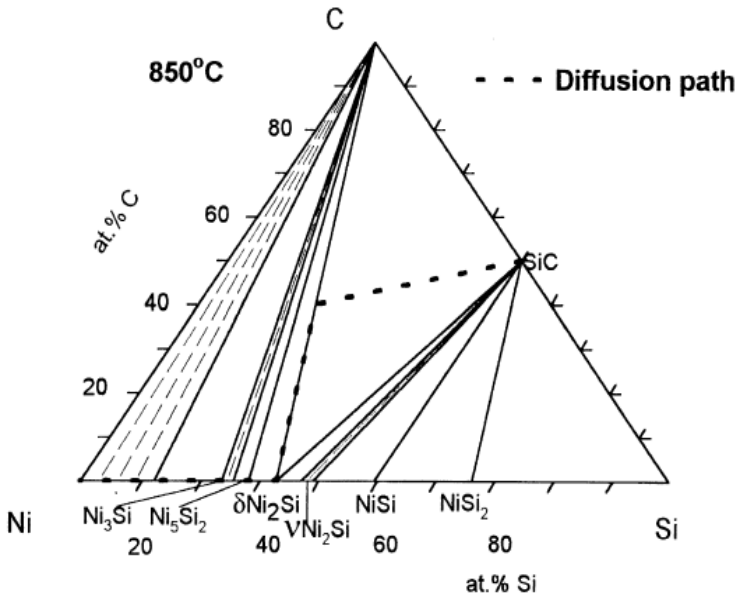

Figure 2.22: Schematic presentation of the Ni-Si-C isothermal section at 850^0C. The dotted line represents the diffusion path determined by the diffusion couple (Bhanumurthy and Schmid-Fetzer, 2001).

2.8.3 Pd-Si-C system

The Pd-Si-C system is relatively simple since Pd is not a carbide forming metal and there are no ternary phases expected to form. Figure 2.23 shows the ternary phase diagram of the Pd-Si-C determined by Bhanumurthy and Schmid-Fetzer at a temperature of 800^0C. In this diagram several phases which are also observed in the Pd-Si binary phase diagram are also observed in this system. The observed phases are Pd_9Si_2, Pd_3Si and Pd_2Si. The PdSi phase which is observed at higher temperatures in the binary system is also not observed at 800^0C is not observed in the ternary system.

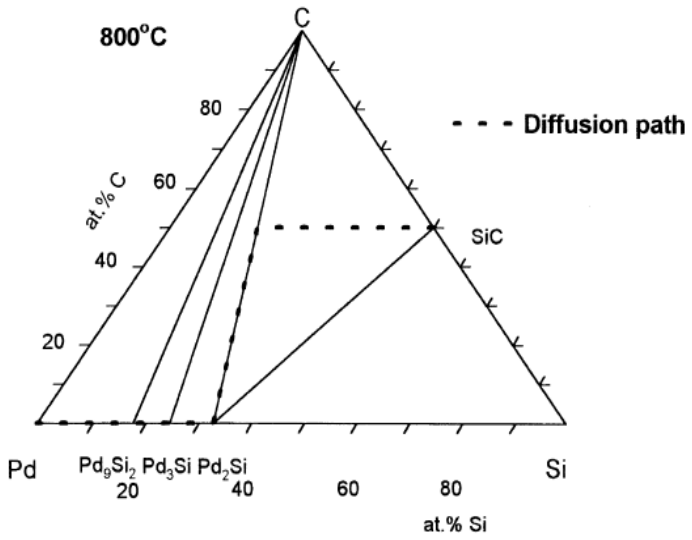

Figure 2.23: Pd-Si-C isothermal section (800^0C) with dotted lines representing the diffusion path determined by the diffusion couple (Bhanumurthy and Schmid-Fetzer, 2001).

The formation of the periodic layered structures was also observed in the 6H-SiC/Pd/HIP-SiC system. In this system the Pd reacted with Si to form silicides and a free carbon. The phases Pd_2Si close to the Pd_3Si without the graphite and the formation of the Pd_2Si with the graphite in the dark band close to SiC was observed. The sequence of the phase formation is represented by the diffusion path shown in figure 2.23 determined by the diffusion couple.

Reference

Bené R.W., 1982, Appl. Phys. Lett. **41**, 528.

Bhanumurthy K., Schmid-Fetzer R., 2001, Compos. Part A-Appl. Sci. **32**, 569.

Chang Y.A and Kao C.R., 1994, Pure Appl. Chem., **66(9)**, 1797.

Crank, J, 1975, The mathematics of diffusion, 2nd Ed., Clarendon Press, Oxford, pg 2.

Du Z., Guo C., Yang X., Lui T., 2006, Intermetallics **14**, 560.

d'Heurle F.M and Gas P., 1986, J. Mater. Res. **1(1)**, 205.

Dybkov V.I, 1992, J. Phys. Chem. Solids **53**, 703.

Gas P., d'Heurle F.M., LeGaues F.K., Laplace S.J., 1986, J. Appl. Phys. **59**, 3458.

Gas P. and d'Heurle F.M., 1993, Appl. Surf. Sci. **73**, 153.

Gülpén J.H., 1995, "Reactive phase formation in the Ni-Si system", Eindhoven University of Technology, Eindhoven, Netherlands.

Devendra G., 2005, Diffusion processes in advanced technological materials, William Andrew publishers, Norwhich, NY, USA.

Jan C.H., Chen C.P., Chang Y.A, 1993, J. Appl. Phys. **73**, 1168.

Kao C.R., Chang Y.A., 1993, Acta Metall. Mater., **42(12)**, 3463.

Kubaschewski O and Alock C.B., 1979, "Metallurgical Thermochemistry", 5th Ed., Pergamon Press, Oxford pg 1.

Laurila T and Molarius J., 2003, Critical Reviews in Solid state and material science **28(3)**, 185.

Osinski K., 1983, "The influence of Aluminium and Silicon on the reaction between Iron and Zinc", PhD thesis, Eindhoven University of Technology, Eindhoven, Netherlands.

Ottaviani G., 1984, Thin-films and interfaces II, Material Research society Vol. 25 Elsevier Science Publishing Co., Inc, pg 21-33

Park J.S., Landry K., Perepezko J.H, 1999, Mat. Sci. Eng., **A259**, 279.

Poate J.M, Tu K.N, Mayer J.W, 1978, "Thin film-interdiffussion and reactions", John Wiley & Son, pg 358.

Ronay M., 1983, Appl. Phys. Lett. **42**, 577.

Pretorius R., 1993, Mat. Sci. Eng. R. **10**, pg 8.

Rijnders M.R, 1996, "Periodic layer formation during solid state reactions", Eindhoven University of Technology, Eindhoven, Netherlands.

Selman G.L., Ellison P.J. and Darling A.S., 1970, Platinum Met. Rev., **14**(1), 14.

Shewmon P., 1989, "Diffusion in solids", The mineral, metals and material society, USA, pg 57.

Theron C.C, 1997, "In-situ, real time characterization of solid-state reaction in thin-films", PhD thesis, University of Stellenbosch, South Africa.

van Loo F.J.J, 1971, "Diffusion in the Titanium-Aluminium system", Eindhoven University of Technology, Eindhoven, Netherlands.

van Loo F.J.J and Kodenstov A.A., 1998, Pure and Appl. Chem., **70(2)**, 501.

Wakelkamp W.J.J., 1991, "Diffusion and phase relations in the systems Ti-Si-C and Ti-Si-N", Eindhoven University of Technology, Eindhoven, Netherlands.

Walser R.M, Bené R.W, 1976, Appl. Phys. Lett. **28**, 624

Chapter 3

Experimental

Experimental Techniques

The solid-state interaction of Pd on single crystalline SiC is investigated using the following techniques: Rutherford Backscattering Spectrometry (RBS), Time of flight Energy recoil detector (ERDA), Glancing incident X-ray diffraction (GIXRD) and scanning electron spectroscopy (SEM). This chapter presents all the experimental work performed in preparing and analyzing the samples.

3.1 Sample Preparation

The starting material for this study were a single crystal 6H-SiC with a diameter of 50.8mm and a thickness of $368 \pm 25\mu$m produced by Cree Inc®. Prior to deposition the samples were cut into 5×1 mm^2 using a diamond scriber before any wet chemical treatment. In order to remove any natural contamination and oxides on the layer of the surface the following cleaning procedure was adhered to: the samples were cleaned ultrasonically by using trichloroethylene (10min), acetone (10 min), methanol (10 min) followed by a dip in 10% diluted hydroflouric acid (10 min) succesively. The degreased samples were then rinsed with de-ionised water after each cleaning step and blown dry by using nitrogen (N_2) gas before deposition.

3.1.1 Film deposition

For Pd deposition the degreased samples were mounted onto a steel sample holder which can hold up to eight samples at a time, and were transfered into the vacuum chamber. In order to obtain the desired pressure for deposition the turbo and the backing pump were used to reduce the pressure inside the vacuum chamber. The deposition was performed in a high vacuum system with a base pressure of 1.8^{-7} mbar and 9×10^{-6}mbar during evapouration. The Pd thin-film with a thickness of $500\mathring{A}$ measured by the crystal monitor was deposited on the degreased 6H-SiC samples mounted on the steel sample holder by using the resistive evapouration technique.

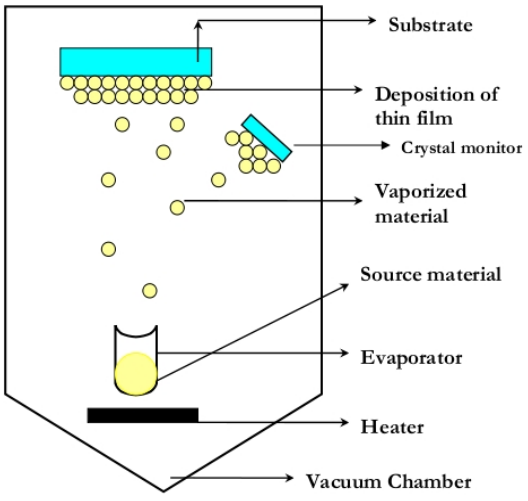

Figure 3.1: A schematic representation of the physical vapour deposition systems, showing the deposition that is taking place in the vacuum chamber.

A PENNINGVAC PAM 410 was used to supply the amount of current needed to thermally heat the crucible and melt Pd solid source material which was contained in a tungsten crucible

coated with Al_2O_3. During deposition, a high current of 25 A was supplied to the crucible, until the Pd heated beyond its melting point, thereby causing the Pd to evaporate. The evaporated atoms from the solid material traveled through the reduced background pressure in the vacuum chamber and condensed on all the cooled surfaces in the vacuum chamber including the SiC substrate. The rate of deposition was kept between 0.2 and 0.4$\mathring{A}$/s. Figure 3.1 shows the deposition process taking place in the vacuum chamber, the deposition of the Pd only takes place in the side that is facing the crucible as depicted in the figure 3.1.

3.1.2 Annealing systems

Some of the as-deposited samples, were heat treated in order to investigate the Pd/SiC after thermal annealing. These samples were annealed at different temperatures for each different as-deposited sample for a period of 1 hour. The annealing temperatures chosen for this study ranged between 200^0 to 800^0C. For the study of the reaction between Pd and SiC, the samples were annealed in the vacuum controlled tube oven which can attain a maximum temperature of 1200^0C. The oven temperature is regulated by the thermocouple and the maximum temperature of the oven is reached in the center of the oven and it decreases towards the edges of the oven. The quartz tube in this type of annealing system is attached to the turbo pump which is used to achieve the desired pressure. For each annealing step at a specific temperature, the samples were mounted onto a sample boat centered inside the quartz tube.

Prior to annealing the tube was evacuated to a pressure below 10^{-6} mbar and the temperature of the oven was preset at the desired temperature value and was allowed to stabilize before being moved over the stationary tube containing the sample. During annealing the temperature of the sample was measured using the thermocouple situated near the sample. After annealing for a period of 1 hour the oven was moved away from the sample position and the annealed samples were allowed to cool down to room temperature before being taken out. The as-deposited sample together with all the annealed samples were then examined by RBS, GIXRD and SEM.

Analytical Techniques

3.2 Rutherford Backscattering Spectrometry (RBS)

The RBS technique originates from the field of low energy nuclear physics. The main component of RBS, is the principle of surface analysis, which gives quantitative information on chemical composition, depth distribution and crystal quality. This can be done by measuring the backscattering of the beam of high energy ions impinging on the sample (Feldman *et al.,* 1982).

RBS is a very simple experimental procedure based on the principle that, when light ions for example, He^+ or H^+ in the MeV range are incident on a target material, they will undergo collisions with the electrons and the nuclei of the atoms of the target material. The majority of the ions will come to rest in the solid while a small percentage of ions which come close to the nucleus are scattered back at angles larger than 90^0 relative to the direction of incidence. These backscattered particles can then be detected at a set angle. By measuring the energy of these backscattered incidented ions it is possible to obtain the information about the nature and the concentration of the target atoms and their depth distribution.

3.2.1 The Kinematic factor

The energy of the backscattered particle is determined or depends on its own mass m, the mass of the target M and the scattering angle θ. Figure 3.2 shows a geometry representation of a two-body elastic collision system between the projectile atom and the target atom with a scattering angle θ of 165^0 which is defined as the angle between the projectile incident direction and the scatter angle. The incoming projectile atom with mass m and an energy of E_0 collides with the target atom of mass M and becomes backscattered at an angle of 165^0 with an energy of E_1, which is then detected by the detector.

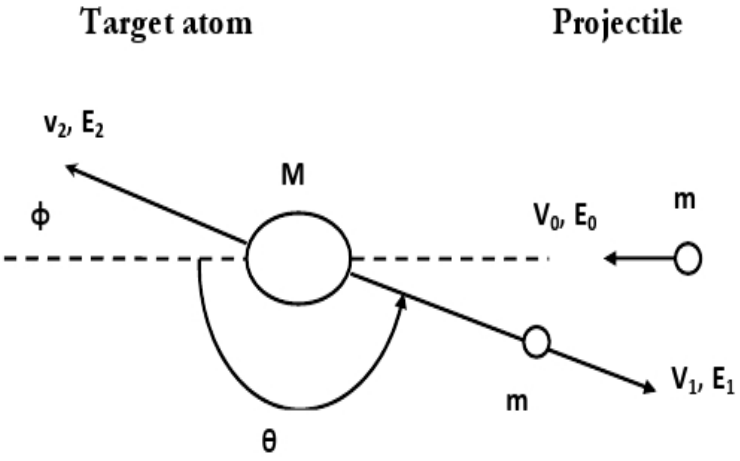

Figure 3.2: Schematic presentation of a two-body collision system between projectile and the target.

From figure 3.2 the particles which are backscattered relative to the surface of the target atom have an energy given by the following kinetic equation (Poate *et. al*, 1978),

$$K = \frac{E_1}{E_0} \tag{3.1}$$

where K is defined as the kinematic factor, E_0 and E_1 are the projectile energies before and after the collision respectively. The kinematics of the simple elastic collision can be solved by applying the principle of conservation of energy and momentum. The solution when $m < M$ is given by

$$K = \frac{E_1}{E_0} = \left[\frac{mcos\theta + \sqrt{M^2 - m^2 sin^2\theta}}{m + M}\right]^2 \tag{3.2}$$

The kinematic factor K, is only depended on the masses and on the scattering angle. Knowing the energy of the incident beam and the energy of the backscattered ions, the mass of the target atom can be calculated. Thus the kinematic factor is suitable for mass analysis.

The signal originating from the surface of each element in an RBS spectrum is defined by the kinematic factor (K) of the element and the α-particle energy. In a spectrum the backscattering particle will have the highest possible energy provided that the backscattering event occurs at the surface and that the high energy edge is given by $K_x E_0$, where E_0 is the incident energy of the projectile and K_x is the corresponding kinematic factor. The kinematic factor of an element gives the position of the edge of each element. It also determines the position in which the element will appear in an RBS spectrum. Thus, the element with the larger kinematic factor will appear at the highest energy in the RBS spectrum and the element with the lowest kinematic factor will appear at the lowest energy in the RBS spectrum.

3.2.2 Depth Profiling

When a projectile ion hits and penetrates a target, it loses progressively its kinetic energy through out its path by interacting with the electrons of the target atom through the processes of ionization, excitation and also by nuclear collisions. The backscattered projectiles will have different energies due to the fact that they are backscattered at different depth. The ability to resolve the energy differences between particles backscattered at different depths within the target material is one of the key aspects of RBS. In the case where the scattering of the projectiles is below the surface of the target material, the energy E_0 of the incident projectile is greater than the energy E found immediately before scattering. After scattering, the projectiles continues to lose energy on its outward path, emerging from the target atom with an energy of E_1 . This energy E_1 is then used to related the depth at which the particle scattering event occurred. Figure 3.3 shows the geometry of the scattering of the projectile with an initial incident energy of E_0.

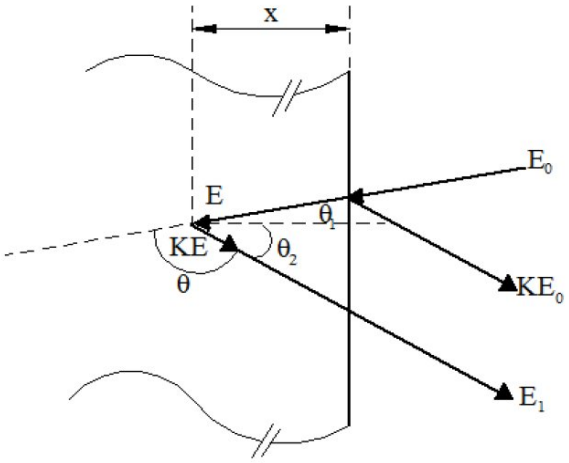

Figure 3.3: Schematic presentation of the energy loss of a projectile from depth x (Chu *et al.*, 1987).

In order to calculate the energy of the projectiles that backscatters at depth x, it is essential to consider the fact that the projectile loses its energy on its way into the target material and on its way out. From figure 3.3 the energy E immediately before scattering can be related to the incident path length $x/\cos\theta_1$ of the incident path can be related by

$$\frac{x}{\cos\theta_1}\alpha - \int_{E_0}^{E} dE/(dE/dx) \tag{3.3}$$

and the the outward path length $x/\cos\theta_2$ is related to the kinetic energy and E_0 by

$$\frac{x}{\cos\theta_2}\alpha - \int_{KE}^{E_1} dE/(dE/dx) \tag{3.4}$$

where θ_1 and θ_2 from equation 3.3 and 3.4 are the angle between the sample normal and the direction of the incidented beam. If one assumes that the value of dE/dx along the inward and the outward path is constant, equation 3.3 and 3.4 reduce to

$$E = E_0 - \frac{x}{\cos\theta_1}\frac{dE}{dx}\bigg|_{in} \tag{3.5}$$

and

$$E_1 = KE - \frac{x}{\cos\theta_2}\frac{dE}{dx}\bigg|_{out} \tag{3.6}$$

where the subscripts *in* and *out* refer to the constant values of dE/dx along the inward and the outward path respectively(Chu *et al.*, 1978).

From figure 3.3 the energy KE_0 is the energy that corresponds to the energy of the particles backscattered from the atoms at the surface of the target, while E_1 is the energy measured value of the particles scattered from an atom at depth x. Thus the energy difference between E_1 and KE_0 is given by

$$\triangle E = KE_0 - E_1 = [S]x \tag{3.7}$$

where the backscattering energy loss factor $[S]$, relates the depth x to the energy difference $\triangle E$. The energy loss factor $[S]$ is defined as

$$[S] = \left[\frac{K}{\cos\theta_1}\frac{dE}{dx}\bigg|_{in} + \frac{1}{\cos\theta_2}\frac{dE}{dx}\bigg|_{out}\right] \tag{3.8}$$

The energy difference equation can be given in-terms of the stopping cross-section rather than dE/dx (Chu et al., 1978)

$$\triangle E = [\epsilon]Nx \tag{3.9}$$

where N is the density of atoms and $[\epsilon]$ is the stopping cross section factor given by

$$[\epsilon] = \left[\frac{K}{\cos\theta_1}\epsilon_{in} + \frac{1}{\cos\theta_2}\epsilon_{out}\right] \tag{3.10}$$

The stopping cross-section ϵ_{in} and ϵ_{out} are evaluated at energies E_0 and KE_0 (Chu *et al.*, 1978). The stopping cross-section $[\epsilon]$ or the backscattered energy loss factor $[S]$ can be used to determine the depth scale of the backscattering energy spectrum. Therefore, the energy spectrum can be converted directly into depth scale by determining the depth per channel of the spectrum.

For a compound target such as SiC the loss of energy must be obtained from the stopping power of the projectile in the compound target. That is, the projectile will penetrate the target and will lose energy as a result of interacting with more than one element and the stopping cross-section will depend on the sample composition. In order to calculate the energy E_1 of the detected backscattering ions to the depth x, Bragg's rule on the additivity of stopping cross-sections of the elements making up the target is used (Chu *et al.*, 1978). If the compound is defined as A_mB_n, with E_{1A} and E_{1B} denoting the energy loss of the particles backscattered from element A and element B at depth x. The energy loss of the particle backscattered from element A at depth x is given by:

$$\triangle E_A = [\epsilon]_A^{AB} N^{AB} x = \left[\frac{K_A}{\cos\theta_1}\epsilon_{in,A}^{AB} + \frac{1}{\cos\theta_2}\epsilon_{out,A}^{AB}\right] N^{AB} x \tag{3.11}$$

similarly for element B in the compound

$$\triangle E_B = [\epsilon]_B^{AB} N^{AB} x = \left[\frac{K_B}{\cos\theta_1}\epsilon_{in,B}^{AB} + \frac{1}{\cos\theta_2}\epsilon_{out,B}^{AB}\right] N^{AB} x \tag{3.12}$$

where K_A and K_B are the kinematic factors of the element A and element B in the compound and $[\epsilon]_A^{A_mB_n}$ and $[\epsilon]_B^{A_mB_n}$ are the stopping cross-section of the elements in the compound. The values of $[\epsilon]^{A_mB_n}$ are determined by assuming a linear additivity of the elemental cross-section making up the target used. This is known as Bragg's rule (Grob and Siffert, 1984)

$$[\epsilon]^{A_nB_m} = m[\epsilon]^A + n[\epsilon]^B \tag{3.13}$$

where ϵ^A and ϵ^B are the stopping cross-sections of the target atoms A and B. Therefore the total energy loss in the compound will be given as

$$\triangle E = \left[\frac{m}{m+n}[\epsilon]_A^{AB} N_A^{AB} x\right] + \left[\frac{n}{m+n}[\epsilon]_B^{AB} N_A^{AB} x\right] \tag{3.14}$$

3.2.3 Differential Cross Section

The scattering cross-section σ is the likelihood that a collision in a two-body system will occur. It determines the probability that a given collision between the projectile and the target will result in a scattering event. It can also be used to estimate how frequently a collision occurs and ultimately the scattering yield at a certain angle.

The force between the projectile ion and the target atom can be described by the Coulomb repulsion of the two nuclei provided that the distance of closest approach between the projectile ion and the target atom is large compared to the nuclear dimensions, but small enough when compared to the Bohr radius (0.53 $\AA$). If these conditions are satisfied the differential cross-section shown in equation 3.13 can be used (Chu *et al.,* 1978).

$$\frac{d\sigma}{d\Omega} = \left(\frac{zZe^2}{4E_0}\right)^2 \frac{4\left[\sqrt{M^2 - m^2\sin^2\theta} + M\cos\theta\right]^2}{M\sin^4\theta\sqrt{M^2 - m^2\sin^2\theta}} \tag{3.15}$$

where z, m and Z, M are the atomic numbers and mass numbers of the projectile and the target atom respectively, E_0 is the energy of the projectile before scattering and Ω is the finite solid angle subtended by the detector.

Since the differential cross section is directly proportional to the Z^2 and inversely proportional to E_0, it indicates that the sensitivity of the RBS is high for heavy target atoms at small scattering angels which makes it suitable for quantitative analysis (Mayer and Nicolet, 1978). This equation is directly related to the scattering probability and it connects the backscattering yield to the quantitative analysis, which means that one could expert more backscattering yield if working with lower energies than higher energies.

Thus from equation 3.13 the Rutherford backscattering probability depends on the following (Grob and Siffert, 1984)

- The atomic number of the projectile z. $d\sigma/d\Omega \propto z^2$ that is the yield increases quickly with the atomic number.
- The atomic number of the target atom Z^2. $d\sigma/d\Omega \propto Z^2$ since RBS is more sensitive to heavy elements
- The incident angle θ, that is, the yield increase quickly when the angle θ is reduced.
- The inverse proportionality of $d\sigma/d\Omega \propto E^{-2}$ shows that the backscattered yield decreases rapidly with higher energies.

For a target of a thin-film with a thickness of x, the scattering yield Y detected at the solid angle $\triangle\Omega$ at a particular scattering angle θ is given by

$$Y(\theta) = (N.x) \times \frac{d\sigma}{d\Omega} \times \frac{\triangle\Omega Q}{cos\alpha} \tag{3.16}$$

where N is the atomic density of the target, Q is the number of incident ions which can be obtained by time integration of the current of charged particles incidented on the target and α is the incident angle (Feldman *et al.*, 1982).

3.2.4 Energy Straggling

One of the important concepts in RBS is the energy straggling. This concept arises from the fact that identical energetic particles with the same initial velocity do not have exactly the same

energy after passing through a target medium. That is the spread of the energy of the ion after penetrating a target with a thickness $\triangle x$ is subject to statistical fluctuations in the number of collision it encounters.

This phenomenon is known as the energy strangling. Energy straggling places a limit to which losses and therefore depth can be resolved in a backscattering spectrometry. Due to statistical uncertainty in the energy of particles entering the target material, both the number and size of events for a certain depth of penetration will have a certain distribution. As a result the energy profile broadens as a function of the distance traveled through the target (Bird and Williams, 1989). If a particle has lost an average energy $\triangle E$ over a given path $\triangle x$, the energy straggling around $\triangle E$ has the variance given by (Grob and Siffert , 1984).

$$\Omega^2 = 4\pi z^2 e^4 Z N \triangle x \tag{3.17}$$

where z and Z are atomic numbers of the ion and the target respectively. In this work, the energy straggling phenomena was not taken into consideration due to the small thickness of the deposited layer.

3.2.5 RBS experimental setup

A monoenergetic beam of a ions (He^+, impinge on the target material, 6H-SiC deposited with a thin-film of Pd. The charged He^+ particles are produced by an ion source situated in the accelerator. The accelerator used in this study is the Van de Graaff accelerator at the University of Pretoria as shown . The accelerator has a maximum voltage of 2MV.

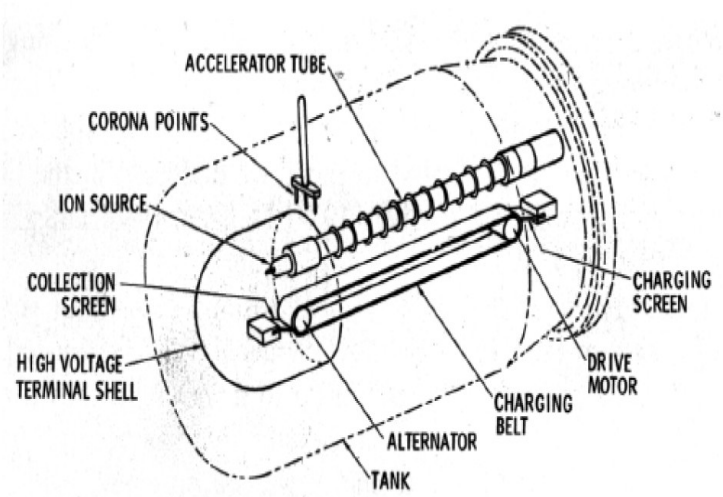

Figure 3.4: Van de Graaff accelerator. Taken from Chu *et. al.,* (1978).

In order to perform any backscattering experiments an ion beam has to be produced and accelerated. The ions to be accelerated are first produced in the accelerator tank, which houses the ion source, accelerator tube, charging belt and the components providing the electrostatic environment of the accelerator (figure 3.4). The accelerator tan is filled with dry gases such as N_2 and CO_2 to allow a standoff of the high voltage on the terminal-from-ground potential (Chu *et al.,* 1978).

Therefore the ions of the desired species are produced in the ion source, and are accelerated through an accelerating column. From this column, the ions enter the analyzing magnet where a number of ion species are separated and only those needed for the experiment are selected, thus the analyzing magnet acts as an energy and mass separator. After passing the analyzing magnet the beam passes through the high and low energy slits and it is directed to the centre of the scattering chamber with a beam spot size of 1mm. Inside the scattering chamber there is a passivated implanted planar silicon (PIPS) partially depleted (PD) surface detector which has a reversed biased with 40V and a three axis goniometer system with a 0.01^0 precision. The schematic set-up of the Van de Graaff accelerator of the Department of Physics at the University of Pretoria is shown in figure 3.5

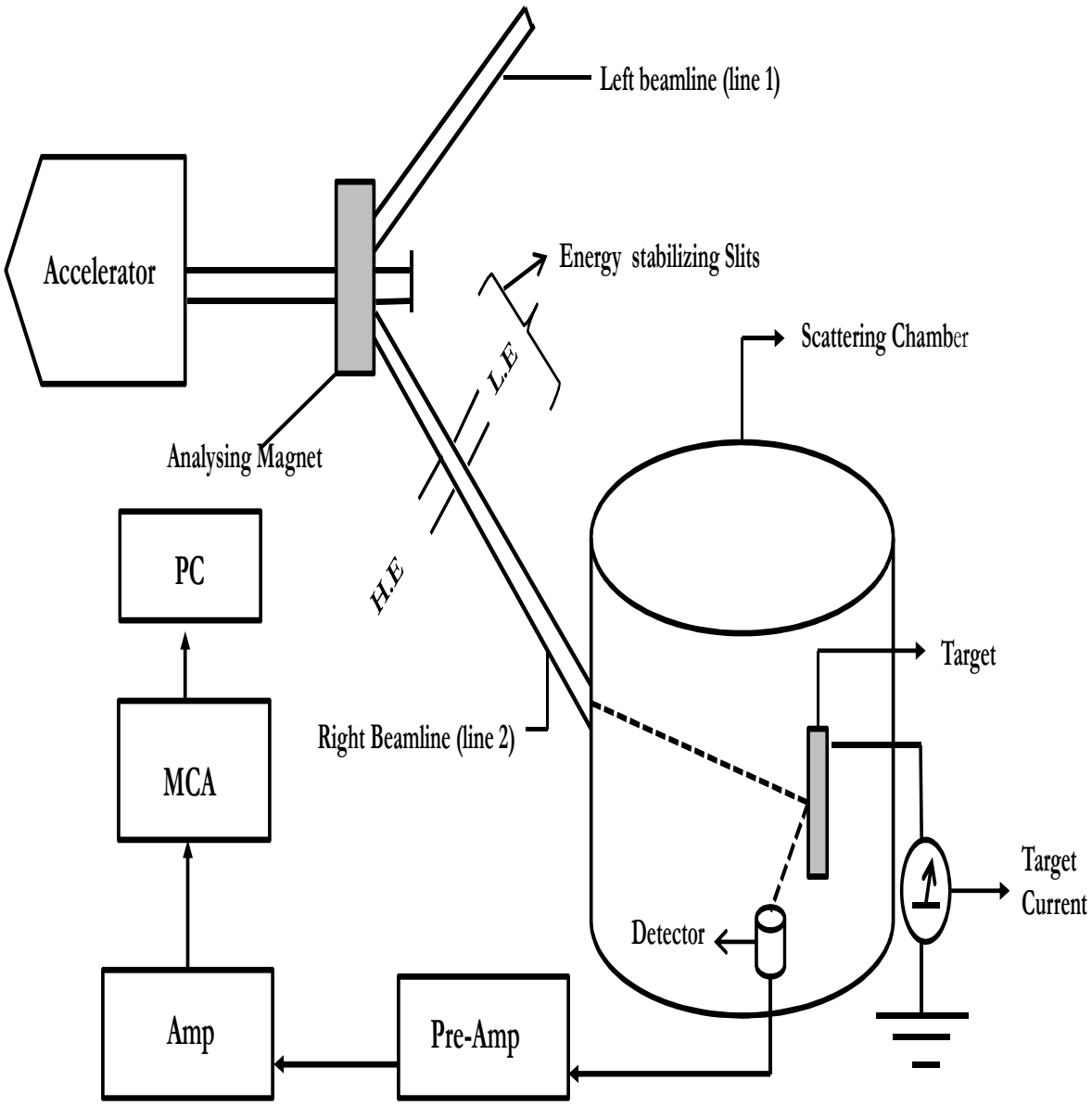

Figure 3.5: Schematic presentation of the Van de Graaff accelerator at the University of Pretoria.

3.2.6 Data Acquisition

When a monoenergetic high energy He^+ beam impinges on the target, some of the particles will be absorbed and some will be backscattered; part of these backscattered ions are analyzed and counted. The backscattered ions are detected by a Canberra PIPS surface barrier detector with an area of $25mm^2$ situated at an angle of 165^0 relative to the incident. A bias voltage of about +40V is supplied to the detector by the high voltage supply. An output charge signal from the detector which is proportional to the energy of the backscattered particle is transfered to the pre-amplifier which converts this charge signal pulse into a voltage pulse. The amplitude of this voltage pulse will be proportional to the energy of the of the backscattered particles.

This voltage pulse will then be further amplified and shaped to meet the requirements of the pulse-height analysis by the amplifier. That is, the amplifier will accept the voltage pulse from the pre-amplifier and amplifies it into a linear voltage range. The amplifier therefore creates a suitable pulse shape optimizing the resolution and count-rate capability. There are generally two main reasons for pulse height shaping: (a) to avoid pulse pile up and (b) to enhance the signal-to-noise ratio. The amplifier produces two types of signals namely, a unipolar and signal on the front and rear panel. The front panel is connected to the input of the oscilloscope in order to monitor the signal while the back panel is fed into the MCA. The current generated at the back of the samples is connected to the current integrator. The sample holder is insulated from the chamber and has a voltage of -300V used to suppress the secondary electrons. The logic signal from the current integrator is responsible for the initiation and termination of signal processing by both the MCA and the counter. The signal from the current integrator is then connected to the charge counter and its output connected to the MCA.

The MCA is used for pulse-height analysis, voltage sampling and multichannel scaling, it sorts and collects the pulse signal from the amplifier to produce a digital and visual presentation of the pulse height signal spectrum produced by the detector. The final output of the MCA is depicted on the personal computer (PC), which gives a visual representation of the counts versus the channel number of the spectrum. The schematic representation of the data acquisition system at the University of Pretoria is shown in figure 3.6.

3.2.7 Data Analysis

The backscattered spectra of the backscattering yield against the channel number were obtained by collecting a total charge of $8\mu C$ for each sample during the investigation. This was done to minimize the statistical error. The vacuum of the scattering chamber was maintained at a pressure well below 10^{-6} mbar in order to minimize carbon deposition on the sample, which is caused by the collision between the projectile particles with residual gases that are present in the chamber. During the analyses the high energy beam had a current of 10 nA to avoid heating the sample and to reduce the pile-up affects. Pile-up effects can occur when the events encountered by the detector are too high and the detector system is unable to separate these events individually. If the pile-up event can occur, two different events can be detected as one event, which may result in false measurements.

To obtain the energy per channel for the calibration of the system, the backscattered spectra were obtained at two different energies of 1.6 MeV and 1.4 MeV. The positions of C, Si and Pd channel number at the different energies were plotted against the corresponding energies. The calculated slope of the plots gave the energy calibration of the system which is the energy per channel of keV/channel used in the simulation of the RBS spectra.

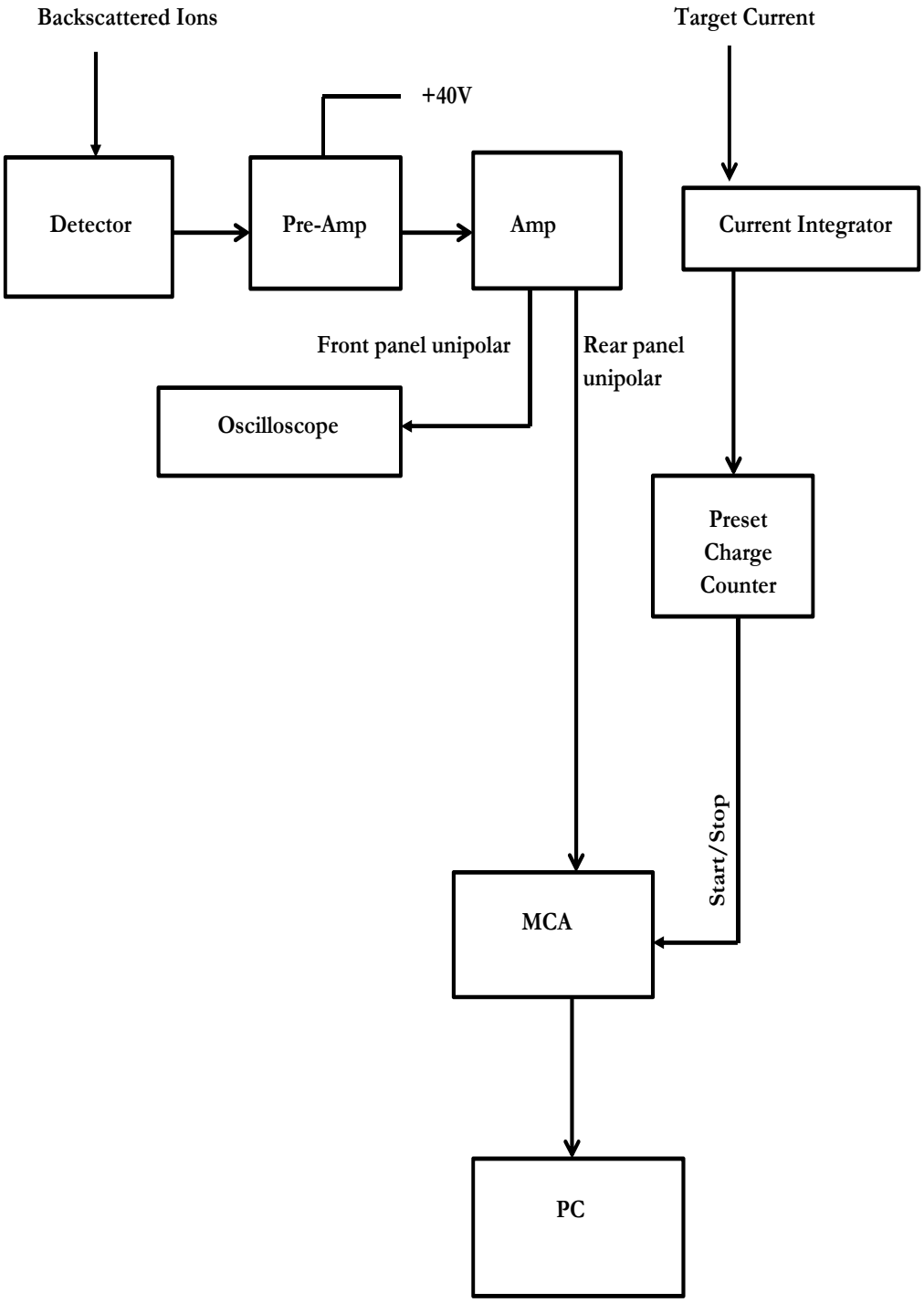

Figure 3.6: Schematic presentation of the electronics used for data acquisition in the RBS at the University of Pretoria.

3.2.8 Rutherford Universal Manipulation Program (RUMP)

In determining the elemental concentrations the experimental spectra are usually analysed by means of a computer simulation program known as RUMP. In RUMP, the samples to be analysed is considered to be a stack of layers each with uniform compositions. A hypothetical description of the sample such as elemental composition and thickness of the layers must be specified. The measurements or the experimental parameters used when analysing the spectra of the sample must must also be specified. These include the projectile type, the energy of the projectile, its charge, current and the angle of orientation of the sample during analysis must be specified. Once the parameters have been inserted the RUMP code will generates a theoretical spectra for thick or thin targets bombarded by light projectiles with specified incident energies. It will also generate the depth profile of the sample.

The simulation software package RUMP is used to fit and analyze the experimental data presented with the yield normalized to the incident beam current. The incidented angle (θ), which is the angle between the sample normal and the incoming beam measured from the sample normal, was kept at an angle of -7^0 to avoid channeling in the substrate and the angle(ϕ), which is the angle between the incoming beam and the detector measured from the incoming beam, was also kept at 15^0 during the course of the experiments.

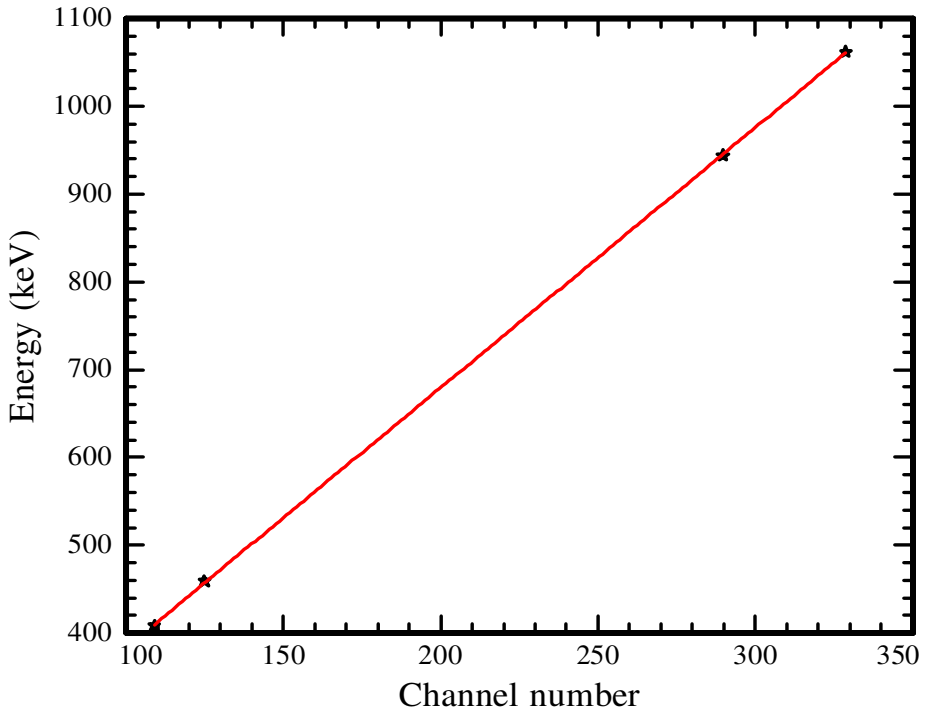

Figure 3.7: The energy calibration curve.

The energy conversion factor between the ADC reading and the actual energy was obtained by energy calibration of the RBS system. The energy calibration curve shown in figure 3.7 was obtained by calculating the surface positions of two elements, carbon and silicon in energy and plotted in keV in the y-axis. The channel numbers were read from the RBS spectra and were plotted against energy values on the x-axis. This then resulted in a straight line fit. The slope of the straight line calculated above is 2.962 keV / channel and the offset at channel zero is 46.976

keV(0). The simulating parameters used in fitting the experimental data are tabulated in table 3.1 below.

Parameter set	Command set
Beam	1600 keV
Charge	8μC
Current	10 nA
Theta	-7^0
Econv	2.962(keV/ch) +46.979 keV(0)
Omega	3.5 mSr

Table 3.1: Initial parameters set for sample simulation.

3.3 Time Of Flight-Energy Recoil Detector

The Time of flight - Elastic Recoil detector (ToF-ERD) is a technique used for quantitative analysis of light elements in a solid material. In ToF-ERDA heavy incident ions are used to kinematically recoil sample atoms off from the sample. In ToF-ERDA the mass of the incident ions must be greater than that of the target nucleus. If we consider a positive beam of ions striking a solid target, the heavy ion projectiles can easily recoil the lighter ions in the target which in turn can be ejected from the target and be detected provided that the geometry is right. Figure 3.8 shows the ToF-ERD set-up at iThemba LABS. The heavy ion ERD at iThemba LABS consists of a time of flight detector, built with two timing detectors T1 and T2, situated in a flight distance of 0.584 m apart and a silicon surface barrier detector (SBD). The SBD is placed at a distance of 6.5 cm behind the second time detector and it is used for energy measurements (Msimamga *et al.*, 2009). In the spectrometer, the sample to be studied is bombarded with heavy ions (copper ions) generated from the a Tandem accelerator.

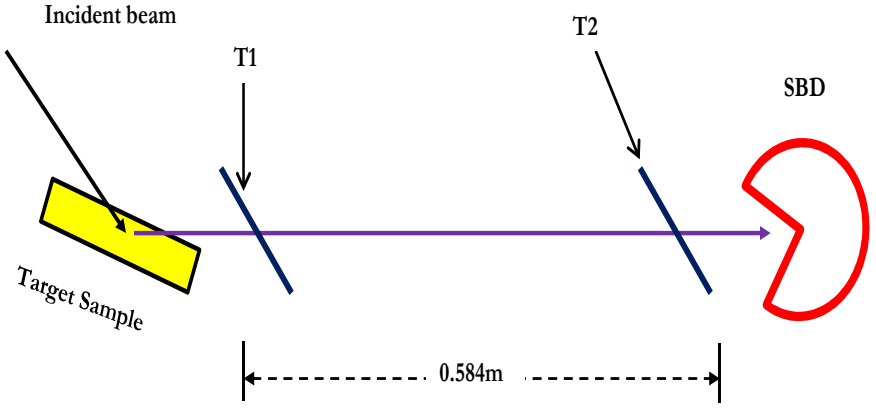

Figure 3.8: A schematic diagram showing the ToF-ERD spectrometer setup

During the ToF-ERD measurements the incident heavy ion strikes the target sample and recoils the elements in the sample. The ejected or recoiled atoms are directed towards the two timing detectors T1 and T2. If the target contains different elements with different masses, each of these particles will be detected by two timing detectors T1 and T2 to give the time of flight signal. The SBD signal will then give the energy signal of the particles arriving at the detector.

If both the energy and the ToF are plotted against one another one can separate all the masses present in the sample into different banana curves and the depth profile of the elements in the sample can be determined.

3.4 X-ray Diffraction

3.4.1 Principles of X-ray diffraction

X-rays are electromagnetic radiation with a wavelength ranging from $0.1-5\mathring{A}$, which is equivalent to an energy range of about 12.5keV to 125keV (Dinnebier and Billinge, 2009). They belong to the electromagnetic spectrum overlap with the gamma-rays in the shorter wavelength and with ultraviolet in the longer wavelength. They can be described in terms of the wavelength λ, frequency ν and photon energy E as follows:

$$E = h\nu \tag{3.18}$$

X-ray diffraction (XRD) phenomenon was discovered by a German physicist Max von Laue in the 1912. Before the discovery of X-ray diffraction, crystallographers had analysed the information about crystals mainly by measuring the interfacial angles, chemical analysis and by physical properties. However, little was known about the interior structure of crystals. In his work von Laue argued that if the crystals were composed of regularly spaced atoms which might act as scattering centers for X-rays and if the X-rays were electromagnetic waves with a wavelength equal to the interatomic distance in crystal, then it should be possible to diffract the X-rays by using a crystal (Cullity, 2001). This phenomenon was then named diffraction shown in figure 3.9.

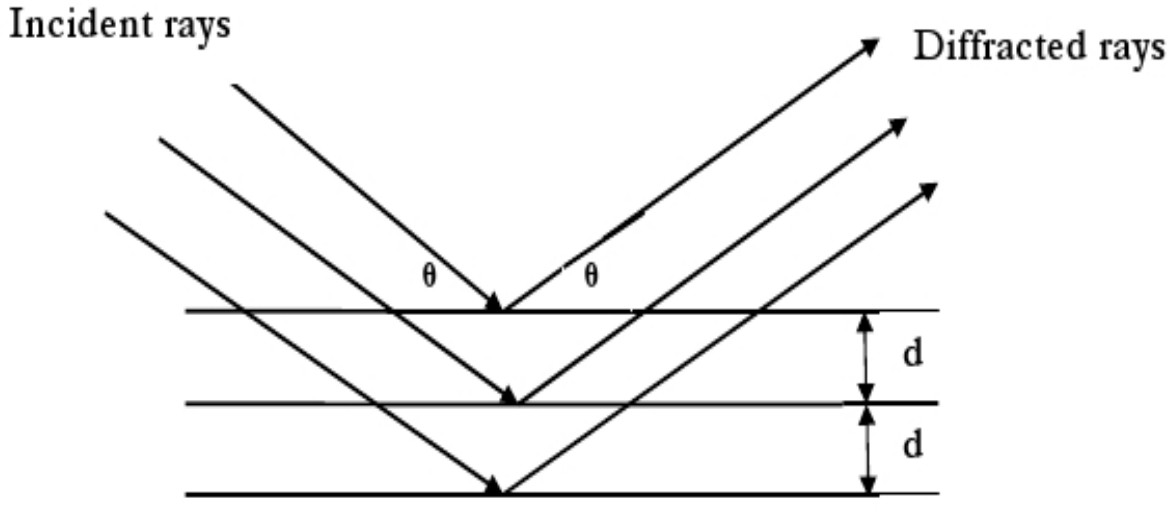

Figure 3.9: Bragg diffraction of X-rays by a crystal.

The X-rays can be diffracted when a monochromatic X-ray beam with a wavelength λ is projected into a crystalline material at an angle of θ. Some of the X-ray beam will be absorbed

and the other part of the X-ray beam will become scattered or reflected and the generated scattered X-rays will have the same wavelength as the incident beam and these can then be detected.

3.4.2 Braggs law

Since the atoms in a lattice are arranged periodically, the X-rays scattered from a crystalline solid can constructively interfere and produce a diffracted beam when the path differences are $n\lambda$. The Bragg equation gives the basis for X-ray diffraction and describes the conditions for constructive interference of the X-rays scattered from a plane of atoms. The Bragg's equation is given by

$$2dsin\theta = n\lambda \tag{3.19}$$

where

- λ is the wavelength of the incident X-ray beam
- d is the spacing between the atomic planes
- θ is the Bragg angle
- n is the integer

For diffraction the smallest value of $n = 1$ and it is taken as the first order, $n = 0$ corresponds to the beam diffracted in the same direction as the transmitted beam and cannot be observed.

A diffracted pattern from the crystal has many sharp peaks corresponding to various crystal planes based on the Bragg-law. The peaks at low 2θ are from the crystal planes of large d-spacing and the peaks at high 2θ are from the crystal planes of small d-spacing. To satisfy Bragg's condition at all crystal planes, the crystal diffraction pattern is generated mostly from the polycrystalline materials or powder material. In single crystal the diffraction pattern is collected with the provision that the sample is rotated at various angles during data collection so that the Bragg law condition can be satisfied by different d-spacings.

3.4.3 Glancing-Incident diffraction

X-ray radiation is known of its large penetration depth into any matter. This property of X-rays makes normal XRD not to be surface sensitive. The thin-film layers in a sample have a small diffracting volumes, which results in low diffracted intensities when compared to the substrate and the background diffracting intensities. The combination of the low diffracted signal and the high background make it very difficult to identify phases present.

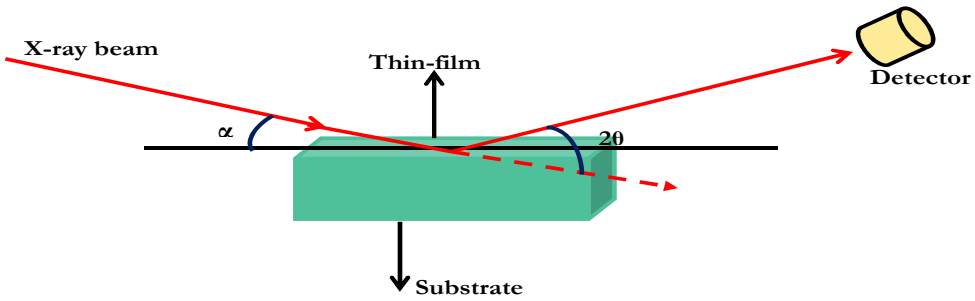

Figure 3.10: Schematic representation of the glancing-incident XRD technique.

Glancing incident XRD is able to overcome this restriction by using very small incident angles to maximize the signal from the surface layers as shown in figure 3.10.

In glancing-incident, the stationary incident beam makes a very small angle ($\approx 1^0$)with the surface which increases the path length of the X-ray beam in the thin-film. This results in the increase of the diffracted intensity on the thin-film at the same time reduces the diffraction intensity from the surface. Due to the increase in the path length when the glancing incident is used, the diffraction volume increases proportionally.

In this study an XRD instrument used for phase analysis was the Bruker D8 Advanced XRD situated at the South African nuclear energy corporation (NECSA). This XRD equipment is equipped with glancing incident capabilities. During the experiment X-ray beam (Cu-Kα radiation) was kept at an incident angle of 1^0 relative to the surface and the diffraction pattern was collected at a 2θ range from 26^0 to 95^0 . During the collection of the diffraction spectrum, only the detector rotates through the angular range, thus keeping the incident angle, the beam path length, and the irradiated area constant.

3.4.4 Phase Identification

XRD is one of the mostly used tools for identifying the unknown crystalline phases. In material science, a phase is defined as a region that has relatively uniform chemical composition and physical properties including crystal structure. Thus each phase has its own unique diffraction pattern, which can precisely determine the content of the sample.

XRD comprises of two analyzing methods namely qualitative and quantitative analysis. Qualitative analysis involves the identification of phases in a specimen by comparing the positions and the intensities of the diffraction peaks with a reference pattern or library of known crystalline phases. Qualitative analysis can also estimate the proportions of different phases in a multi-phase specimen by comparing the peak intensities attributed to the identified phase. Quantitative analysis on the other hand involves the determination of the amounts of different phases in a multi-phase specimen. In quantitative analysis the structural characteristics and phase proportions from the experimental data can be determined. In this study qualitative analysis was used.

3.5 Scanning Electron Microscope

Scanning electron microscopy (SEM) is a type of microscope which depends on electrons rather than light. It is mainly used for various purposes such as topographic studies, chemical composition, elemental mapping and microstructure analysis. In SEM, the primary electron beam is produced in the electron gun by a cathode filament (tungsten (W) or lanthanum hexaboride (LaB_6)) or by a field emmision gun (W-tip) (Lawes, 1987). After the electrons have been produced they are accelerated with a velocity which is highly depended on the accelerating voltage. This accelerating voltage can range from 200V to 30kV depending on the type of microscopy used. The electron beam with a specific energy is then directed towards the scanning coils and over to the specimen surface. The image of the specimen will then be formed by scanning the beam across the specimen and detecting the secondary electrons emitted from the sample. Figure 3.11 shows a schematic presentation of the SEM.

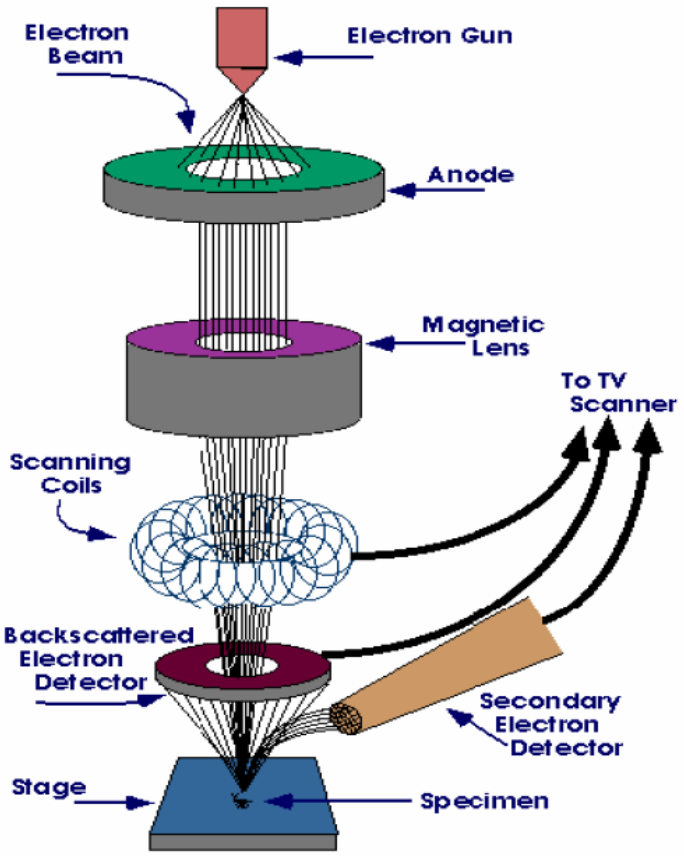

Figure 3.11: Schematic presentation of SEM. Taken from [www.purdue.edu/rem/rs/sem.htm; accessed on 25-04-2012]

.

3.5.1 Electron-Specimen Interaction

There are a number of possible interactions between the specimen and electron the beam that can take place when the beam of electrons strikes the specimen. The focused electron beam can generate a variety of signals at the surface of the specimen. These signals carry different types of information and are used for different purposes. Figure 3.12 shows the different types of information obtained when the electron beam interacts with the sample and region where the information is produced.

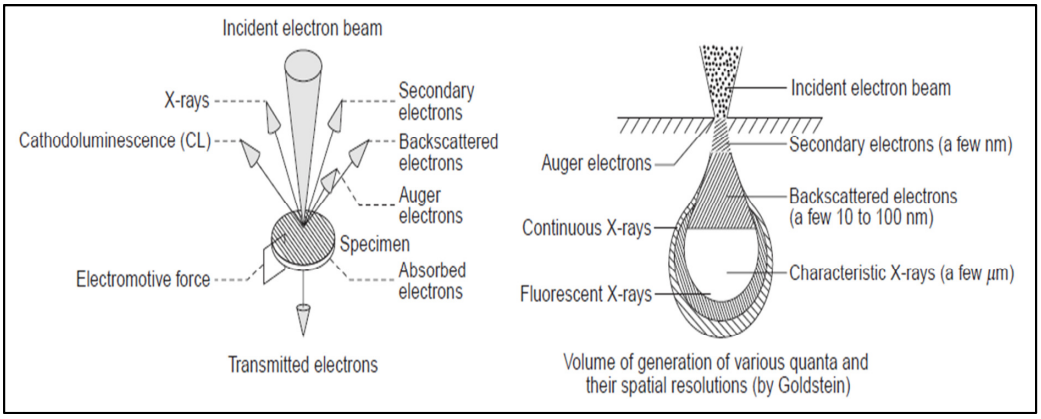

Figure 3.12: A schematic representation showing the interaction of electron with a sample in SEM. *Left panel*: shows the different types of information obtained. *Right panel*: shows the regions where the information is produced. Taken from [www.jeolusa.com/DesktopModules/ accessed on 25-04-2012].

There are three most commonly used signals from SEM : secondary electron signal, backscattering signal and the X-ray signals. The secondary electron signals come about as a result of inelastic scattering between the incident electrons and the specimen. Inelastic collision occurs when the incident electrons interact with the orbiting shell electrons and the nuclei. In this case the incident electrons transfer a large proportion of their kinetic energy. The incident electrons will knock out the loosely bounded electrons in the atom of the specimen. The weak-electrons may escape as low energy secondary electrons and their signal is collected for imaging. Secondary electrons of about 1-50eV are mostly used for imaging the topographically contents of the surface. The secondary electron signal depends on the surface undulation of the specimen, moreover the energy of this signal is very low and their generation is limited to a thin layer close to the specimen surface which is what makes it more suitable for observing a specimen surface topography.

The backscattering electron signal comes about as a result of elastic scattering. Elastic scattering of electrons involves the electrons which change direction when passing very close to a positively charged nucleus. As a result elastically scattered electrons tend to maintain all their energy. During the elastic scattering event, the electrons become deflected and their deflected angle depends highly on their energy and on how closely it passes to the nucleus. The deflected electrons are called backscattered electrons when collected as a signal for imaging. The signal for the backscattered depends highly on the angle between the incident beam and the surface of the specimen and on the atomic number Z which is useful for obtaining Z-contrast. The energy of the backscattered electrons is very much higher than that of the secondary electrons, thus they carry information from deeper layers of the specimen surface. Therefore the backscattered electron image will show the compositional difference found on the sample.

The characteristics X-ray emitted from the specimen when the electron beam irradiates it can be detected and analysed in order to identify the elements contained in the specimen (qualitative analysis). Also one can determine the weight concentration of the contained elements (quantitative analysis).

Reference

Bird J and Williams J, 1989, "Ion Beams for Materials Analysis", Academic Press, Australia, pg 620.

Chu W., Meyer J. and Nicolet M., 1978, "Backscattering Spectrometry", Academic Press, New York.

Cullity B.D. and Stock S.R., 2001, "Elements of X-ray Diffraction", Third Edition, Prentice Hall.

Dimmebier Robert E., Billinge Simon J. L., 2008, "Powder Diffraction Theory and Practice", The Royal Society of Chemistry (RSC).

Feldman L.C., Mayers J.W., Picraux S.T, 1982, "Materials Analysis by ion channeling, "Academic Press", New York.

Grob J. and Siffert P., 1984, J. Cryst. Growth. **8**, 59.

Guilhaus Michael, 1995, J. Mass Spectrom., **30**, 1519.

Lawes Grahame, 1987, "Scanning electron Microscopy and X-ray microanalysis", John Wiley & Sons.

Mayer James W, Nicolet Marc-A., 1978, Backscattering Spectrometry, John Wiley & Sons Inc.

Msimanga M, Comrie C.M., Pineda-Vargas C.A., Murray S., Bark R., Dollinger G., 2009, Nucl. Instrum. Meth. B **267**, 2671.

Poate J.M, Tu K.N , Mayer J.W, 1978, "Thin films-Interdiffusion and reactions", John Wiley & Sons Inc.

Chapter 4

Results and Discussion

4.1 Results

The aim of this study is to investigate the interaction of Pd with single crystal SiC by employing thin-film diffusion couples at room and elevated temperatures. Literature showed that Pd reacts with SiC to form more than one phase at low temperature, with these phases converting to a single phase as the annealing temperature is increased. Studies have also shown that a number of metal-rich phases tend to form at low temperatures with low-metal rich silicides forming at elevated temperature. This behavior was largely observed in Pd/SiC diffusion couples consisting of a thick layer of Pd. A phenomena of phases forming as periodic layered structures was also observed in these diffusion couples resulting from the interaction of the metal with the SiC atoms to form silicides with the Si and and an immobile carbon which accumulated in this study. Therefore this study aims to identify the phases that form for thin-film diffusion couples at low and elevated temperatures and also aims to investigate the behavior of phase formation sequences for thin-film Pd/6H-SiC diffusion couples.

The interaction of Pd with SiC was investigated using four techniques outlined in chapter 3: (i) RBS for compositional and interaction analysis with the help from RUMP simulation software, (ii) ToF-ERDA for depth distribution of the elements (iii) GIXRD for phase identification and (iv) SEM for surface analysis. The results obtained through out this study are therefore reported now.

4.1.1 Rutherford Backscattering Spectrometry

The diffusion couples employed in this study were prepared by depositing a thin Pd layer of thickness of about 50 nm by using the resistive heating procedure. Two sets of depositions were made namely deposition (a) and deposition (b). Figure 4.1 below summarizes the steps followed in the analysis of the diffusion couples.

A typical RBS spectrum illustrating a random spectrum of Pd deposited onto a SiC is shown in figure 4.2. The energy of the helium beam used in the collection of the RBS spectra was 1.6 MeV at a backscattering angle of 165^0. The charge collected for all the spectra was 8 μC and the current during spectrum collection was kept at 10 nA. For a spectrum shown in figure 4.2, the Pd element which is the element with the highest kinematic factor, appears in the high region of the spectrum with its edge at a channel number of 451, followed by the Si with a channel number of 289 and then C with a channel number of 123. The arrows in the spectrum (as depicted in figure 4.2) indicates the surface position corresponding to the elements in the spectrum namely, Pd, Si and C.

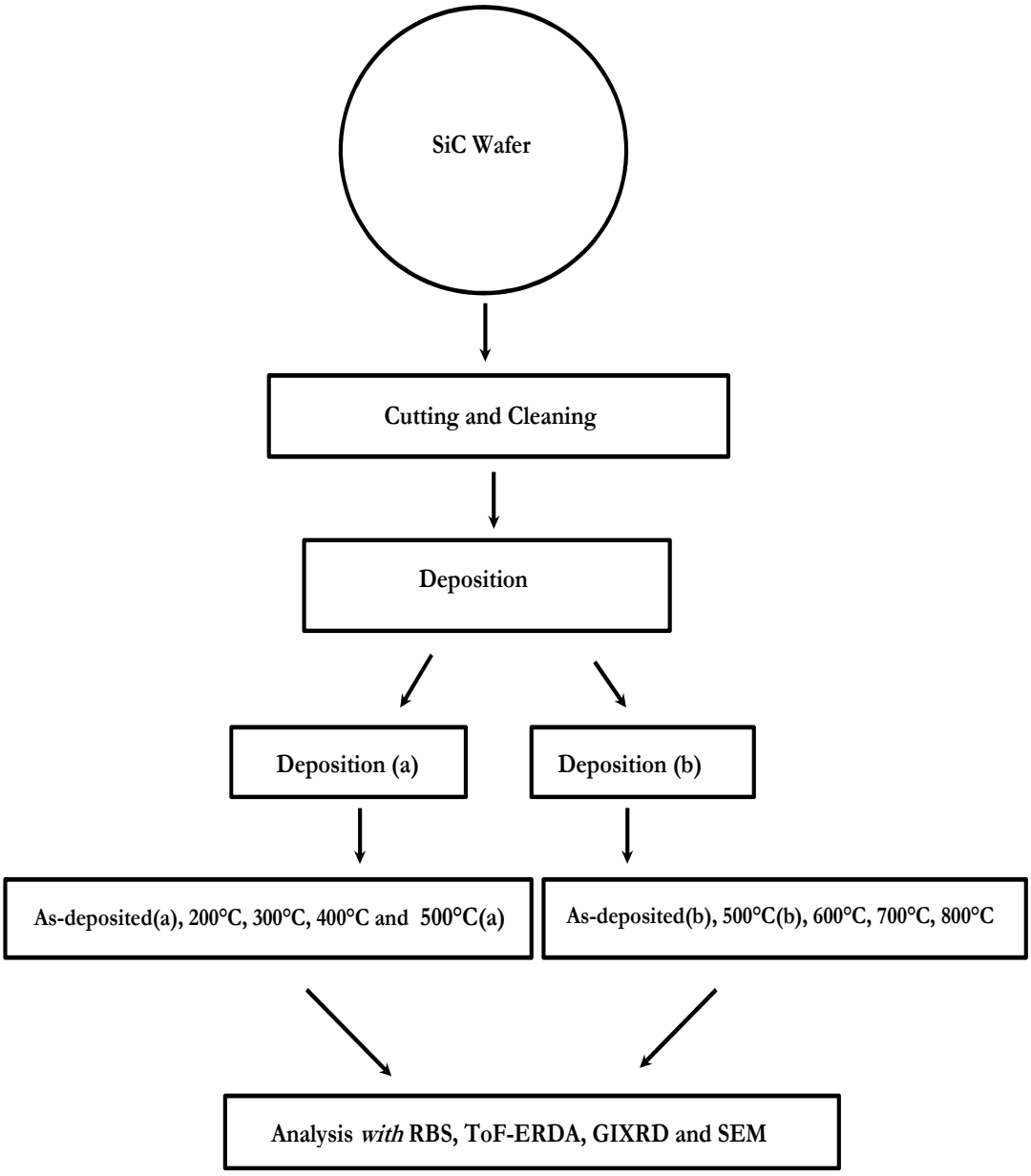

Figure 4.1: A schematic diagram showing the preparation and the analysis of the Pd/6H-SiC samples .

The RBS study was performed in order to determine the layer-by layer composition of the Pd/6H-SiC interface before and after annealing. The RBS spectrum shown in figure 4.2 shows a layer of deposited Pd with a sharp interface with SiC. The plateau in the backscattering yield extending from the Pd peak shows a high Z, but low concentration contamination throughout the Pd layer. If one assumes this to be W then the height of the signal corresponds to 0.3 at.%. Since this peak was present in all the samples prepared from the Pd-source; it could have been contaminated. However, since the concentration is so low it was decides not to take it into account when simulating the spectra.

The as-deposited spectrum of the Pd/SiC presented in figure 4.2 showed no detectable reaction between Pd and SiC at room temperature. Thus the spectrum of the as-deposited sample will serve the purpose of a reference, compared to which the thermally annealed spectra could be analyzed. The samples annealed at 200^0C and 300^0C also showed no detectable reaction between Pd and SiC.

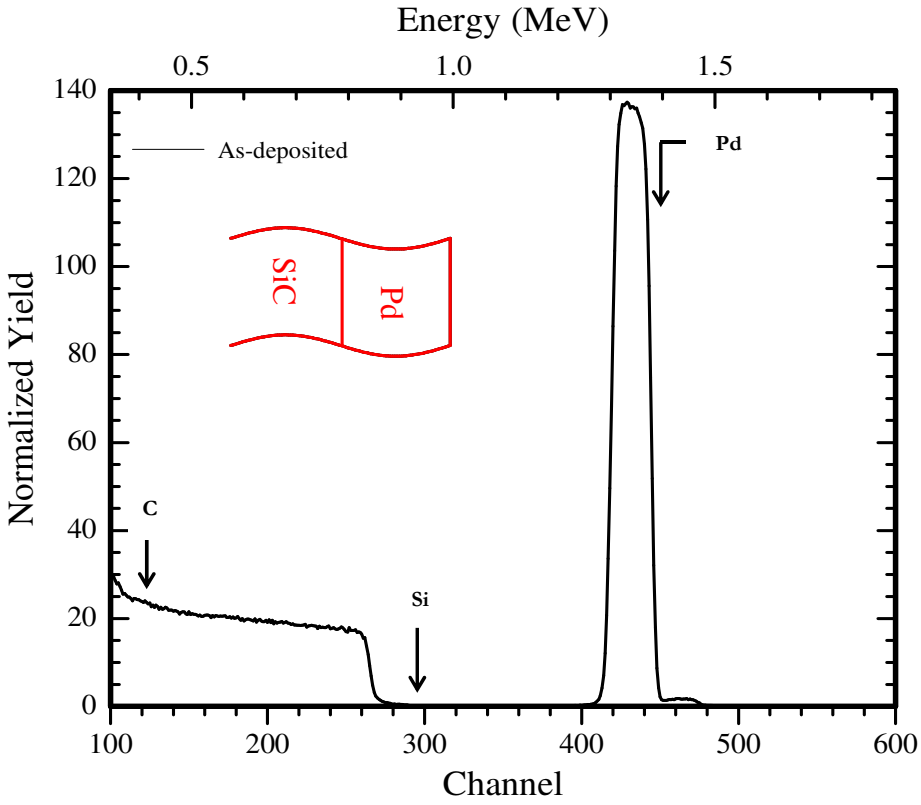

Figure 4.2: RBS spectrum of as-deposited Pd/6H-SiC interfaces.

Figure 4.3 shows the backscattering spectrum of the as-deposited sample compared to the sample thermally annealed at 400^0C for 1 hour in vacuum. The spectrum of the thermally annealed sample showed a relatively less number of Pd atoms per unit energy loss compared to the as-deposited spectrum. Thus indicating the presence of other atoms inside the Pd layer.

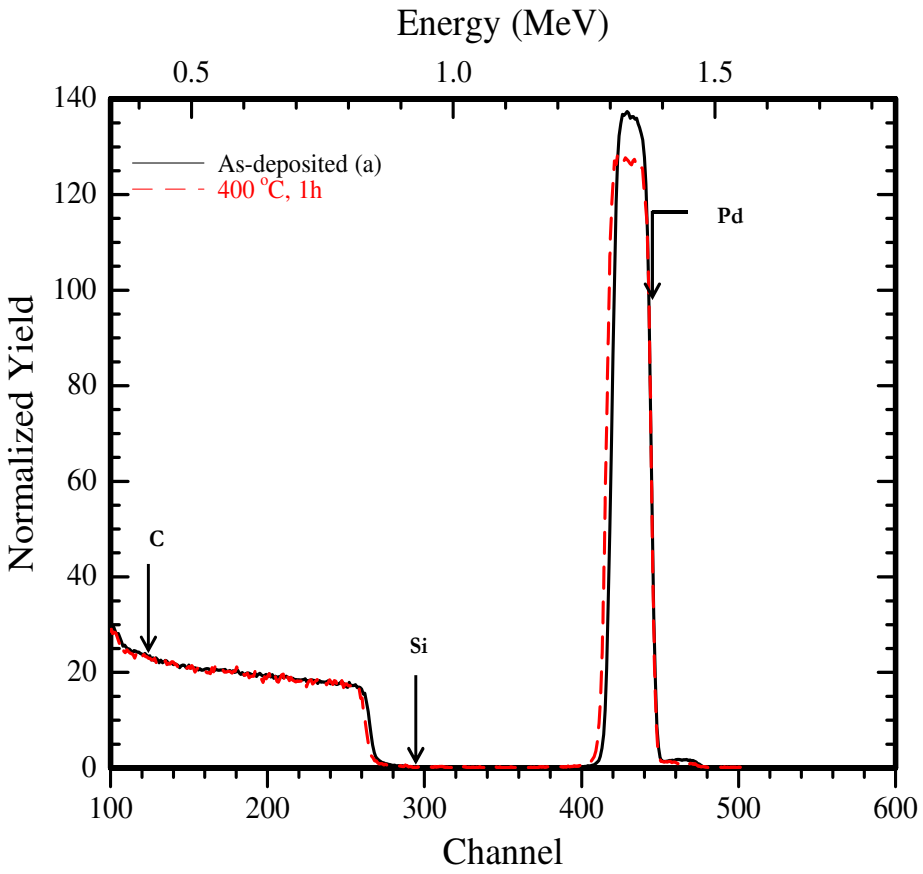

Figure 4.3: RBS spectra of Pd/6H-SiC interface before and after annealing at 400^0C.

The RBS spectra for the Pd/6H-SiC interface for the samples annealed at the temperatures of 500^0C and 600^0C for a period of 1 hour each is shown in figure 4.4. The spectra of the samples annealed at 500^0C and 600^0C are quite different from that of the as-deposited sample as well as the sample annealed at 400^0C. Both spectra show an observable reaction taking place between the Pd layer and the SiC. This is indicated by the Pd layer peak of both samples annealed at 500^0C and 600^0C exhibiting fewer Pd atoms per unit energy loss when compared to the as-deposited sample. The trend of the spectrum around channel number 381 indicates that the Pd signal is seen quite deep into the sample. This could be due to interdiffusion or the formation of a rough interface. The signal of the Si is also observed near the surface. Therefore at these temperatures Pd has completely reacted with SiC to form a phase(s).

The spectra for the samples annealed at higher temperatures of 700^0C and 800^0C shown in figure 4.5 indicated that the Pd has completely reacted with SiC resulting in the formation of reaction compounds. This is shown by the appearance of the Si signal near its surface position. In addition, these spectra show the formation of layered structures observed at the Pd layer. In the case of the samples annealed at higher temperatures, that is, at 700^0C and 800^0C the formation of the two-layered structures is more pronounced with two well defined average compositions compared to the ones annealed at 500^0C and 600^0C. The trend of the spectra around channel number 381 showed an increased in interdiffusion or roughness of the interface.

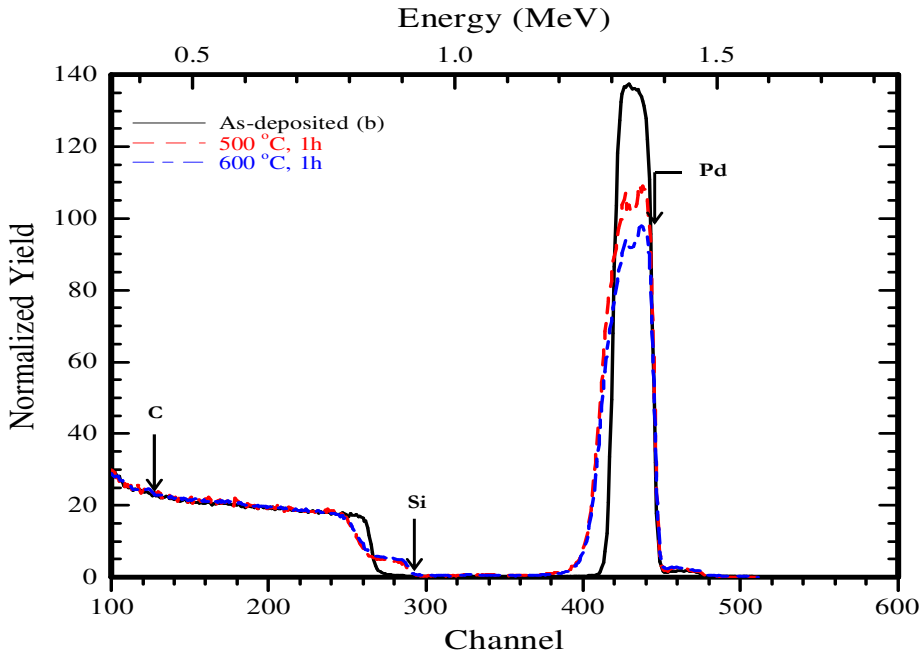

Figure 4.4: RBS spectra of Pd/6H-SiC interface before and after annealing at 500 and 600^{0}C.

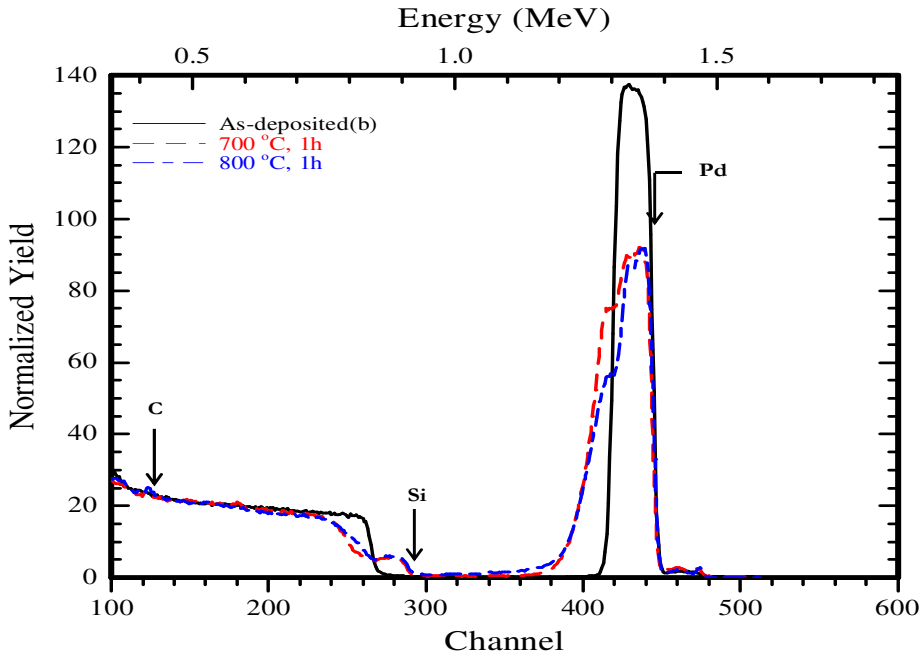

Figure 4.5: RBS spectra of Pd/6H-SiC interface before and after annealing at 700 and 800^{0}C.

4.1.2 Time of Flight-Elastic Recoil Detector

The experimental results obtained from RBS spectra gave clear Pd and Si profiles. Due to the low sensitivity of the backscattering technique for light elements, the amount of C dissolved in the Pd silicide film during reactions could not be accurately determined. This then gave us the opportunity to use ToF-ERDA measurements to accurately determine the C profile in the Pd/6H-SiC interface. The ToF-ERDA measurements were performed using a heavy ion Cu-beam produced by the tandem accelerator to analyze the as-deposited sample in order to determine the C distribution in the samples. The heavy ion Cu-beam was then used to recoil / scatter the elements contained in the samples. Elements such as Si, C and oxygen (O) were successfully recoiled by the Cu ions and the ToF against energy plot of the recoils together with the forward scatter of the Cu-beam are shown in figure 4.6 for the as-deposited sample. However, the Cu-beam was not an ideal beam available for the scattering the Pd atoms. This is due to the Pd being much heavier than Cu (Cu < Pd), which resulted in a noisy scatter plot for Pd as shown in figure 4.6. Despite the non-ideal measurement conditions, certain features could be deduced.

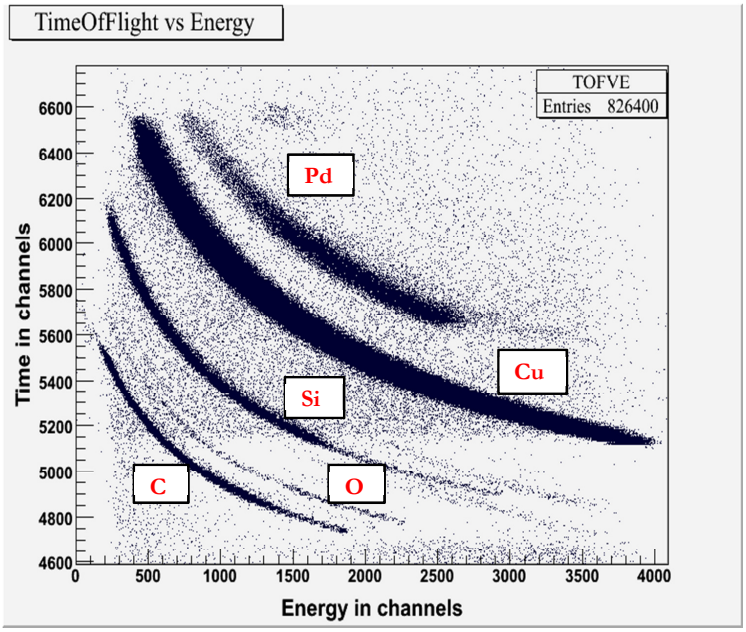

Figure 4.6: ToF vs Energy scatter plot of recoils (and forward scattered Cu-beam) from the as-deposited sample.

Figure 4.7 shows the overall energy spectra of Pd, C and Si recoils from the as-deposited sample extracted from the 2D-scatter plot.

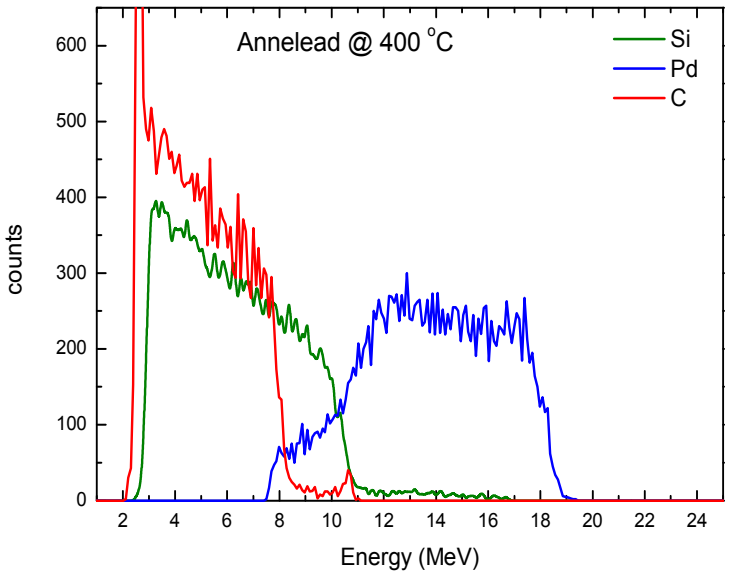

Figure 4.7: Energy spectra of Pd, Si and C recoils from the as-deposited sample.

The information obtained from the ToF against energy scatter plot can be used to convert each elemental spectrum into a depth profiles spectrum using KONZERD software, an energy-depth conversion algorithm. The elemental depth profiles for Pd, Si, C and O are shown in figure 4.8 for the as-deposited sample. The depth profile for the as-deposited sample shown in figure 4.8, indicates that there is some mixing between the Pd and the C at the surface layer, this is indicated by the C and the Si signal not appearing at the same depth. The surface layer also showed the presence of C in significant quantities. The surface layer thickness was estimated at about $5\times\ 10^{17}$ at.cm^{-2} (74nm) with a composition of Pd being around 0.8 and that of C being around 0.1 and the balance being Si and O. The presence of C on the surface layer could be due to surface contamination which occurred during deposition.

The extended Pd profile produced by KONZERD shown in figure 4.8 is worrying as the Pd peak shown in figure 4.7 does not show the same feature. This is being examined by the author of KONZERD.

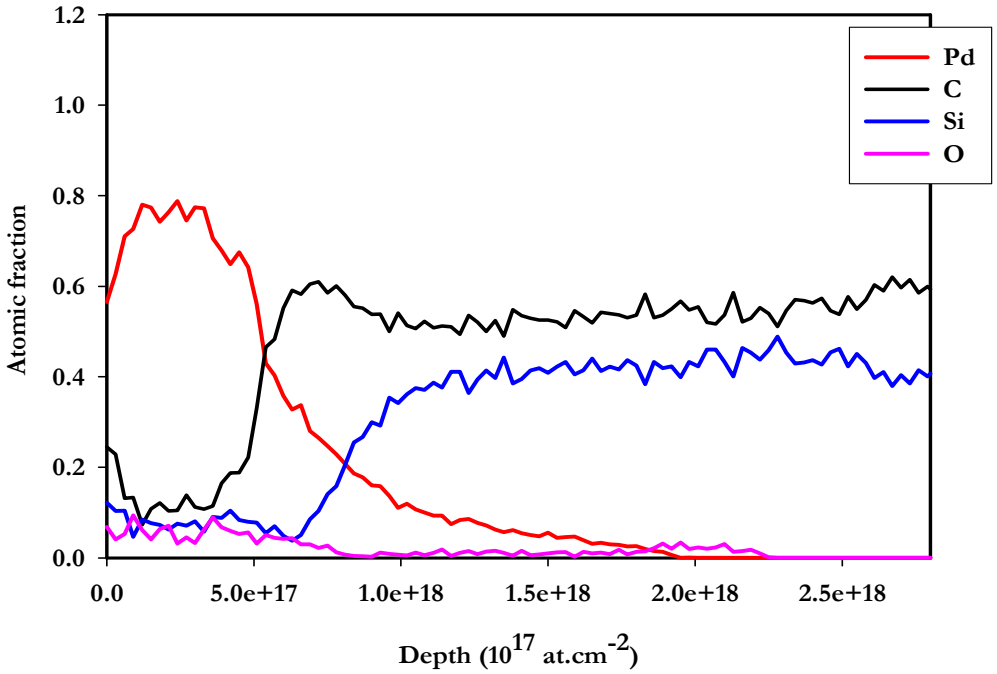

Figure 4.8: Elemental depth profiles of the as-deposited sample obtained using KONZERD, an energy-depth conversion algorithm.

4.1.3 RBS analysis with RUMP

The RBS spectra presented in this section all show the experimental data fitted with the simulated RUMP spectra. The experimental spectra is plotted in black while the simulated spectra are plotted in red. In order to simulate the raw experimental data a number of parameters have to be specified. These include the energy of the incoming beam, the charge and the current collected for each spectra, the incident and the backscatter angle as well as the energy conversion factor which can be obtained by system calibration.

Figure 4.9 shows the as-deposited spectrum which was fitted using the parameters set in table 3.1. In order to simulate the raw experimental data, the thickness and the elemental composition of the deposited layer and the substrate has to be specified. During the simulation of the as-deposited spectrum, the height of pure Pd layer could not be fitted onto the raw experimental data due to the presence of carbon in the Pd layer. This carbon which could have been a result of the hydrocarbon present in the chamber during deposition. Based on the ToF-ERDA results, which was able to determine the amount of carbon to be about 10% after annealing at 400^0C in the thin film, we then decided to include this amount of carbon in the Pd layer in order to be able to fit the as-deposited spectrum. This resulted in the elemental composition of Pd being 90% and that of carbon being 10%. The relative amounts of the Pd:Si:C used in fitting the as-deposited spectrum are shown in table 4.1 and the compositional curve as a function of depth for as-deposited sample is shown in figure 4.10.

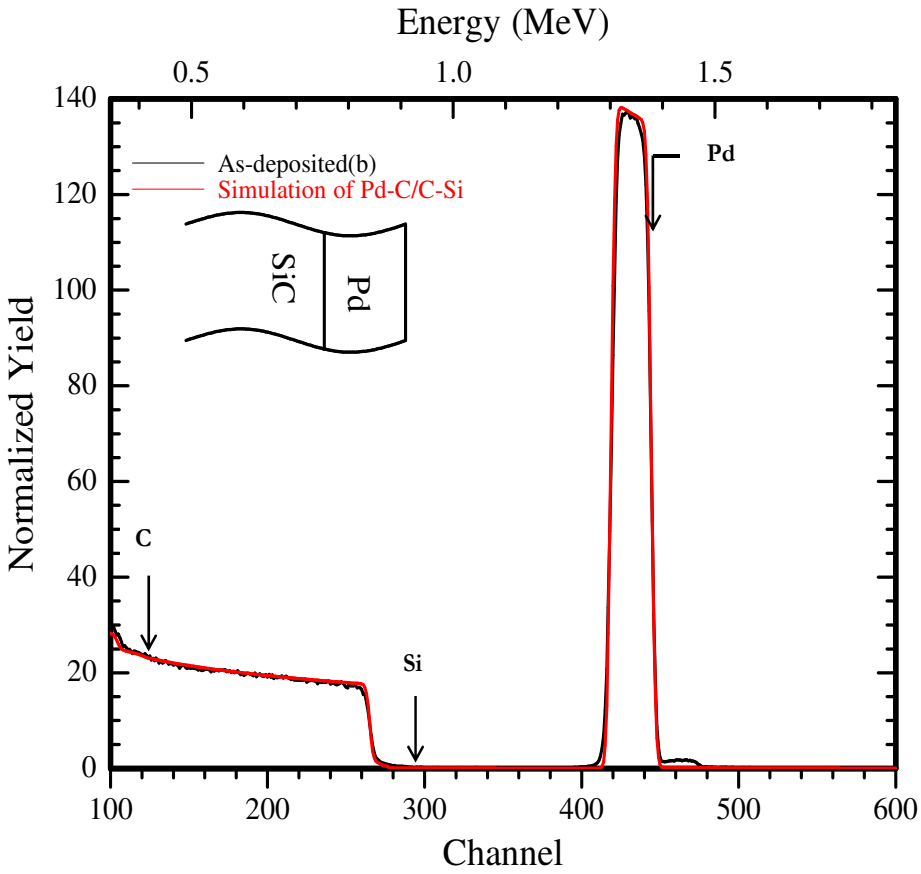

Figure 4.9: A simulated RBS spectrum of the as-deposited sample.

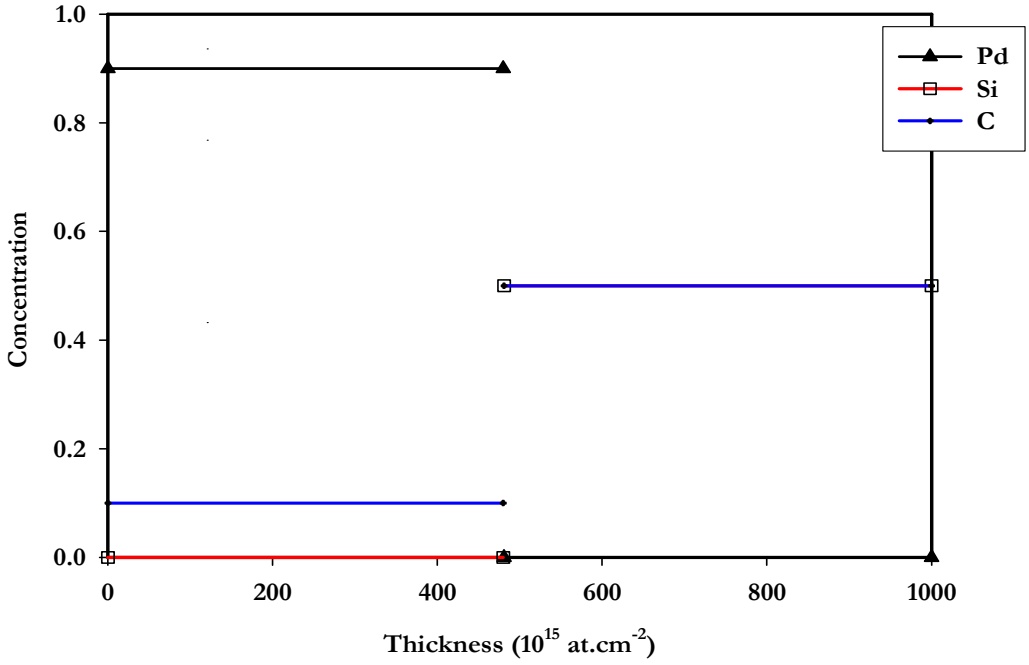

Figure 4.10: Elemental composition of the as-deposited sample as a function of depth.

The RBS / RUMP simulation showed no evidence of the reaction between Pd and SiC.

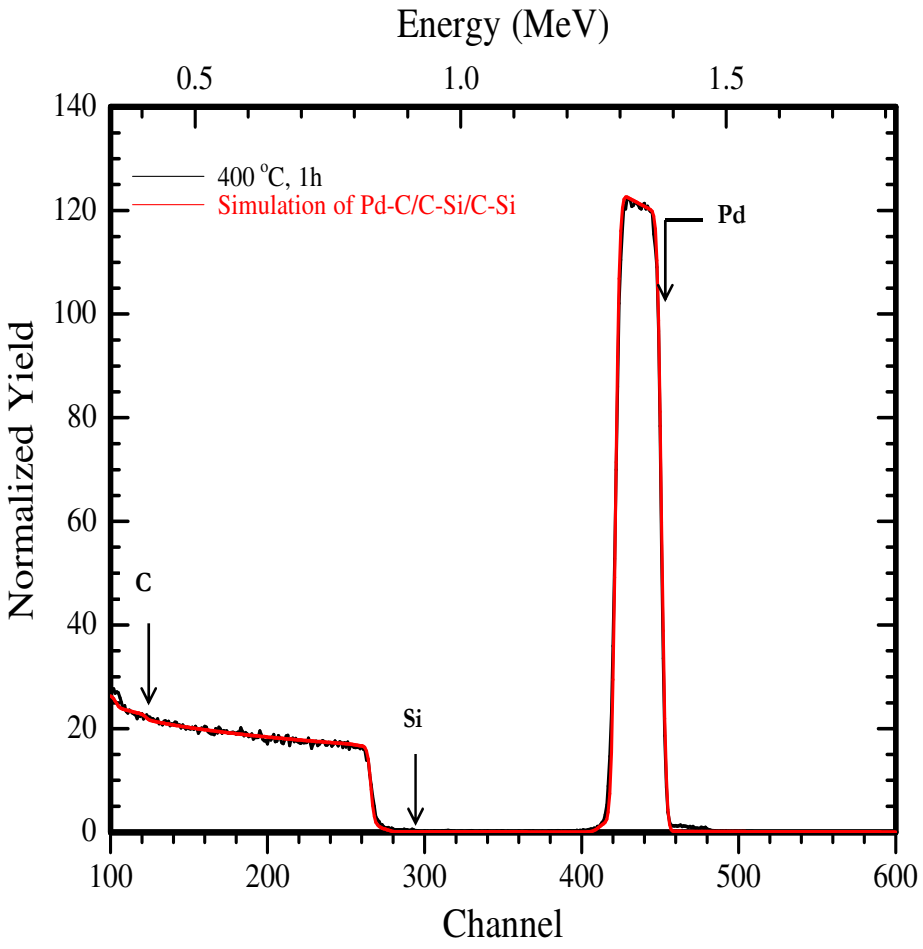

Figure 4.11: RBS spectrum for the sample annealed at 400^0C fitted with RUMP.

The RBS spectrum of the thermally annealed Pd/6H-SiC interface at 400^0 (figure 4.11) showed a decrease in the concentration of Pd atoms in the Pd layer when compared to the as-deposited RBS spectrum. The simulation also indicates a decrease in the number of Pd atoms and an increase in the amount of carbon in the system. The simulation shows that the elemental composition of Pd decreased from 90% to ≈70% and the carbon increased from 10% to ≈20%. The layer of the Pd was observed to have a thicker surface layer. Figure 4.12 shows the concentration profile of the sample annealed at 400^0C and the relative amounts used in fitting this spectrum are tabulated in table 4.1.

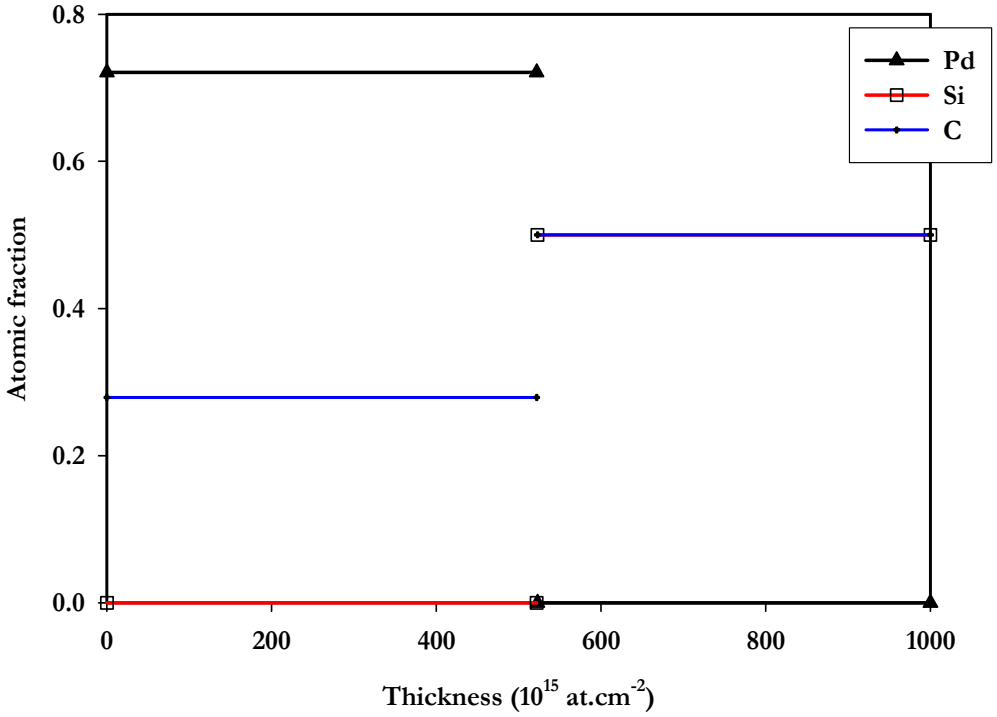

Figure 4.12: Elemental composition of the sample annealed at 400^0C as a function of depth.

The RBS / RUMP spectra for the samples annealed at 500^0C and 600^0C are shown in figure 4.13 and figure 4.15 respectively. Two significant features were observed in these spectra. Firstly, the concentration in the Pd layer showed a significant decreased in both spectra. Secondly, the formation of more than one phase was also observed in the surface layer and lastly the Si appeared at its surface. These RBS spectra proved to be difficult to fit as the phase formation in these system is quite complex.

In order to fit these spectra a two-layered structure model was employed. This model suggested that the reaction taking place at the Pd/SiC interface results in the complete consumption of the Pd metal. The Pd metal at high temperatures will completely react with Si from the SiC substrate to form more than one compound structure. Another aspect which has to be considered when simulating these spectra in the mass balance between the Si atom and the carbon atom. Since Pd is a non-carbide forming metal, it is expected that for every Pd atom that reacts with a Si atom to form a silicide, a free carbon atom has to be expelled into the system. That is, the carbon atom is left immobile in the system. Therefore during the simulation the mass balance between Si atom and the C atom was checked.

Figure 4.14 and 4.16 shows the composition of the elements as the function of depth obtained by using a two-layered model employed in fitting the spectra of the sample annealed at 500^0C and at 600^0C. The interface of Pd/SiC in these spectra was also found to be relatively rough. Therefore due to the roughness of the interfaces, the reaction layers had to be fuzzed in order to fit the rough interfaces. The dotted line in the elemental composition for the samples annealed at 500^0C, 600^0C, 700^0C and 800^0C indicates a fuzzed (rough) interface. The relative amounts of the Pd:Si:C used in the simulation are shown in table 4.1.

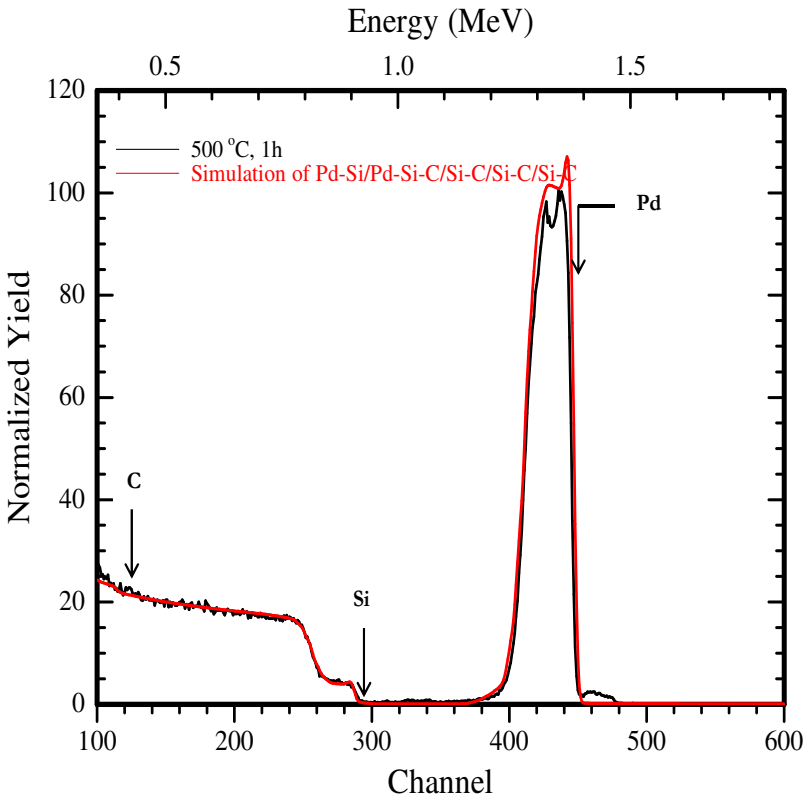

Figure 4.13: RBS spectrum for the sample annealed at 500^0C(b) fitted with RUMP.

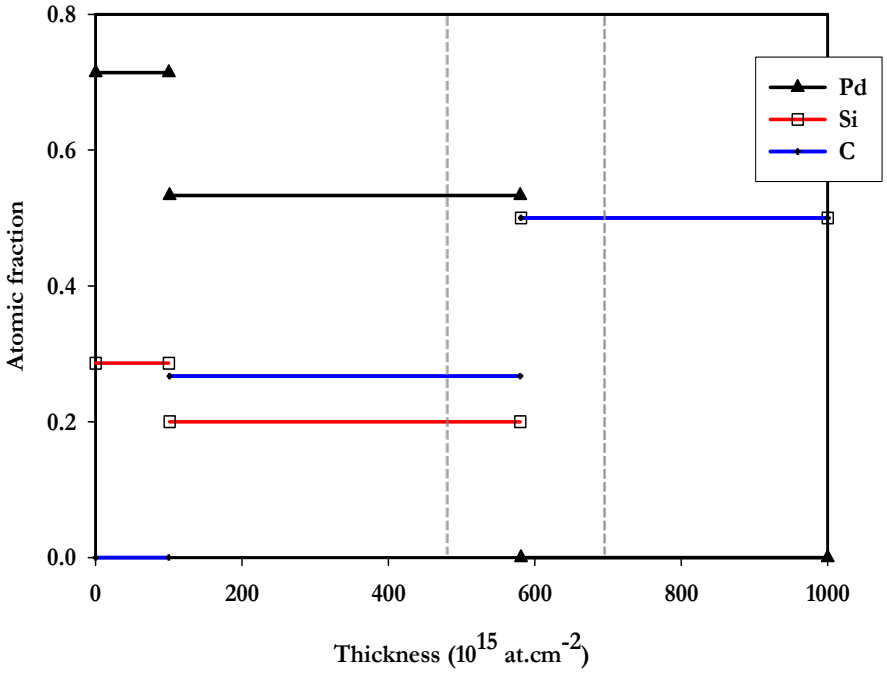

Figure 4.14: Elemental composition of the sample annealed at 500^0C(b) as a function of depth. The dotted line indicates fuzzing of 200 in 5 steps of the rough interface of the second layer.

The RBS / RUMP simulated spectra corresponding to the samples annealed at 700^0C and 800^0C are depicted in figure 4.17 and 4.19 respectively. The spectra also indicated a featured loss of the Pd signal from the top surface as refered to the as-deposited sample. The leading edge of the Si signal indicated the formation of compound silicide. The formation of the two-layered structure is more pronounced in the samples annealed at these temperatures, therefore the proposed two-layered structure model was again used in determining the layer-by-layer composition in the spectrums. Figure 4.18 and 4.20 shows the elemental composition curves as a function of depth for the samples annealed at 700^0C and 800^0C respectively obtained by using the two-layered structure model.

In ideal simulations, the interface between the layers are absolutely sharp and planar. However, in reality the interfaces are slightly fuzzy or non-uniform. Thus the fuzz command simulates the literal non-uniformity by averaging several structures with a slightly different layer thickness. Therefore, for each layer to be fuzzed, it is necessary to specify the layer number, the average thickness of the layer (fuzz amount) and the number of iterations. Therefore, due to the roughness of the interface of Pd/SiC, the dotted lines in the graphs indicates a fuzzed interface. For the sample annealed at 800^0C the first layer was not fuzzed but the second layer was quite non-uniform in thickness and thus fuzzing was used. The relative amount of the Pd, Si and C for both layers are also indicated in table 4.1.

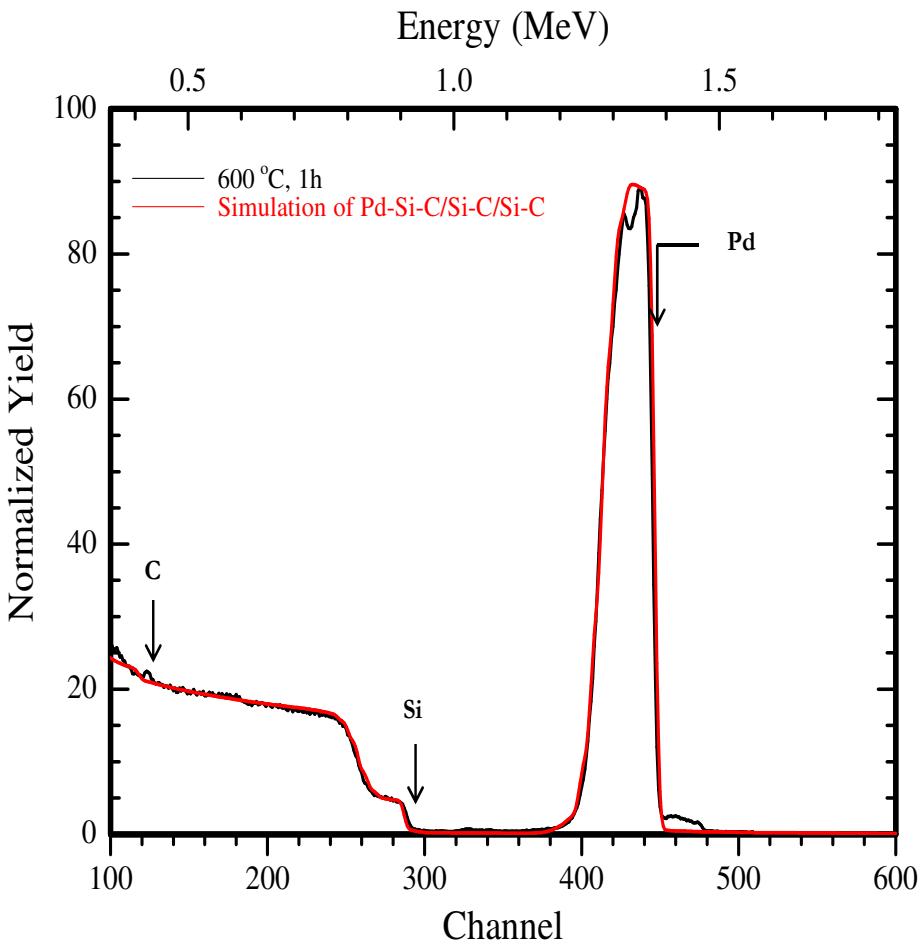

Figure 4.15: RBS spectra for the sample annealed at 600^0C fitted with RUMP.

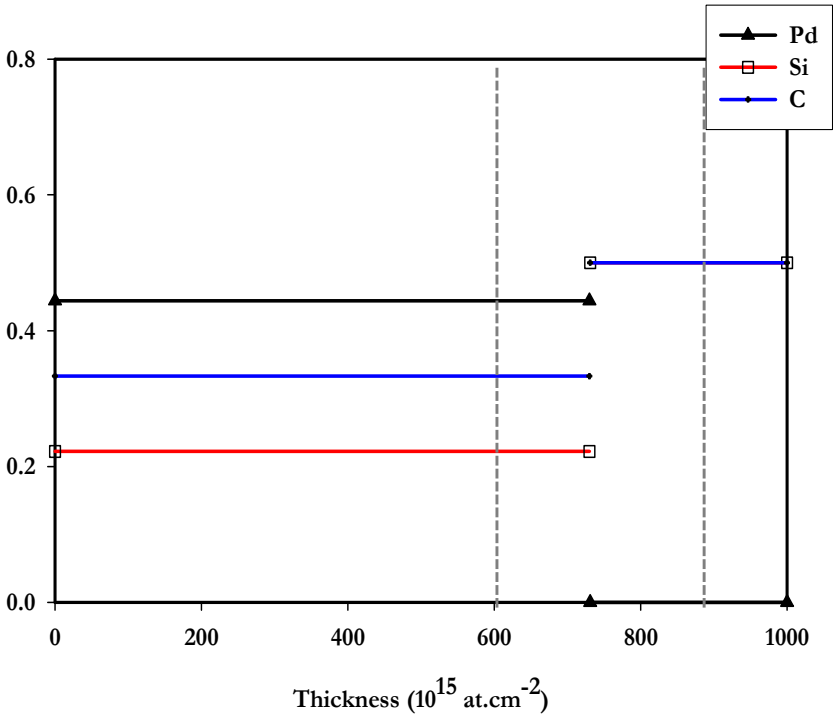

Figure 4.16: Elemental composition of the sample annealed at 600^{0}C as a function of depth. The dotted line indicates the fuzzing of the rough interface with a fuzzing of 250 in 5 steps for the entire layer.

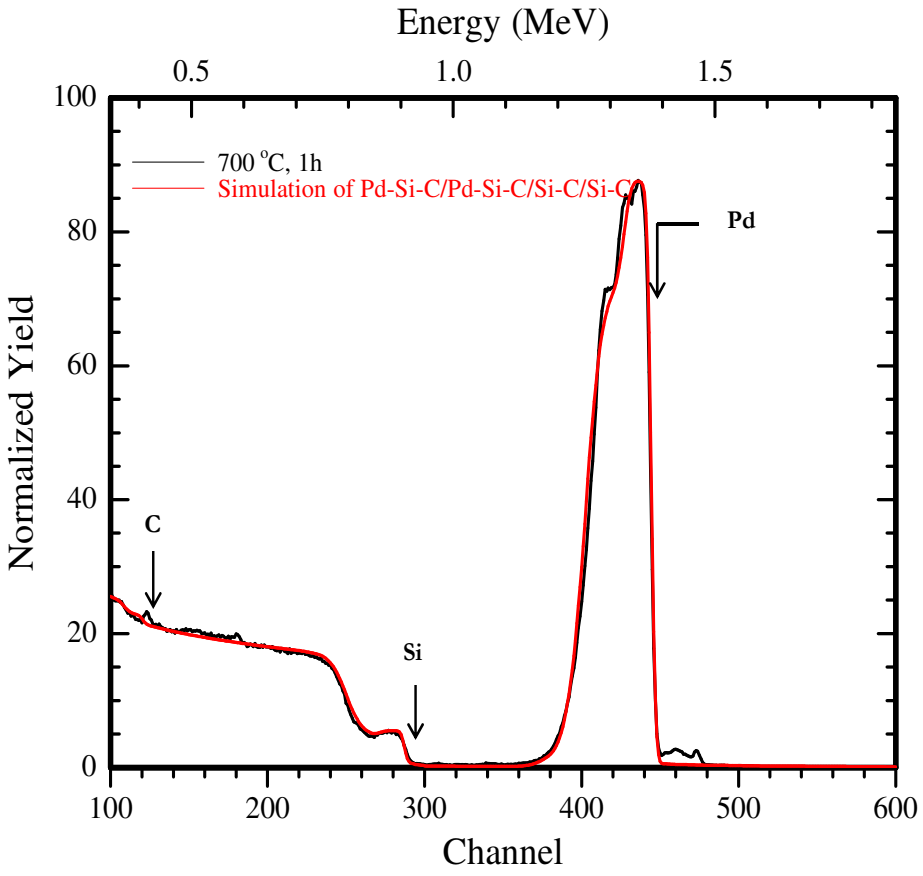

Figure 4.17: RBS spectrum for the sample annealed at 700^{0}C fitted with RUMP.

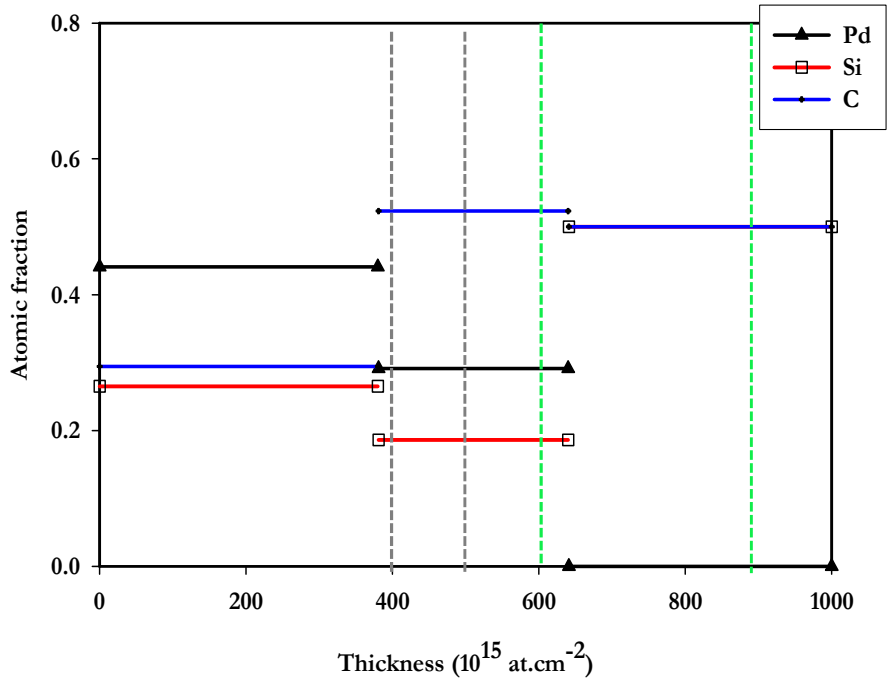

Figure 4.18: Elemental composition of the sample annealed at 700^{0}C as a function of depth. The dotted line indicates that the first layer has been fuzzed by 100 in 5 steps and the second layer has a fuzzing of 250 also in 5 steps during the simulation.

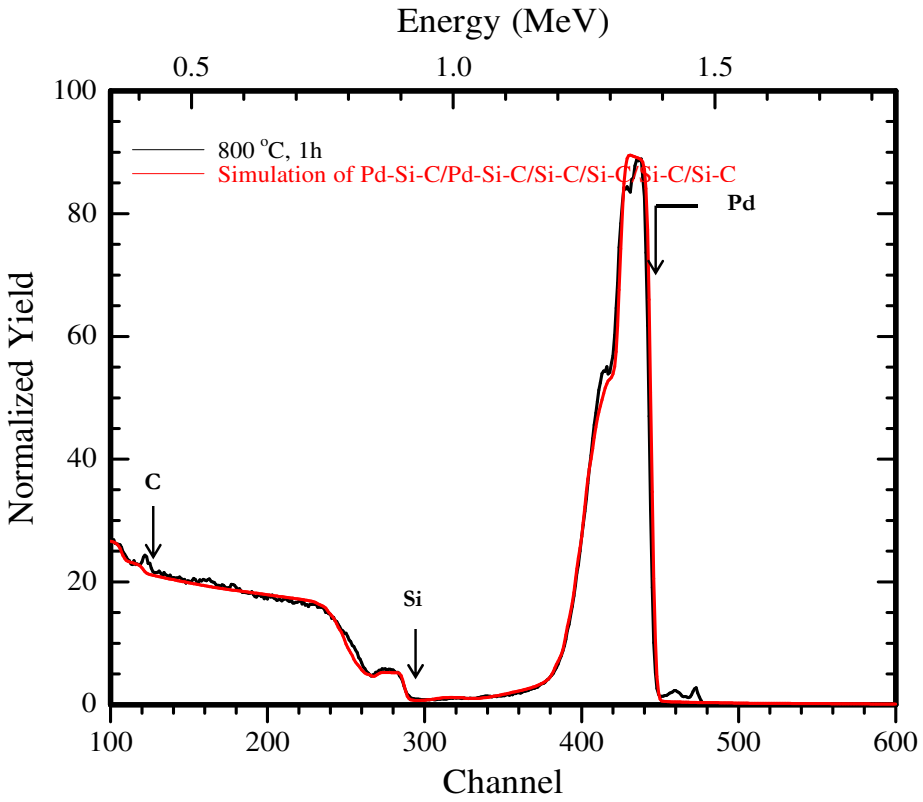

Figure 4.19: RBS spectrum for the sample annealed at 800^{0}C fitted with RUMP.

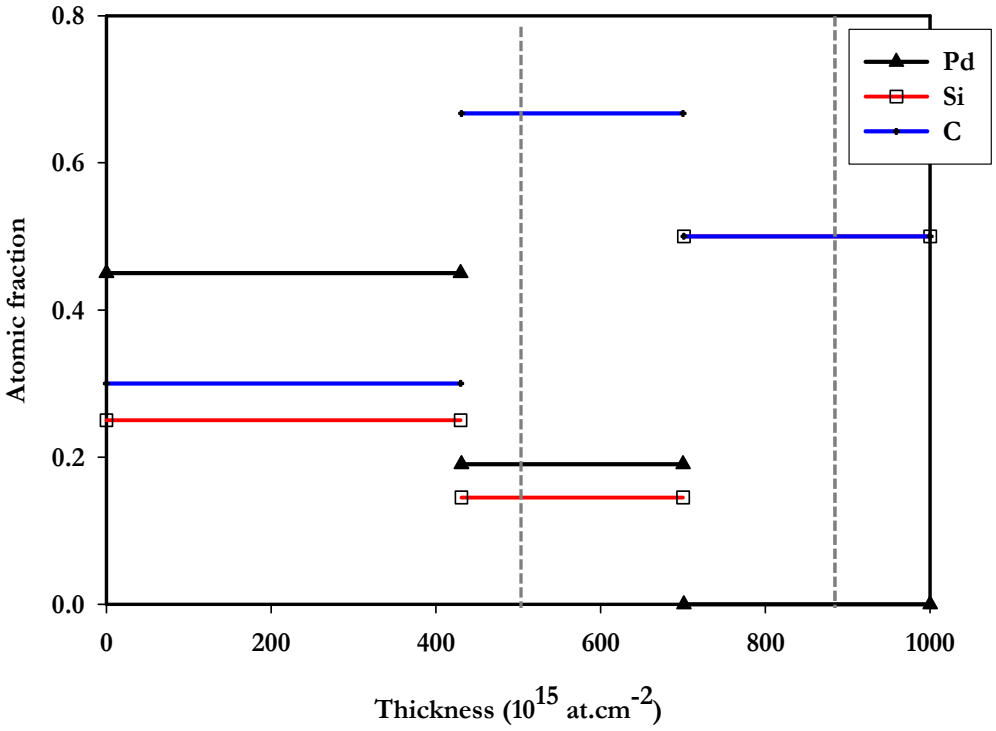

Figure 4.20: Elemental composition of the sample annealed at 800^{0}C as a function of depth. The dotted line shows that only the the rough interface of the second layer was fuzzed at 400 in 5 steps, the first layer was not fuzzed during the simulation.

Temp(^{0}C)	First layer		Second layer	
	Thickness (10^{15}at.cm^{-2})	Rel. amount(%) Pd:Si:C	Thickness (10^{15}at.cm^{-2})	Rel. amount(%) Pd:Si:C
25	480	90:0:10	0	...
400	521	72.1:0:27.9	0	...
500	100	71.4:28.6:0	580	53.3:20:26.7
600	730	44.4:22.2:33.3	0	...
700	380	44.1:26.5:29.4	640	29.1:18.6:52.3
800	430	45:25:30	700	19.1:14.3:66.7

Table 4.1: Relative amounts of the reaction products and their thicknesses.

4.1.4 Glancing-Incident X-ray Diffraction analysis

Glancing-Incident X-ray Diffraction (GIXRD) study was used to identify the Pd silicide phases, if any, at the Pd/6H-SiC interfaces. The angle of incident of the X-ray beam (Cu) was kept at an angle of 1^0 with respect to the sample surface. The minimum contribution from the substrate. The diffraction spectra shown from figure 4.21 to 4.26 were collected at 2θ range between the angles of 26.5^0 and 95^0 since the major peaks of Pd and Pd silicides appear within this range. The experimentally obtained diffraction patterns were compared with the International Center for Diffraction Data (ICDD) powder diffraction database for peak identification.

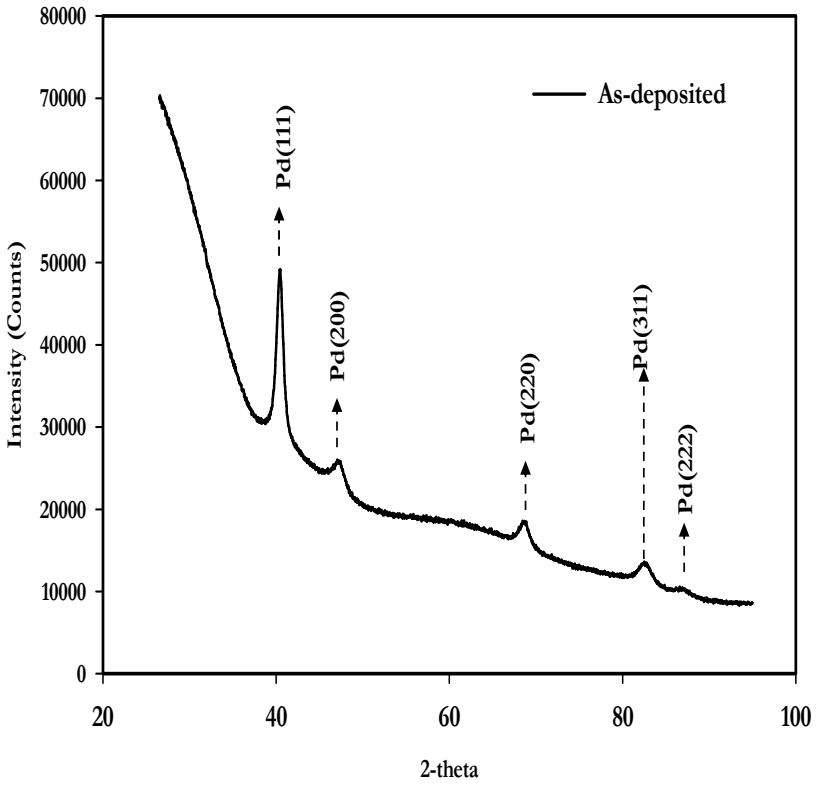

Figure 4.21: As measured diffraction pattern of the as deposited Pd-SiC sample.

The diffraction spectra recorded on as-deposited Pd/6H-SiC interface (figure 4.21) showed no evidence of any peak that can be attributed to Pd silicides. The diffraction spectra for the samples annealed at 200^0C and 300^0C also showed no peak which could be attributed to the Pd silicides. These results further ratifies the RBS/RUMP analysis which indicate that the Pd top layer remains unreacted with SiC after annealing at 200^0C and 300^0C for a period of one hour each.

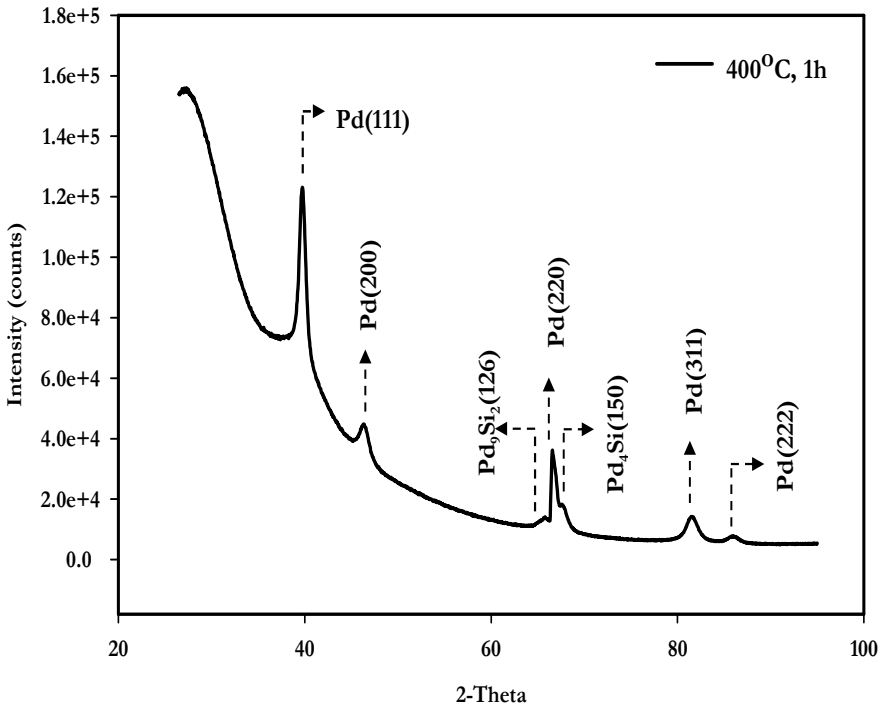

Figure 4.22: As measured diffraction pattern of the sample annealed at 400^0C.

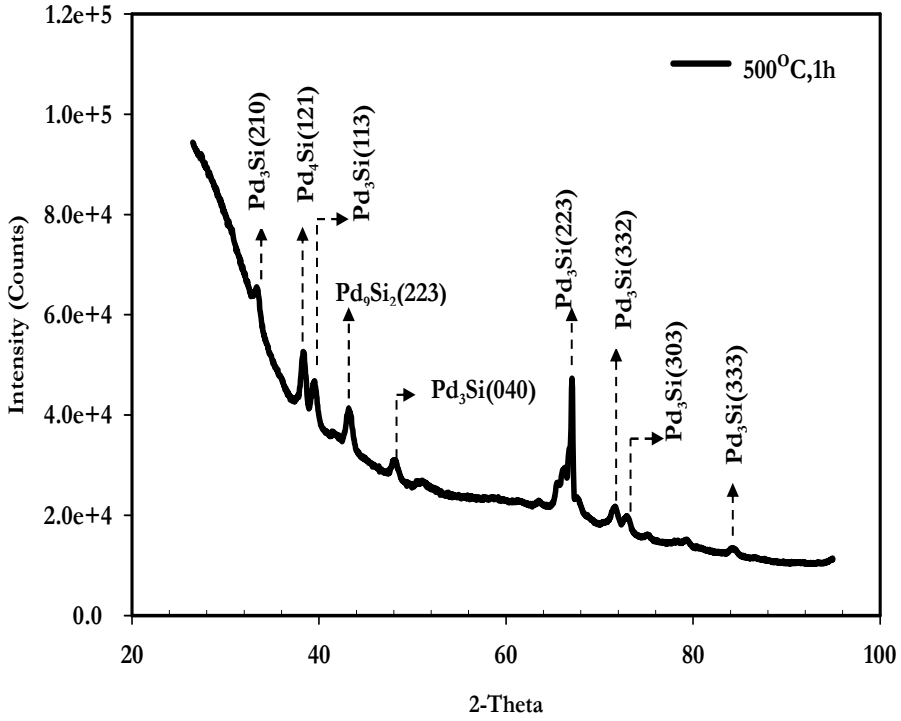

Figure 4.23: As measured diffraction pattern of the sample annealed at 500^0C.

For the sample annealed at 400^0C two metal-rich silicides were identified together with the unreacted Pd as shown in figure 4.22. The two identified metal-rich silicides were Pd_4Si, Pd_9Si_2. Thus annealing the Pd/SiC interface at 400^0C resulted in the formation of the metal-rich silicides and unreacted Pd.

The diffraction pattern showed in figure 4.23, is the diffraction pattern for the sample annealed at 500^0C. A large number of metal-rich Pd silicides were identified in this spectrum namely Pd_3Si, Pd_4Si and Pd_9Si_2. From the diffraction pattern of this spectrum one notices an addition new phase Pd_3Si forms when annealing at 500^0C apart from the two phase observed at the 400^0C diffraction pattern.

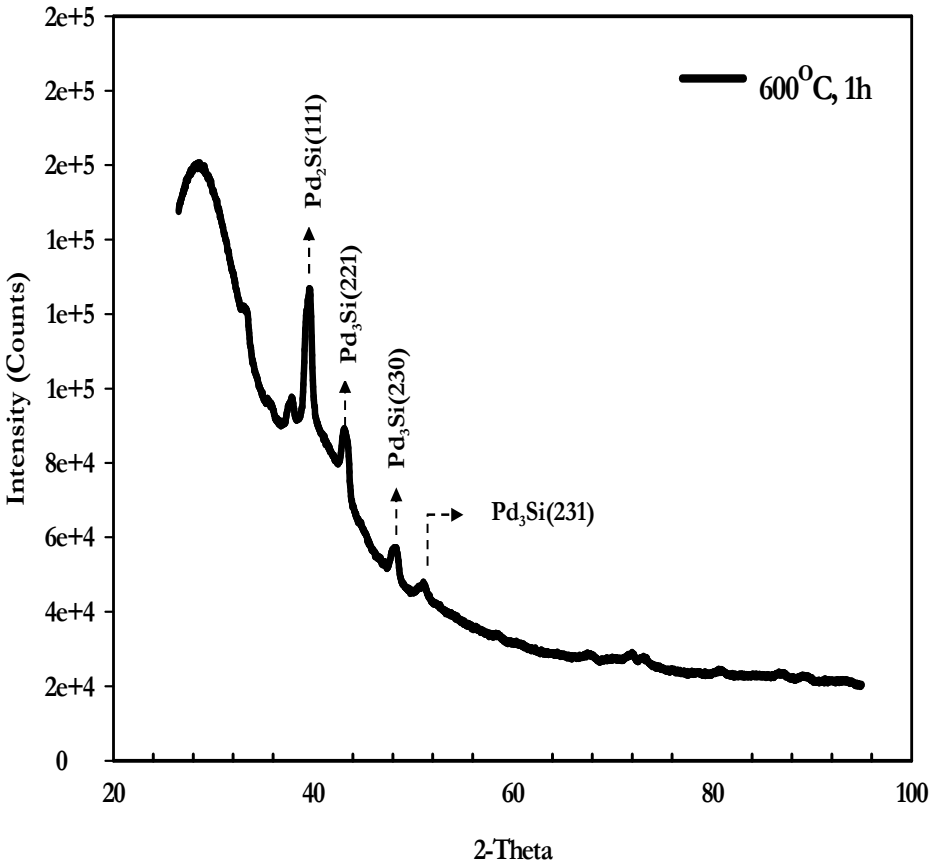

Figure 4.24: As measured diffraction pattern of the sample annealed at 600^0C.

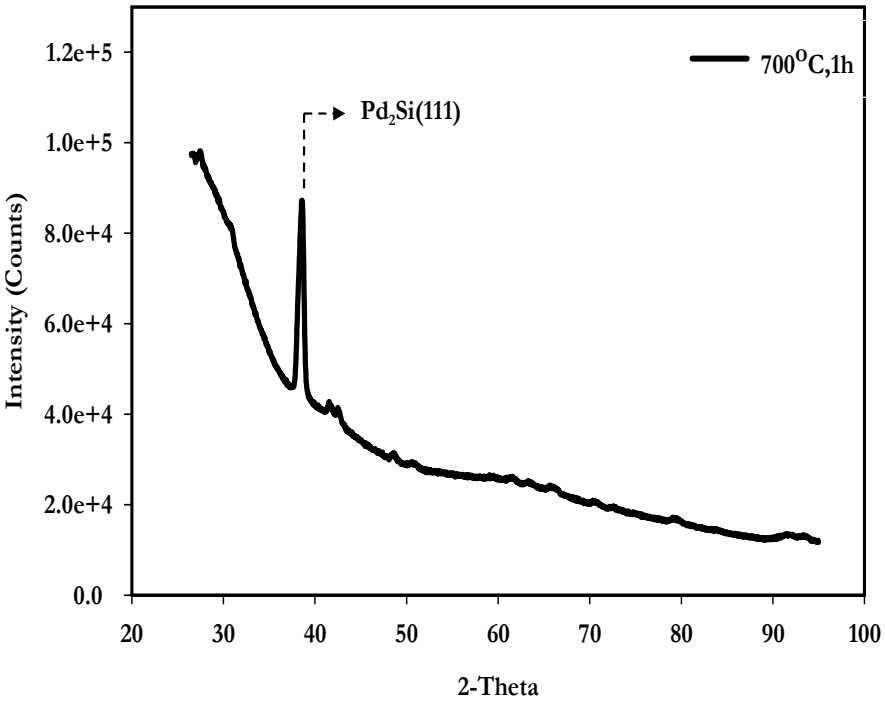

Figure 4.25: As measured diffraction pattern sample annealed at 700^0C.

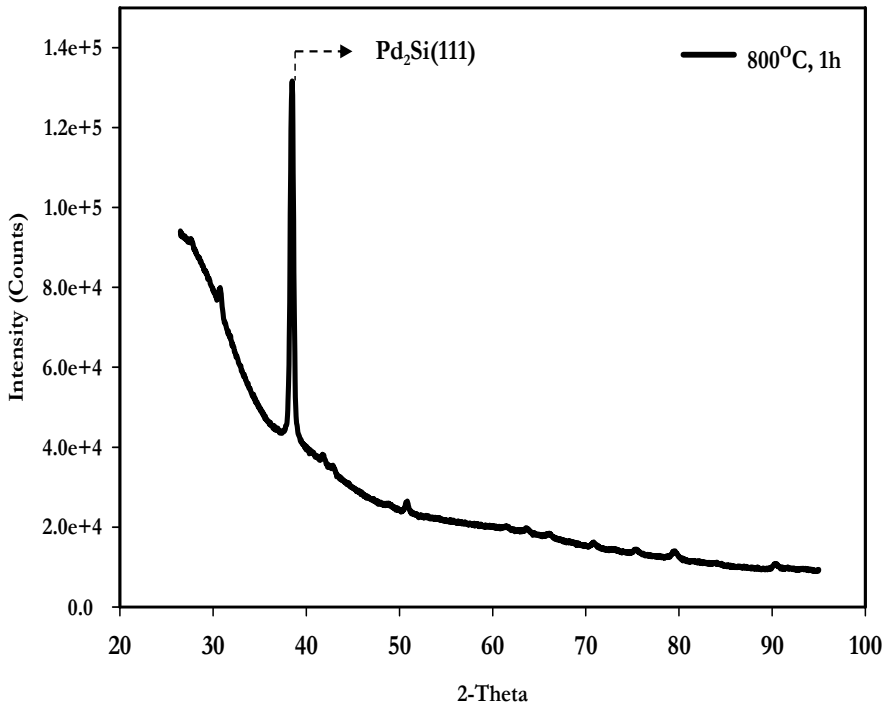

Figure 4.26: As measured diffraction pattern sample at 800^0C.

The diffraction pattern of the sample annealed at 600^0C is shown in figure 4.24. In this diffraction pattern metal-rich silicide Pd_3Si was observed followed by the formation of the Si-rich silicides Pd_2Si, the other metal-rich silicides observed on the samples annealed at 400^0C and 500^0C were found to have disappeared. For the samples annealed at 700^0C and 800^0C only Si-rich compound of Pd_2Si was found to be stable and the other metal-rich silicides observed previously were not identified. It can also be noted that from 600^0C to 800^0C the Pd_2Si (111) reflection increases in intensity.

Temperature (^{0}C)	Phase Identified
As-deposited	Pd
200	Pd
300	Pd
400	Pd, Pd_4Si, Pd_9Si_2
500	Pd_3Si, Pd_4Si,Pd_9Si_2
600	Pd_2Si, Pd_3Si
700	Pd_2Si
800	Pd_2Si

Table 4.2: Phase identification of the Pd/SiC interface at different temperatures.

Table 4.2 gives a list of the phases observed at different temperatures. The XRD results observed above show that the interaction between Pd and SiC commences at a temperature of 400^0C where the is an intermixing of the atoms resulting in the formation of metal-rich silicides. It should however be noted that the results also indicate that although the Pd reacts with SiC at this temperature not all the Pd atoms participates in the reaction. This is indicated by the presence of the unreacted Pd peak observed in figure 4.22. At 500^0C, the results shows that the Pd continues to interact with SiC also forming the metal-rich silicides. In addition to these phases which were also observed at 400^0C another metal-rich phase Pd_3Si appears and the Pd phase disappears. When annealing at higher temperatures, 600^0C only one metal-rich silicide is observed followed by the formation of the Si-rich silicide. Annealing at 700^0C only one Si-rich phase Pd_2Si is observed and this phase becomes stable even after annealing at 800^0C.

Our GIXRD study indicates that Pd only starts to reacts with SiC at the temperature of 400^0C which complements the results obtained by RUMP simulation. The invisibility of the reaction observed with the RBS spectrum could be due to the fact that the silicides formed are not thick enough to be detected by RBS. However, the RBS spectrum does show a decrease in Pd concentration and an increase in the carbon content in the top layer. This carbon can only come from the dissociation of the SiC, which would indicate the start of silicide formation. Looking at the diffraction patterns, one notices the broad diffraction peaks, the peak broadening could be due to the very thin-layer of palladium resulting in the small grain size formation during the reaction, therefore the smaller the grain sizes the broader the peak will appear. In some instances however, the broadening of the diffraction peaks could be as a result of the multi-phase formation which are overlapping onto one another resulting in the broadening of peaks.

4.1.5 Scanning Electron Microscopy

Figure 4.27 shows the SEM micrographs of the surfaces for the as-deposited samples and the samples annealed at temperatures of 400^0C to 800^0C each for a period of 1 hour. The surface analysis of these samples was performed using the ZEISS ULTRA 55® SEM at the University of Pretoria. The electron beam with a low accelerating voltage of 1kV for high surface resolution was used and the secondary electron images were obtained.

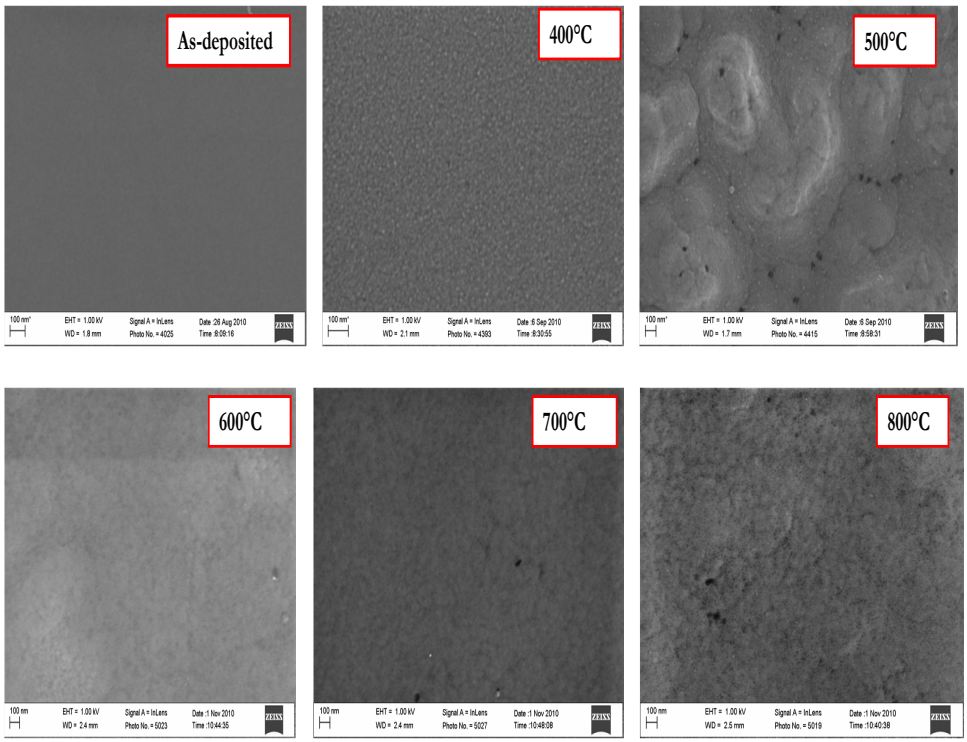

Figure 4.27: Scanning electron microscopy images of surface before and after annealing at 400^0C to 800^0C with a magnification of 100nm and energy of 1kV.

The micrograph of the as-deposited sample indicates a smooth / uniform deposition of the layer of Pd on the SiC substrate. No evidence of the reaction taking place at the surface is observed for the as-deposited sample. The surface of the samples annealed at 200^0C and 300^0C were similar to the as-deposited sample surface. For the sample annealed at 400^0C, the surface topography indicated the formation of light phases partially covering the surface layer.

For the sample annealed at 500^0C significant changes in the surface is observed when compared to the surface of the as-deposited and the surface of the sample annealed at 400^0C. The surface of the sample after annealing at this temperature became rough and showed the formation of structures covering the entire surface of the sample. These structures were observed to be surrounded by dark areas. For the sample annealed at 600^0C the surface indicated the traces of the structures observed on the 500^0C surface, but these structures were less pronounced. Also the dark areas decorating the structures observed on the surface of the sample annealed at 500^0C were not observed on the surface of the sample annealed at 600^0C.

The surface area for the samples annealed at 700^0C and 800^0C showed the evidence of the reaction between Pd and SiC. The surface area of these anneals became rough but the structures structure observed in the samples annealed at 500^0C and 600^0C were not observed. The dark

areas decorating the structures which were observed in the surface area of the sample annealed at 500^0C were also observed in the surface area of these samples but they appeared to be much less.

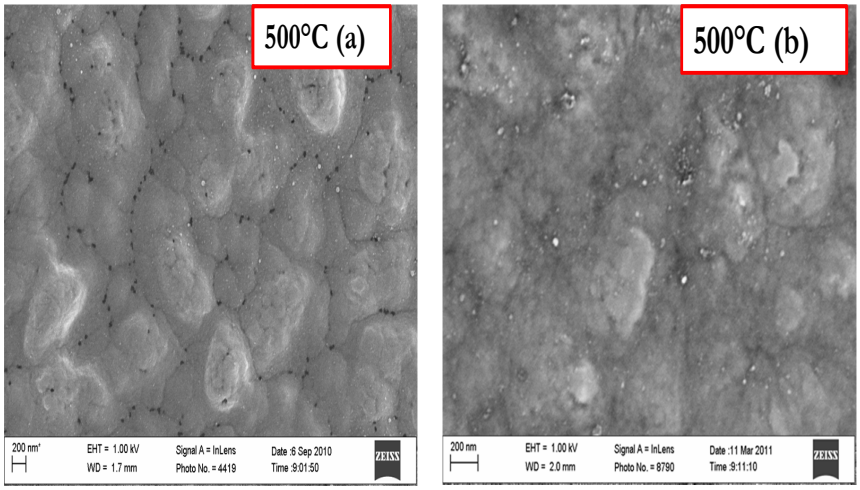

Figure 4.28: Scanning electron images for the samples annealed at 500^0C. *Left panel:* shows the first annealed samples at 500^0C, namely 500^0C (a) and *Right panel:* shows the repeated 500^0C samples, namely 500^0C (b)

.

The results obtained in figure 4.27 showed an drastic change in the sample annealed at 500^0C, with this change not observed at higher annealing temperatures. Therefore, due to the vast differences between the surface appearance of the sample annealed at 500^0C and the samples annealed at 600^0C, 700^0C and 800^0C, a new as-deposited sample was annealed again at 500^0C to confirm the results which were obtained in figure 4.27.

Figure 4.28 shows the secondary electron micrographs for the samples annealed at 500^0C, (a) being the first deposition and (b) being the second deposition of the samples annealed at 500^0C. The 500^0C (b) sample showed the same anomalies as observed in the 500^0C (a) sample. The surface area of these samples appeared to be the same in terms of surface roughness and formation of structures on the surface. However, in the 500^0C (b) surface, the dark areas decorating the structures were not observed.

4.2 Discussion

The results obtained using the backscattering spectrometry showed no detectable reaction of Pd with the single crystal SiC at room temperature. Furthermore no evidence of reaction was observed after annealing at temperatures of 200^0C and 300^0C. These results were complemented by the simulation spectra obtained by using RUMP simulation package, which indicated no phase formation at the Pd/SiC interface. GIXRD, performed on the as-deposited samples and the samples annealed at 200^0C and 300^0C showed no formation of the Pd silicide. GIXRD only indicated the presence of the Pd phase. The surface topography obtained using SEM showed a smooth clean deposition of Pd layer for the as-deposited sample and for the samples annealed at low

temperatures of 200^0C and 300^0C no change in the surface morphology was observed.

Annealing at 400^0C showed a decrease in the concentration of Pd atoms on the surface layer which was attributed to the dissociation of the Si atoms from the tightly bound SiC and their migration to the Pd layer, resulting in the reaction of some of the Pd atoms with the Si from the SiC substrate. However, this reaction is not observed by RBS. The invisibility of the reaction at the Pd/SiC interface on the RBS spectrum for the sample annealed at 400^0C could be due to the insensitivity of the RBS technique for layers with a thickness of less than 10 nm. Simulation by RBS/RUMP indicated an increase in the thickness of the Pd layer, which was associated with some of the atoms from SiC migrating into the Pd layer. The GIXRD identified metal-rich silicides such as Pd_9Si_2 and Pd_4Si as well as unreacted Pd metal. This indicated that at 400^0C not all the Pd is consumed during the reaction which resulted in the formation of silicides. No carbon compounds are observed by RBS/RUMP. The SEM micrograph for the sample annealed at 400^0C showed the formation of light phases partially covering the surface when compared to the as-deposited sample. Since not all the Pd metal is participating in the reaction, the reaction occurring at 400^0C can be summarized by the expression below:

$$Pd + SiC \longrightarrow Pd_xSi + Pd + C$$

Temperature (^{0}C)	Pd:Si ratio by RBS	Phase identified by XRD
25	...	Pd
400	....	Pd, Pd_4Si, Pd_9Si_2
500	2.5 and 2.6	Pd_3Si, Pd_4Si
600	2	Pd_2Si, Pd_3Si
700	1.7 and 1.6	Pd_2Si
800	1.8 and 1.3	Pd_2Si

Table 4.3: Phase and atomic ratios of the reaction products of Pd on SiC.

Annealing at the temperatures of 500^0C and 600^0C resulted a compound formation between the Pd and SiC. The reaction at these temperatures proved to be aggressive with very rough interfaces forming. The leading Si signal edge on the backscatter spectrum indicated that the Si was now on the surface layer and it had completely reacted with all the Pd leaving no free Pd metal during the reaction. The RBS/RUMP simulation was used in simulating the layer-by-layer composition of the reaction products. In the simulation a two-layer structure model is used to explain the formation of the phases and the reaction morphology. This model suggested that when the reaction between Pd and SiC occurs, it does not form a single phase but forms a number of phases in the reaction zone. Our measurements with RBS, only gives the average composition of all the phases in the system, making it impossible to predict or identify these phases using RBS/RUMP. The average composition of these phases is presented in table 4.1. The relative amounts in table 4.1 was used to determine Pd:Si ratio in the reaction products. The Pd:Si ratio after annealing at 500^0C was measured to be 2.5 and 2.6 for the first and the second layer respectively. At 600^0C the Pd:Si atomic ratio is measured to be 2.0.

To identify the phases which form GIXRD was employed and it indicated that all the Pd metal participates in the formation of silicides at temperatures greater and equal to 500^0C. At 500^0C, metal-rich silicides such as Pd_9Si_2, Pd_4Si and Pd_3Si are formed. The surface of the sample annealed at 500^0C as investigated by high resolution SEM, the surface of this sample became rough

when compared to the as-deposited sample and the sample annealed at 400^0C. The formation of structures containing dark areas (carbon) was also observed in the surface. At 600^0C, the rough surface was also observed with the traces of the same structures observed at the 500^0C. However, in this case the dark amorphous carbon areas observed in the surface of the sample annealed at 500^0C was not seen. The reaction occurring for the samples annealed at 500^0C and 600^0C can be summarized by the reaction below:

$$\mathrm{Pd} + \mathrm{SiC} \longrightarrow \mathrm{Pd}_x\mathrm{Si} + \mathrm{C}$$

For the samples annealed at 700^0C and 800^0C a reaction between Pd and SiC is observed on the RBS spectrum and the formation of more than one compound as shown by XRD is more pronounced in the RBS spectra. RBS / RUMP was employed in determining the layer-by-layer composition of the reaction products by also employing the two-layered structure model. Table 4.1 showed the relative amounts of Pd:Si:C used during the simulation and the Pd:Si ratio in the reaction products after annealing at 700^0C were measured to be 1.7 and 1.6 for the first and the second layer respectively. For the sample annealed at 800^0C the relative amounts in table 4.1 were also used to measure the Pd:Si ratio. The ratios were measured to be 1.8 and 1.3 for the first and the second layer as shown in table 4.3.

The relative amount of carbon in the samples annealed at 700^0C and 800^0C showed an increase in the amount of carbon we had to include in during simulation. This increase in the carbon amount is attributed to the incomplete reaction of SiC grains and the free carbon that results when the Si atoms dissociate from the Si-C bond to react with Pd to form a silicide at the interface. That is, at these high annealing temperatures the Pd metal gets quickly consumed during the reaction and there is not enough Pd metal available in the system to react with all the SiC available for the reaction. This phenomena was also observed by Demkowicz *et al.,* (2008) after annealing SiC with Pd at 1000^0C for 10 h (see figure 4.29). Demkowicz *et al.,* (2008) observed that the region adjacent to SiC (figure 4.29 (b)) gave the reaction product consisting of incompletely reacted SiC grains, carbon and $\mathrm{Si}_x\mathrm{Pd}_y$ intermetallics. Therefore the reaction occurring at 700^0C and at 800^0C is most likely consistent with the reaction observed by Demkowicz and co-workers.

GIXRD measurements identified the compounds formed after annealing at higher temperatures and only one Si-rich phase $\mathrm{Pd}_2\mathrm{Si}$ was present for both anneals. The SEM micrographs of both samples showed a rough surface when compared to the as-deposited sample and smoother surface when compared to the samples annealed at 500^0C and 600^0C. The smoothness of the surface could be attributed to the disappearance of the metal-rich silicides leading to the formation of Si-rich structures . The amorphous free carbon present as dark areas on the surface of the sample was also observed at high annealing temperatures.

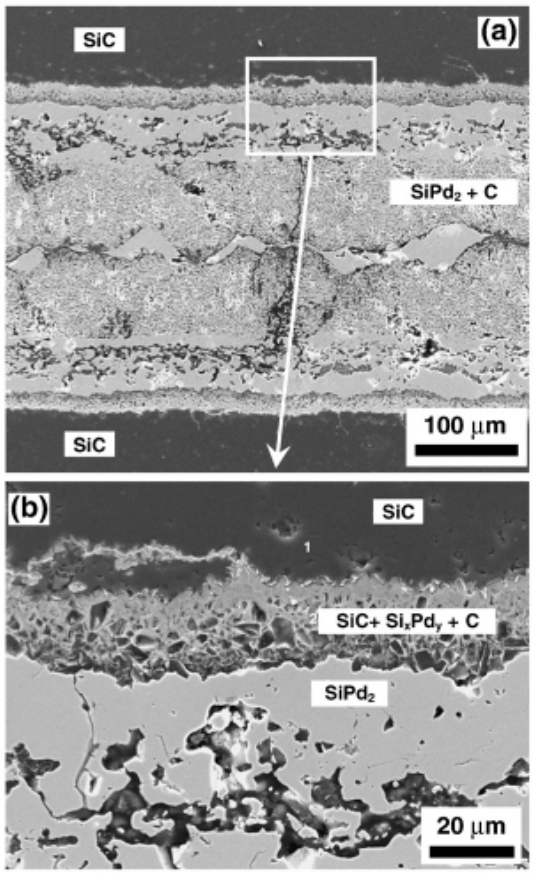

Figure 4.29: Pd-SiC interface annealed at 1000^0C for 10 h (Demkowicz *et al.*, 2008).

Silicide formation by solid-stated reaction between Pd and Si shows that metal-rich silicides form first with some free Pd still available in the system at low temperature. At high temperatures, metal-rich silicides are also observed and they continue to grow until all the Pd is consumed. When the Pd has been consumed, Si-rich silicides start appearing and the metal-rich silicide disappear. The Si-rich silicides continue to grow by simply consuming all the metal-rich silicides and reach a stage where a uniform phase is formed due to the fact that there is not enough Pd metal available in the system to form any other phases.

Our study shows that no carbon compounds are found to form during the reaction, thus confirming that Pd is a non-carbide forming metal. Therefore the formation of the Pd silicides will be accompanied by free carbon which is immobile in the system. The formation of the phase sequence can be predicted by using an isotherm ternary phase diagram such as the one obtained by Bhanumurthy and Schmid-Fetzer (2001), shown in figure 4.30. The ternary diagram shows the phase formation sequence indicated by the diffusion path for a diffusion couple annealed at 800^0C. The phase diagram shows that at this temperature three phases Pd_9Si_2, Pd_3Si and Pd_2Si co-exist with each other.

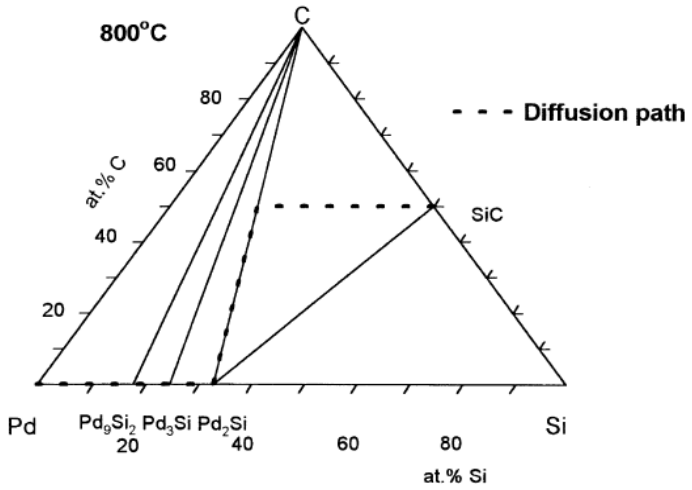

Figure 4.30: Pd-Si-C isothermal section (800^{0}C) with dotted lines representing the diffusion path determined by the diffusion couple (Bhanumurthy and Schmid-Fetzer, 2001).

Therefore the reaction morphology or phase formation in thin-film diffusion couples between Pd and 6H-SiC depends on three parameters, temperature, time and the availability of the Pd metal. That is, the reaction taking place at the Pd/6H-SiC interface at low temperatures for a given period of time, will proceed slowly resulting in the formation of the metal-rich silicides. However, due to the time available the reaction taking place at low temperature does not have sufficient time for the entire Pd metal to react and to afford an opportunity for other silicides such as the Si-rich silicide Pd_2Si to grow. Therefore, if the reaction taking place at low temperature had enough time for the reaction to continue, it is speculated that all the Pd metal will be consumed and Si-rich silicides will begin to appear. At high annealing temperatures for the same given period of time, the reaction occurring at the Pd/SiC interface occurs very rapidly and the Pd in the system gets quickly consumed resulting in the formation of metal-rich silicides first followed by the formation of Si-rich silicides such as Pd_2Si which become stable at high temperatures investigated in this study.

The reaction sequence taking place at the Pd/SiC after annealing will consist of silicides with free carbon. At low annealing temperatures, an unreacted Pd and silicides with carbon will result and at high annealing temperatures silicides with free carbon and an incompletely reacted SiC grains giving an increase in the carbon in the system will result. The phase sequence for the Pd/SiC before and after thermal annealing at temperatures of 400^{0}C, 500^{0}C, 600^{0}C, 700^{0}C and 800^{0}C is summarized as: Pd—Pd_9Si_2 + C— Pd_4Si + C— Pd_3Si + C— Pd_2Si + C.

Our work correlates well with the work done by Pai and co-workers,(1985). The difference being that in their work they reported the reaction between Pd and SiC to only take place after annealing at 500^{0}C with all the Pd reacting with an unspecified polytype of SiC. In their work, Pai *et al.,* (1985), also reported that the metal-rich silicides form first followed by the formation of Si-rich silicides Pd_2Si only appearing after annealing at 700^{0}C with another metal-rich silicide Pd_3Si. At 800^{0}C and 900^{0}C only Pd_2Si was found to be stable. In our study, we observe the reaction between Pd and SiC to take place at a low temperature of 400^{0}C and the appearance of the Si-rich silicide Pd_2Si at a relatively lower temperature of 600^{0}C and the metal-rich silicide Pd_3Si is not seen after annealing at 700^{0}C. The Pd_2Si phase is found to be stable after annealing at 700^{0}C and at 800^{0}C.

The formation of silicides in the Pd-Si-C system is different from the formation of silicides

in the Pd-Si system. Firstly, in the Pd-Si system, the reaction commences at relatively low temperatures of 250^0 resulting in the formation of the Si-rich silicide Pd_2Si. This silicide is found to exist even after annealing at temperatures of 800^0C. In the Pd-Si-C the reaction between Pd and SiC only occurs at 400^0C and results in the formation of metal-rich silicides, rather Pd_2Si. The Pd_2Si phase is only observed after annealing at 600^0C and remains stable at higher annealing temperatures.

Reference

Bhanumurthy K., Schmid-Fetzer R., 2001, Compos. Part A-Appl. Sci. **32**, 569.

Demkowicz P., Wright K., Gan J. , Petti D., 2008, Solid State Ionics **179**, 2313.

Pai C.S., Hanson C.M. and Lau S.S, 1985, J. Appl. Phys. **57**, 618.

Chapter 5

Conclusion

5.1 Conclusion

In this work we set out to investigate the metallurgical interaction of Pd with single crystal SiC for thin-film diffusion couples at low and high temperatures. To do this, 6H-SiC substrate were deposited with a thin-layer of Pd consisting of a thickness of 500$\mathring{A}$ at room temperature. Rutherford backscattering spectrometry in conjunction with RUMP simulation package showed that the Pd does not react with SiC at room temperature for thin-film diffusion couples. GIXRD studies did not identify any Pd silicides at room temperature and the surface micrograph obtained by using SEM showed no evidence of the formation of silicides, instead a smooth uniform deposition of Pd on the surface was observed. The same behaviour was observed for the samples annealed at 200^0C and 300^0C.

Analysis of the sample annealed at 400^0C by RBS and RUMP indicated a decrease in the concentration of the Pd atoms on the Pd peak in the substrate. It also showed the widening of the surface peak with an unspecified thickness, which indicated that some light atoms have diffused into the Pd layer. The GIXRD results revealed the formation of more than one metal-rich silicide layers and an unreacted Pd metal layer. The surface micrographs of the sample annealed at 400^0C showed the formation of light phases covering the surface. Annealing at 500^0C and 600^0C, the reaction between Pd and SiC proved to be more extensive, with the Si signal on the RBS spectrum appearing at its surface. GIXRD results showed that at these annealing temperatures resulted in the formation of two or more metal-rich silicides at 500^0C followed by the formation of Si-rich silicides at 600^0C and the disappearance of metal-rich silicides. The surface micrographs for the samples annealed at 500^0C appeared to be rough when compared to the 600^0C sample with the carbon appearing as dark spots on the samples. The dark areas observed on the sample annealed at 500^0C were not seen on the 600^0C sample.

For the samples annealed at 700^0C and 800^0C, Pd had completely reacted with silicon carbide forming more than one Si-rich silicides. The GIXRD results showed that, the reaction taking place resulted in the formation of a uniform phase with all the other phases observed at the preceding temperature disappearing. The simulation at these temperature revealed a high content of carbon, which was attributed to the free carbon released when Si atom react with Pd and liberating the carbon into the system and the other carbon was from the incompletely reacted SiC grains. The micrographs of the sample annealed at 700^0C and at 800^0C appeared to be rough when compared to the surface of the as-deposited sample and the samples annealed at 400^0C, but the roughness was less when compared to the surfaces annealed at 700^0C and 800^0C. The dark areas observed at the surface of the sample annealed at 500^0C was also observed in the samples annealed at 500^0C and 600^0C. Annealing at a temperature range of 400^0C to 800^0C showed no formation of carbon compounds, therefore the formation of silicides at these temperatures is accompanied by the formation of free carbon.

In general, our study shows that the reaction between Pd and SiC will only take place after annealing at 400^0C and will result in the formation of metal-rich silicides and unreacted Pd. These metal-rich silicides disappear when annealing at high temperatures and the Si-rich silicides start to appear and all the Pd becomes completely reacted. The formation of these silicides is accompanied by the free carbon which remains immobile in the system as stated in the literature (Bhanumurthy and Schmid, 2001).

5.2 Future work

Our research has shed some light in the formation of phase when Pd reacts with SiC at low and high annealing temperature. From the fundamental point of view, additional investigations need to be conducted in order to gain more insight on the phase formation sequence when the reaction between Pd and SiC takes place. Firstly, there is a question of the formation of metal-rich silicides and unreacted Pd metal when the reaction is taking place at low annealing temperature (400^0C) for the given time period used in our study. Literature work showed that when the Pd/SiC interface was annealed at 400^0C for 30 minutes with the thickness of Pd close to the one used in this study, no detectable reaction was observed. Perhaps, annealing the Pd/SiC interface for longer period of time at this temperature where we start to observe the reaction taking place, will result in total consumption of Pd forming metal-rich silicides first, which can later on evolve into Si-rich silicides.

Secondly, investigations should also be performed on the samples annealed at higher temperature for a shorter period than the one used in this study. In doing so, one will be able to determine if the phase formation sequence in Pd/SiC system starts off by forming metal-rich silicides which evolve into Si-rich silicides or if the formation of Si-rich silicides is immediate. Lastly, the crucial issue on the reaction morphology resulting in the formation of periodic structures observed in bulk diffusion couples as discussed in chapter 2 also needs to be addressed. That is, thin-film diffusion couples must be prepared and cross-sectional analysis using the SEM focused ion beam (FIB) technique or TEM in order to observe the formation of these periodic structures.

Reference

Bhanumurthy K., Schmid-Fetzer R., 2001, Compos. Part-A: Appl. Sci.**32**, 569.